

Municipal Solid Waste Incineration (MSWI) Ash Characterization and Physical Concentration

Sharon D. Escalante Pedraza

Thesis submitted to the faculty of the Virginia Polytechnic Institute and State University in partial fulfillment of the requirements for the degree of

Master of Science

In

Mining Engineering

Wencai Zhang, Chair

Aaron Noble

Oscar J. Restrepo

March 30th, 2023

Blacksburg, Virginia

Keywords: Municipal solid waste, Bottom ash, Valuable elements, Characterization, Physical concentration, Acid leaching, Modes of occurrence, Mineralogy, Particle size

Copyright 2023, Sharon E. Pedraza

Municipal Solid Waste Incineration (MSWI) Ash Characterization and Physical Concentration

Sharon D. Escalante Pedraza

ACADEMIC ABSTRACT

Bottom ash (BA), generated from the incineration of municipal solid waste (MSW), contains valuable elements which present a potential economic incentive to attempt recovery. The first study of this thesis investigated the physical, chemical, and mineralogical characterization of MSWI-BA sample through a number of experiments. To develop a proper physical characterization of the BA material, the sample was ground and subjected to particle size distribution, wet magnetic separation, and a float-sink test. As for the chemical and mineralogical characterization, the sample was subjected to XRD, XRF, SEM-EDX, and elemental composition analysis. Additionally, sequential chemical extraction and acid-leaching tests were conducted. The results from this section revealed that carrying out a combination of beneficiation processes using the MSWI-BA sample previously classified into the coarse, middle, and fine-size fractions could lead to better metal concentration yield and recovery optimization. The wet magnetic separation showed outstanding metallurgy indicators towards Fe, with enrichment ratios close to 2.0 and recovery values near to 80%. Metals such as Cu and Co were also enriched by 1.51 and 1.66, respectively, suggesting that the magnetic separation performance and enrichment are a function of the bound of multi-metallic oxides fractions. The 2.95 SG density test reached enrichment ratios higher than 2.0 in Fe, Cu, Co, and Ni in the coarse fraction of the BA fraction, which decreases when reducing the size fraction. The results when reducing the density cutoff showed that the sink fraction yield increased as the medium density decreased, and the enrichment ratios of the minor elements (Mn, Co, Ni, Sn, and V) were similar across the different size fractions. Complementary information was obtained by the mineralogical characterization of the enriched streams from the physical concentration test, which explains the results obtained. The Cu speciation and mineral phases identified were copper oxide, copper sulfate, and cupric sulfite. While, the main Fe-rich constituents existed in chemical forms of iron oxides, such as magnetite, hematite with substituted varieties, spinel group, and metallic inclusions. The enrichment ratios of Mn, Cr, Cu, and Ni obtained through magnetic separation can be explained by the presence of metallic inclusions, where these elements exhibit an affinity for the iron-bearing particles. The acid leaching test revealed that metals such as Fe, Mn, Co, Cu, and Zn can be efficiently leached by using 1M HCl within the 30 min of reaction.

The second part of this research study constituted the evaluation of the effect of the particle size reduction, which was performed to assess the intraparticle heterogeneity of MSWI BA. The evaluation consisted of particle size reductions by crushing and grinding for different residence times and then subjecting the sample to a sequence of physical concentration tests, such as particle size distribution, froth

flotation, and wet magnetic separation. Additionally, the elemental composition after each test was determined through ICP-MS analysis to compare the particle size effect in the recovery and concentration of the valuable elements. The elemental composition results revealed that the comminution process promotes the interaction of Fe, Zn, and Cu, in the fine fraction, by generating more surface area. In contrast, the minor elements were not significantly enriched by reducing the size fraction, suggesting that the comminution process does not impact the mobility and redistribution of the elements in low concentrations. The froth flotation performed in this study showed that when using 0.338 g/ton diesel as a collector, adjusting and controlling the pH between 8.8 to 9.2 throughout the test, the organic matter content can be efficiently reduced in the BA sample from 14.73% to 4.25% when the sample has been previously ground for 30 min. Slight enrichment ratios were observed in the concentrate stream of the forth flotation, suggesting that these elements are associated with the organic matter in the BA sample. In contrast, the wet magnetic separation results revealed significant enrichment ratios of Fe, Mn, Co, and Ni after 10 min of grinding.

Municipal Solid Waste Incineration (MSWI) Ash Characterization and Physical Concentration

Sharon D. Escalante Pedraza

GENERAL AUDIENCE ABSTRACT

The Bottom Ash (BA) generated by the incineration of household solid waste has been identified as a promising source of valuable elements. However, a comprehensive understanding of the BA sample's properties is required in order to determine the most suitable mineral processing method to enrich the elements. The first study of this research consisted of evaluating BA ash's physical, chemical, and mineralogical properties in the BA sample. Following the characterization study, the effect of particle size, as a function of the grinding time, in the valuable elements' enrichment was evaluated. The results suggest that Ti, Fe, Cu, and Zn are the major and most valuable elements, while Mn, Co, Ni, Sb, and V are valuable elements in a minor concentration in the BA samples. Some elements, such as Ti, Sc, Co, Mn, Ni, Sn, and V, have been declared by the US Department of the Interior as critical minerals due to their economic importance and vulnerability to supply chain disruption. Although Fe and Cu are not considered critical minerals, their consumption in 2022 was 40 and 1.9 million metric tons, respectively. The development of national industry and enhancing the understanding of the alternative sources for the valuable elements present an opportunity to diversify local suppliers, pursue a vertical integration of the economic model, and reduce the third-party international vendors' dependency. Likewise, this research supports the aims to reduce the demand for primary natural resources and contribute to the circular economy model, in which energy, resources, and material are kept in a lifecycle while reducing landfilling disposal.

Dedication

“...Put God first in everything you do. Everything that you think you see in me. Everything that I’ve accomplished, everything that you think I have... Everything that I am and have, is by the Grace of God... I’ve been protected, I have been directed and I have been corrected by Him... I did not always stick with him, but he always stuck with me.”

- Adapted from Denzel Washington’s speech at Dillard University.

Lovingly dedicated to my beloved mother, Johanna Pedraza, and my sister Valeria Ortega. They are my anchor, my compass, and my north. I would not accomplish this goal without their advice, patience, unconditional support, and faith in me. Mom, you postponed your dreams and your goals to raise me. You gave me life and then, with my sister, a reason to live for. You did **EVERYTHING** and nothing less than you could, sparing no details for me to build a life that I am proud to live. You two are and will always be my engine to keep going and never give up.

Acknowledgements

First, I would like to express my gratitude to my advisor, Dr. Wencai Zhang, for his understanding when I needed it the most and for sharing his infinite knowledge, commitment to academia, and continuous mentoring, which has culminated in this thesis. He is brilliant at what he does and achieves everything he sets out to do. His tough but accurate feedback has made me a better researcher, author, engineer, and overall professional. I am and always will be grateful to him for this incredible opportunity to come to the U.S. and pursue my master's degree. It is something that has changed my life entirely.

I want to thank my committee members, Dr. Aaron Noble, who taught me and led by example. Moreover, I'm thankful for Dr. Oscar Restrepo, my words fall short to describe his teachings, advice, and genuine desire to help and support every Colombian student selflessly. I could not have had a better professional development and life mentor.

Sincerest thanks are extended to Dr. Erik Westman and Dr. Kray Luxbacher, the Mining and Minerals Department's Head during my time at Virginia Tech, who never hesitated to listen and support me. Thank you for always being available and for your understanding and support. This triumph belongs to you too.

My special thanks are extended to Senior Research Associate Stephen McCartney from the Nanoscale Characterization and Fabrication Laboratory (NCFL) for his patience and willingness to help and teach me how to use, manage, and interpret the SEM-EDX results.

Assistance provided by my research group members, Bin Ji, and Qi Li, was greatly appreciated. Thank you for your support, help, and guidelines when needed. Special thanks to my colleague and friend Zhongqing Xiao, who always made the lab work more enjoyable. His comments, jokes, and conversations lifted me whenever I needed them.

I would not have accomplished this without the Equine Volunteer Program. I want to thank and acknowledge the Equine Center Manager, Natalie Duncan. I will never forget the happy dances in the sunshine surrounded by horses, the serious conversations I had with Murphy, Kwil, Captain, and Reggie, seeing foal Amaretto grow, and the immediate smile on my face every time I had the chance to be around the horses. Thank you, Natalie for all your work and effort with them. You helped me to discover something that brings me so much joy. You make people happy just by doing your job.

Last but not least, I want to thank my friends, Nestor Santa, Carolina Benavides, Juan Monsalve, Ali Hassani, and Lizeth Jaramillo, for their continued support, advice, and company during these years. The members from LAIGSA were always a great reminder of my roots, culture, and home. My boyfriend,

August Greth, for his tremendous effort and unconditional support. For helping me go through difficult times and never letting me down. His tireless effort and push me to strive for excellence and pursue my goals. For believing in me anytime, even when I did not. You have always gone above and beyond, and you will always have my heartfelt gratitude.

The information, data, or work presented herein was funded in part by the Advanced Research Projects Agency-Energy (ARPA-E), U.S. Department of Energy, under Award Number DE-AR0001397. The views and opinions of authors expressed herein do not necessarily state or reflect those of the United States Government or any agency thereof.

Table of Contents

Preface.....	xiv
Chapter 1 Literature Review	1
1.1 Municipal Solid Waste.....	1
1.2 MSW generation by region	1
1.3 MSW composition	3
1.4 MSW treatment and disposal	5
1.5 Energy recovery	7
1.6 MSW incineration (MSWI) by-products composition.....	8
1.7 Developments in Valuable Elements Recovery from MSWI by-products	10
1.7.1 Pretreatment methods.....	11
1.7.2 Treatment operations.....	12
1.8 Aims and objectives of the research	15
Chapter 2 Materials and methodology.....	17
2.1 Materials	17
2.1.1 Sample collection and preparation.....	17
2.2 Methodology	17
2.2.1 Physical characterization.....	18
2.2.2 Mineralogical characterization.....	20
2.2.3 Chemical characterization.....	21
2.2.4 Statistical analysis	27
Chapter 3 Characterization results	28
3.1 Elemental composition.....	28
3.2 Transfer coefficients and elements distribution	31
3.3 Leachability of the valuable metals	33
3.4 Modes of occurrence and association of the valuable elements.....	36
3.5 Mineralogical characterization.....	37
Chapter 4 Physical concentration results	41
4.1 Wet Sieving.....	41
4.1.1 Size fractionation characteristics.....	41

4.2	Magnetic separation	43
4.2.1	Magnetic separation performance indicators	43
4.2.2	Mineralogical characterization of the magnetic fraction.....	45
4.3	Density separation.....	48
4.3.1	Density separation performance indicators	48
4.3.2	Mineralogical characterization of the Sink fraction	51
4.4	Statistical analysis	55
Chapter 5 Evaluation of the effect of the particle size reduction.....		60
5.1	Materials and methods	60
5.1.1	Materials	60
5.1.2	Physical characterization.....	60
5.2	Results and discussions.....	63
5.2.1	Size fraction characterization and elemental composition	63
5.2.2	Flotation test.....	66
5.2.3	Magnetic separation	69
5.2.4	Leachability of the valuable metals.....	70
5.3	Conclusions.....	72
Chapter 6 Conclusions and recommendations for future work		74
6.1	Conclusions.....	74
6.2	Recommendations for future work	76
References.....		79
Appendix A: Particle Size Distribution.....		94
Appendix B: Permission for Release		97
Bunge, 2019		97
World Bank Group.....		99

List of Figures

Figure 1. Waste generation and urbanization rate by region.	2
Figure 2. Average waste generation per capita by region, 2016.	2
Figure 3. U.S. municipal solid waste generation 1960-2018.	3
Figure 4. Global waste composition	4
Figure 5. United States' waste composition.	4
Figure 6. Waste Management Hierarchy	5
Figure 7. Global Waste Treatment and Disposal.	7
Figure 8. Schematic diagram of Waste to Energy facility	8
Figure 9. Bottom ash composition.	9
Figure 10. The circular economy model applied to the consumer goods lifecycle from MSW	11
Figure 11. Scheme of the magnetic separation's working principle.	13
Figure 12. Eddy current separation working principle scheme.	13
Figure 13. Sensor sorters working principle.	14
Figure 14. MSWI systematic characterization plan.	18
Figure 15. Comminution process (a) BA sample pulverized in an electric mill, b) FA non-mechanical comminution.	18
Figure 16. Float- Sink test set up.	20
Figure 17. The procedure of microwave-assisted digestion used to determine the BA and FA samples' elemental composition.	23
Figure 18. Sequential chemical extraction protocol used for this study.	25
Figure 19. Experimental set up used for the acid leaching tests.	26
Figure 20. XRD pattern of the bottom ash sample.	28
Figure 21. XRD pattern of the fly ash sample.	30
Figure 22. Mn, Co, Ni, and Zn distribution between BA and FA samples calculated following the expressions (7) and (8).	32
Figure 23. Ti, Fe, Sn, and Cu distribution between BA and FA samples calculated following the expressions (7) and (8).	33
Figure 24. Effect of the acid concentration on the valuable elements' recovery from the BA sample with (a) HCl and (b) HNO ₃	34
Figure 25. Leaching kinetics of the valuable elements from BA sample using (a) 1 M, (b) 1.5 M, and (c) 2 M HCl.	35

Figure 26. Effect of the temperature on the leaching recovery of the valuable metals from BA sample using HCl at 2 M.	36
Figure 27. Distribution of the occurrence modes of the valuable elements from the BA sample.	37
Figure 28. EDX spectra of Particle 1 (left) and particle 2 (right).	38
Figure 29. BSE image (top left), elemental maps (bottom left), and EDX spectra (right) of particle 3.	38
Figure 30. (a) BSE image and (b) elemental maps of a Fe-P metallic inclusion from the BA raw sample.	39
Figure 31. BSE image (top left), elemental maps (bottom left), and EDX spectra (right) of (a) octahedral substitution of Fe^{3+} by Si^{4+} and Al^{3+} , and (b) tetrahedral substitution of Fe^{2+} by Mg^{2+} , Ca^{2+} , and Mn^{2+} from the MSWI -BA sample.....	40
Figure 32. Systematic physical characterization flowsheet of the BA sample.	41
Figure 33. Valuable elements' enrichment ratios per size fraction in the BA sample for (a) Ti, Sc, Fe, Cu, and Zn and (b) Mn, Co, Ni, Sn, and V.....	42
Figure 34. Cumulative particle size distribution pattern of BA sample using Rosin Rammler Regression.	43
Figure 35. Magnetic separation enrichment ratio for (a) Ti, Sc, Fe, Cu, and Zn and (b) Mn, Co, Ni, Sn, and V.....	44
Figure 36. Magnetic separation recovery for (a) Ti, Sc, Fe, Cu, and Zn and (b) Mn, Co, Ni, Sn, and V of the MSWI bottom ash sample per size fraction.	44
Figure 37. BSE image (top left), elemental maps (bottom left), and EDX spectra (right) of a Fe-rich constituent from the magnetic fraction enriched with (a) Mn and Cr, and (b) Ni, and Cr.....	45
Figure 38. BSE image (left) and EDX spectra (right) of a possible Fe-Cu metallic inclusion, surrounded by Ca – Si matrix from the magnetic fraction of the BA sample.....	46
Figure 39. (a) BSE image and (b) elemental maps of a Fe-rich particle embedded in Si-Ca enrich matrix from the magnetic fraction of the BA raw sample.....	47
Figure 40. BSE image (left), and elemental maps (right) of (a) Cu-S-O particle, and (b) Zn-S-O particle from the non-magnetic fraction of the BA sample.....	47
Figure 41. Density separation enrichment ratios for (a) Ti, Sc, Fe, Cu, and Zn and (b) Mn, Co, Ni, Sn, and V at 2.95 specific gravity of the MSWI-BA sample per size fraction.	50
Figure 42. Density separation recovery for (a) Ti, Sc, Fe, Cu, and Zn and (b) Mn, Co, Ni, Sn, and V at 2.95 specific gravity of the MSWI-BA sample per size fraction.	50
Figure 43. Density separation enrichment ratio for (a) Ti, Sc, Fe, Cu, and Zn and (b) Mn, Co, Ni, Sn, and V at 2.6 specific gravity of the MSWI-BA sample per size fraction.	51
Figure 44. Density separation recovery for (a) Ti, Sc, Fe, Cu, and Zn and (b) Mn, Co, Ni, Sn, and V at 2.6 specific gravity of the MSWI-BA sample per size fraction.	51

Figure 45. BSE image (left), EDX spectra (top right), and elemental maps (bottom right) of most likely magnetite with aluminum/calcium-silicate mineral phases association from the sink fraction of the BA density test.	52
Figure 46. BSE image (left), and elemental maps (right) of a Fe-spinel group with Cr^{3+} substitution (iron chromite) from the sink fraction of the BA density test.....	52
Figure 47. BSE image (left) and elemental maps (right) of a copper oxide particle from the sink fraction of the BA density test.....	53
Figure 48. BSE image (left), elemental maps (middle and top left), and EDX spectra (right) of a Cu-S metallic inclusion, surrounded by CaO and CaTiO_3 from the sink fraction of the BA density test.....	54
Figure 49. BSE image (left) and elemental maps (right) of a calcium titanate particle from the sink fraction of the BA density test.....	54
Figure 50. Froth flotation experiment set up.....	62
Figure 51. Particle size distribution of the BA sample subjected to different grinding times.	64
Figure 52. (a) Major and (b) minor elements distribution per size fraction from the BA raw sample.	65
Figure 53. (a) Major and (b) minor elements distribution per size fraction from the BA sample after 10 min grinding time.....	66
Figure 54. (a) Major and (b) minor elements distribution per size fraction from the BA sample after 30 min grinding time.....	66
Figure 55. Effect of the grinding residence time of the BA sample in the enrichment ratio of (a) Ti, (b) Sc, (c) Fe, (d) Cu, and (e) Zn from a forth flotation carried out under different set up conditions described in Table 8.	68
Figure 56. Effect of the grinding residence time of the BA sample in the enrichment ratio of (a) Mn, (b) Co, (c) Ni, (d) Sn, and (e) V from a froth flotation carried out under different set up conditions described in Table 8.	69
Figure 57. Effect of the grinding time of the BA sample on the (a) major elements and (b) minor elements recovery after a wet magnetic separation.....	70
Figure 58. Valuable elements leachability at (a) 0.5 M HCl, (b) 1.0 M HCl, (c) 1.5 M HCl, and (d) 2.0 M HCl as a function of the grinding time.....	71
Figure 59. Effect of the (a) 10 min, (b) 30 min, (c) 60 min, and (d) 90 min grinding time on the leaching kinetics of the valuable elements using 1.0 M HCl.	72

List of Tables

Table 1. List of chemicals used and related information.	22
Table 2. Elemental contents of major elements, minor elements, and main rare earth elements in the MSWI BA and FA samples.	29
Table 3. Estimated minerals in MSWI-BA and density (g/cm ³).....	49
Table 4. <i>p</i> -values of paired t-test for valuable elements content among magnetic, non-magnetic, float fraction, sink fraction at 2.95 and 2.6 specific gravity of the BA sample.....	55
Table 5. Relative enrichment coefficient of valuable elements in the magnetic material per size fraction of the UB sample.....	57
Table 6. Relative enrichment coefficient of valuable elements in the sink material from the density test at (a) 2.95 SG and (b) 2.6 SG per size fraction of the UB sample.....	58
Table 7. Grinding residence time used.....	61
Table 8. Experimental conditions used for the froth flotation tests.	62
Table 9. Loss of ignition of the concentrate stream generated by the forth flotation tests.	67

Preface

This thesis is composed of six chapters in a traditional format. Chapter 1 presents the introduction and literature review related to the Municipal Solid Waste, generation, composition, and management. It also presents an explanation in detail about the “Energy recovery” process and the developments registered in the literature regarding the recovery of the valuable elements identified in the by-products generated during the combustion process. Chapter 2 describes the materials, samples and methodology used to carry out this research. The characterization, physical concentration and the evaluation of the particle size reduction results obtained in this research are present in Chapter 3, 4 and 5, respectively. The overall conclusions and recommendations for future work are presented in Chapter 6. Permission for release used and adaptations of the figures used in Chapter 1 from the corresponding authors and publishers can be seen in Appendix B.

Abbreviation	Meaning
AS	Acid soluble
BA	Bottom ash
EC	Enrichment coefficient
COD	Chemical oxygen demand
DI	Deionized water
ECS	Eddy Current Separation
EDX	Energy Dispersive X-Ray Spectroscopy
EPA	Environmental Protection Agency
FA	Fly ash
GDP	Gross Domestic Product
GHG	Greenhouse Gases
HIMS	High-intensity magnetic separation
ICP-MS	Inductively coupled plasma spectrometry
IE	Ion-exchange
In	Insoluble
LIMS	Low-intensity magnetic separation
LMT	Lithium metatungstate
MSW	Municipal Solid Waste
MSWI	Municipal Solid Waste Incineration
NFe	Non-ferrous metals
Ox	Oxidable fraction
Re	Reducible fraction
REE	Rare Earth Elements
SCE	Sequential chemical extraction
SEM	Scanning electron microscopy
WL	Water leaching
WtE	Waste-to-Energy
XANES	X-ray absorption near edge structure
XRD	X-ray Diffraction
XRF	X-ray fluorescence spectrometry

Chapter 1 Literature Review

1.1 Municipal Solid Waste

Municipal solid waste (MSW), as the name implies, is waste generated from different sources such as households, shops, offices, public institutions, etc. (Tiseo, 2022). Its management has become a worldwide major issue in terms of public health, land-use, pollution and economic development. Globally, 2.01 billion metric tons of MSW were generated in 2016, from which at least 33% was not properly managed and disposed. East Asia and Asia-Pacific Rim Countries have the highest waste generation with 468 million metric tons per year, followed by Europe and Central Asia with 392 million metric tons. Together, this represented 43% of the total global production according to the World Bank (Tiseo, 2020).

1.2 MSW generation by region

Some studies have found a positive correlation between MSW generation and economic development, urbanization and industrialization and population (Kaza et al., 2018). Usually, waste generation increases with the increase in goods and services consumption. The same tendency is followed by urbanization and industrialization rates. Studies have shown that rural areas tend to purchase fewer store-bought items, which means less packaging disposal. In addition, rural residents have higher rates of recycling and reusing of discarded materials compared to the urban areas, where more than 50% of the world population is concentrated. Kaza et al. (2018) designed a prediction model to determine MSW generation at a specific time, in which the correlation with economic and population growth is assumed. Figure 1 (Kaza et al., 2018) shows the relation between MSW generation per capita and the urbanization rate percentage by region, and the bubble size denotes total MSW generation in millions of tons per year. The bigger bubbles refer to Europe and Central Asia region and East Asia and Pacific, which produced 860 tons per year; however, they are located in the bottom right of the chart, meaning that their per capita production is low (lower than 1.5 kg/capita/day), and high urbanization rate (above 55%). In contrast, the North American region, comprised of the U.S., Canada, and Bermuda (UK), generates on average 289 tons per year with a per capita production of about 2.5 kg/capita/day. The Middle East and North Africa have the lowest MSW generation, with 129 tons per year, a per capita production below 1.0 kg/capita/day, and an urbanization rate close to 65%.

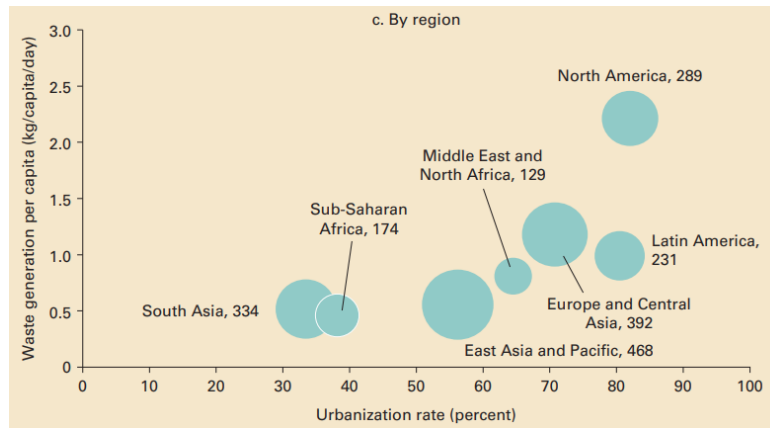


Figure 1. Waste generation and urbanization rate by region. Used with the permission of World Bank Group.

Currently, the average waste generation per capita is 0.74 kg/day. However, this index is highly variable according to the regional differences in waste generation rates. Countries known for their high income, such as the United States which concentrates less than 5% of the global population, generates almost 14% of the global solid waste, for an average of 2.21 kg/capita/day. From East Asia and Asia-Pacific Rim Countries, China accounts for 70% of the regional total solid waste, corresponding to 15.55% of the global MSW production. However, its actual per capita waste generation is only 0.6 kg/per day, because this country concentrates 18.47% of the world's population.

Figure 2, taken and adapted from the World Bank “What a waste 2.0” report from 2018, summarizes the waste generation per capita per region.

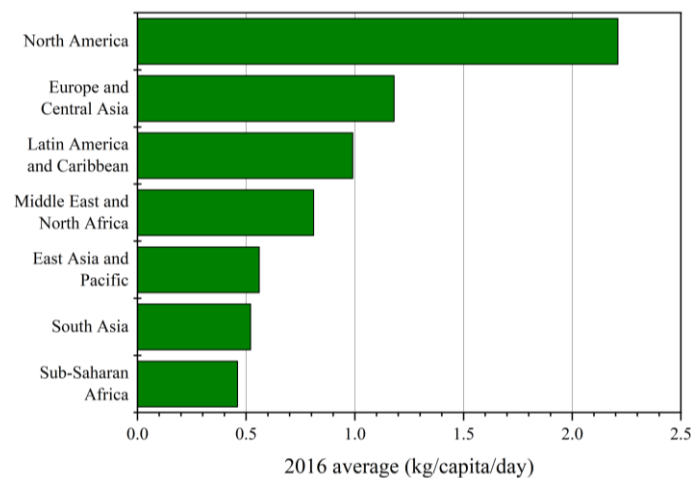


Figure 2. Average waste generation per capita by region, 2016. Adapted from Kaza et al., 2018¹.

¹ This is an adaptation of an original work by The World Bank. Views and opinions expressed in the adaptation are the sole responsibility of the author or authors of the adaptation and are not endorsed by The World Bank.

The United States Environmental Protection Agency (EPA) has been collecting and reporting waste generation and disposal data for over 35 years. Figure 3 shows that over the past 60 years, the U.S. increased its MSW generation rate from 88.1 to 292.4 million metric tons per year (Tiseo, 2022). World Bank studies suggest that the increment is due to the high urbanization rate and economic development, evaluated through Gross Domestic Product (GDP) growth. The GDP is the total value of goods and services that a country provides in a specific time period. Thus, MSW generation also increases as a country's industry expands and its output grows. Kaza et al. (2018) projection determine that the U.S.'s total MSW generation is expected to grow gradually given that its urbanization rate it's above 85%, compared to the developing countries with urbanization rates below 70%.

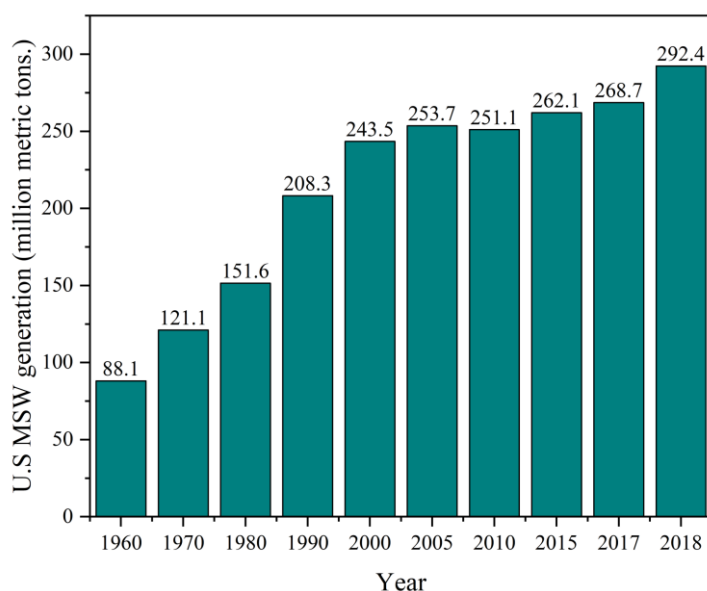


Figure 3. U.S. municipal solid waste generation 1960-2018. Adapted from Environmental Protection Agency, 2020a².

1.3 MSW composition

MSW composition may vary according to the area (rural or urban), season, income level, and urbanization. Nevertheless, at a general level, MSW composition categories are organic (e.g., food and yard trimmings), paper, plastic, glass, metals, rubber and leather, wood and other. The largest category based on dry weight is food and green waste (organic), representing 44% of the MSW composition. Yet, plastic, paper, cardboard, metal, and glass make up 38% (Figure 4) (Kaza et al., 2018).

² This is an adaptation of an original work by the U.S. EPA. The U.S. Government retains a nonexclusive, royalty-free license to publish or reproduce these documents. These documents may be freely distributed and used for non-commercial, scientific and educational purposes.

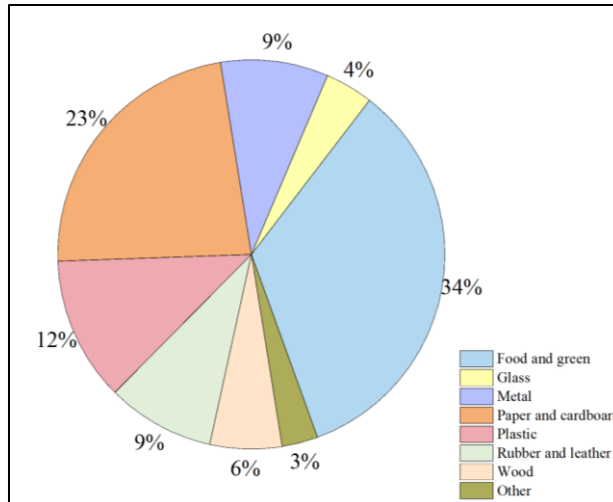


Figure 4. Global waste composition. Adapted from Kaza et al., 2018.

Regarding the composition of MSW generated in the United States, there are slight differences compared to the global average composition. These differences according to Kaza et al., 2018, Šyc et al., 2018, and Muchova et al., 2008, are due to the nation's development, urbanization, and economic activities. Figure 5 summarizes the U.S. MSW composition. Food and garden trimmings represent less than 35%, which is about 10% lower than the global average. While metals and rubber and leather categories account for larger proportions than the global averages (4.8% and 6.9% higher, respectively) (Environmental Protection Agency, 2020a).

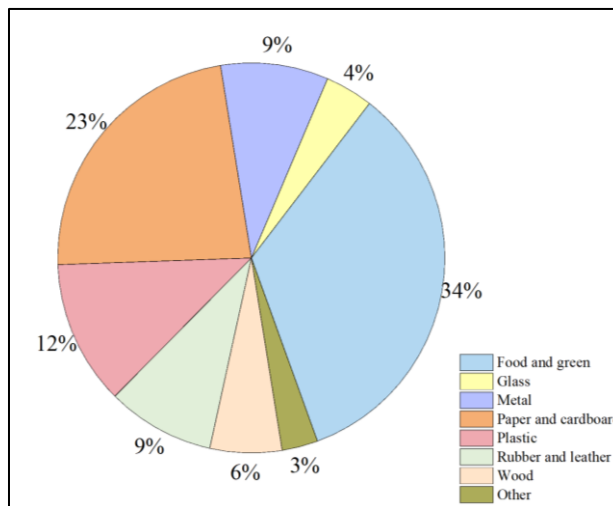


Figure 5. United States' waste composition. Adapted from Environmental Protection Agency, 2020a³.

³ This is an adaptation of an original work by the U.S. EPA. The U.S. Government retains a nonexclusive, royalty-free license to publish or reproduce these documents, or allow others to do so, for U.S. Government purposes. These documents may be freely distributed and used for non-commercial, scientific and educational purposes.

1.4 MSW treatment and disposal

After the inevitable generation of MSW as a result of human and economic activities, it is necessary to treat and dispose of the MSW to avoid socioeconomic, environmental, and public health consequences. It is estimated that about 2 billion people live in areas without MSW collection services or within 10 km of uncontrolled landfills (UNEP & ISWA, 2015). Aiming to reduce the possible outcomes of inadequate MSW management, there are four main strategies for MSW management, which EPA has ranked based on their sustainability (Environmental Protection Agency, 2020b). Figure 6 outlines the preferred, environmentally conscious strategies to manage MSW, focusing on preventing and reducing the generation from the source, followed by recycling and composting, which turn the waste into new products and reduce the energy and natural resources needed to create new products. The next preferable strategy is energy recovery. It involves taking advantage of the heat and energy produced by the combustion of non-recyclable materials. Among the benefits that energy recovery presents are the reduction of carbon emissions by reducing the demand for fossil fuels and the methane generated from landfills. In addition, it helps to reduce the waste volume sent to dumpsites. Finally, the last strategy would be the waste disposal into controlled dumpsites or sanitary landfills, with management practices and engineered design (leachate and gas collection).

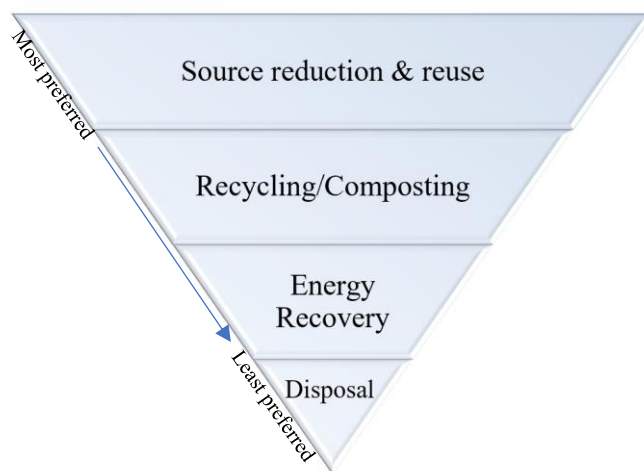


Figure 6. Waste Management Hierarchy. Adapted from Environmental Protection Agency, 2020a⁴.

The report presented by the World Bank in 2012, entitled “What a Waste: A Global Review of Solid Waste Management” compares the strategies for managing MSW according to the income level of the different regions. The three categories according to income are: low, medium, and high. Low- and middle-income countries do not generally have structured programs to reduce MSW generation. In contrast,

⁴ This is an adaptation of an original work by the U.S. EPA. The U.S. Government retains a nonexclusive, royalty-free license to publish or reproduce these documents, or allow others to do so, for U.S. Government purposes. These documents may be freely distributed and used for non-commercial, scientific and educational purposes.

high-income countries have educational programs focused on "the three R's (Reduce, Reuse, Recycle)" and a greater awareness of MSW use, production design and reuse. Regarding recycling and composting, the informal collection and recycling sector plays a fundamental role in low- and middle-income regions, causing the prices for recycled products to be unregulated, and generating a high price fluctuation. In high-income countries, recycling facilities are regulated and equipped with technologies for selection and processing. Likewise, MSW management through composting, both on large and small scales, has become more popular (Hoornweg & Bhada-Tata, 2012).

Regarding the implementation of controlled waste incineration as a strategy to manage MSW, only regions with medium and high incomes implement it. However, some incinerators' operations in middle-income areas are usually financed or subsidized because they are not economically viable on their own. Finally, landfilling occurs more frequently in low-income regions, without environmental or emission controls, near urban centers, aquifers, or bodies of water. In the areas with medium income, it occurs in a similar percentage. However, the medium income areas have environmental controls and regulations with projections to the Clean Development Mechanism Project that allow reducing the emission of greenhouse gases (GHG) (Hoornweg & Bhada-Tata, 2012).

Figure 7 shows the world's MSW management statistics. About 40% of the global MSW generation is disposed of in landfills, while 19% is managed through recycling and composting. Management through energy recovery represents 11%, and the remaining percentage (~30%) is openly dumped, in which there is no control, infrastructure, or engineering design that guarantees safety and security or environmental sustainability (Kaza et al., 2018). The wealthier countries have shown better MSW management due to the availability of investment in more technical processes and awareness campaigns. In the United States, compared to the global distribution, the percentage of MSW treated through recycling and composting is 32%, while only 1.6% is disposed of in landfills or open burning. Controlled incineration for energy recovery accounts for 12%, similar to the global trend.

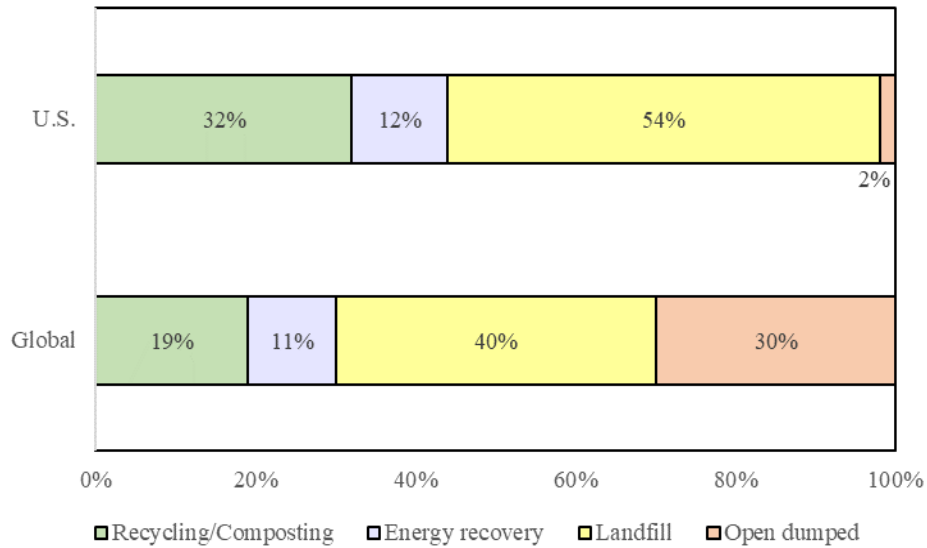


Figure 7. Global Waste Treatment and Disposal. Adapted from Kaza et al., 2018⁵.

1.5 Energy recovery

As was previously mentioned, this strategy consists of the controlled combustion of MSW that allows heat recovery and energy generation. This technology can reduce the volume of waste disposed of by up to 90% (Kaza & Bhada-Tata, 2018). The MSW incineration has been widely used historically, but the potential to be an energy source in addition to a waste management solution is presented as an innovation. However, the associated investment, maintenance cost, and high technical capacity make it a solution primarily used in high-income countries. The trend to manage MSW through energy recovery and controlled incineration in the United States has increased over the last 60 years. By 1980, the controlled waste combustion was 2.76 million metric tons (less than 2% of the total MSW generated by that year), while in 2018, over 34.6 million metric tons were combusted, which represents 12% of the total MSW generated. Over the U.S. territory are 75 facilities (also called waste-to-energy, WtE) that generate about 550 kWh per ton of waste (United States Environmental Protection Agency, 2019).

Figure 8 illustrates a modern controlled waste incineration process, which consists of unloading the material from the collection trucks in a storage area. The waste is classified and taken to a combustion chamber by a crane. When the chamber reaches a temperature between 850 °C and 1450 °C, the combustible materials in the waste burn undergo an oxidation reaction when in contact with oxygen. The generation of heat from oxidation goes to a heat recovery system that uses the heat to produce steam for electricity generation. However, throughout the process, by-products are generated, like Fly Ash (FA), composed of

⁵ This is an adaptation of an original work by The World Bank. Views and opinions expressed in the adaptation are the sole responsibility of the author or authors of the adaptation and are not endorsed by The World Bank.

dust and gaseous emissions containing toxic particles that rise with it, which is captured and treated through a highly advanced air pollution control (APC) process prior to being released into the atmosphere. FA represents ~3-5% by weight of the MSW processed (Kaza & Bhada-Tata, 2018). A second by-product called Bottom Ash (BA) is generated, and as the name implies, it is deposited at the bottom of the incineration chamber (Mutz et al., n.d.). BA's annual production is approximately 25-30% by weight of the total incinerated MSW (Wang et al., 2021) and 80-90 wt.% of the total solid residues from the incineration process (Kaza & Bhada-Tata, 2018).

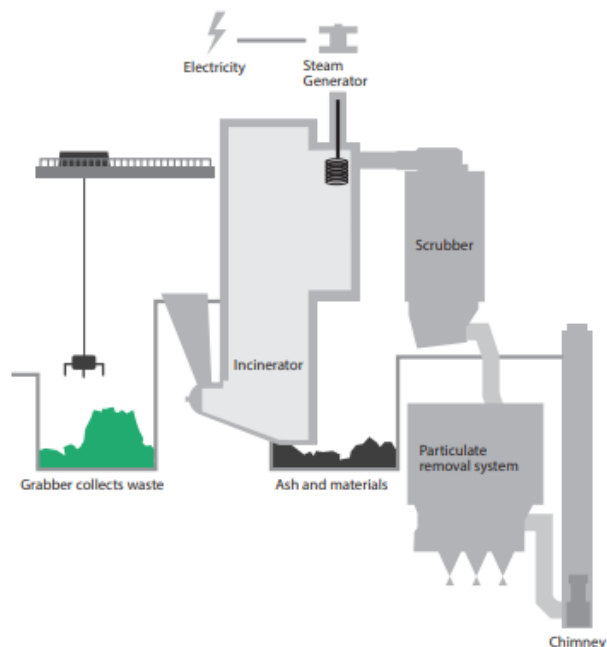


Figure 8. Schematic diagram of Waste to Energy facility. Taken from Kaza & Bhada-Tata, 2018.

1.6 MSW incineration (MSWI) by-products composition

Several studies have been conducted since the 1980s to determine the elemental composition, leachability characterization, and heavy metal content in MSWI ashes due to the environmental concerns (Wang et al., 2021; Pan et al., 2013; Reimann, 1989; Zhang et al., 2008). The studies agreed that BA is a heterogeneous material, and its composition may vary according to incinerated MSW composition, combustion conditions and incinerator type. Kinnunen, 2006, states that due to the heterogeneity of BA, all BA particles have discrete chemical and physical properties.

In a general, it was determined the main heavy metals contained in the by-products were, in decreasing order, $Zn > Pb > Cu > Cr > Ni > Cd$, but their concentrations are higher in the fly ash samples than in the BA samples. The high heavy metal concentration in the fly ash results from the FA's fine particles that provide sufficient specific surface area for metal enrichment. According to Kinnunen, 2006

the Cd and Cr source are colored newsprint and plastic house ware, while Ni and a portion of the Cd come from batteries. The major sources of Pb are plastic films, wood, textiles, and PVC. Electrical appliances are the main Cu source in the MSWI by-products.

Bunge (2019) reported that bulk BA has a density of $\sim 1.2 \text{ t/m}^3$, which could increase up to 1.5 t/m^3 through compaction. The major components in the BA material are classified into mineral fraction, slag, native metals, unburnt organic matter, and grit. Figure 9 shows the components distribution in the BA matrix. The mineral fraction has diameters bigger than 2 mm and usually comprises glass, porcelain, tiles, and cement particles. While slag is molten material partially solidified with a diameter bigger than 2 mm, typically enclosed in foreign materials. 40% of the total iron oxides are contained in this MSWI BA material, presenting some weakly magnetic properties. The native metal fraction represents $\sim 11\%$, comprising ferrous (Fe) and non-ferrous metals (NFe). According to the study by Šyc et al. (2018), ferrous metals can be 5-13% (mainly iron scrap) and 2-5% non-ferrous metals by dry weight. The unburnt organic matter comes from the paper, cardboard, leather, and wood contained in the MSW feedstock. Grit is the fine particles from all the previous categories plus metal oxides.

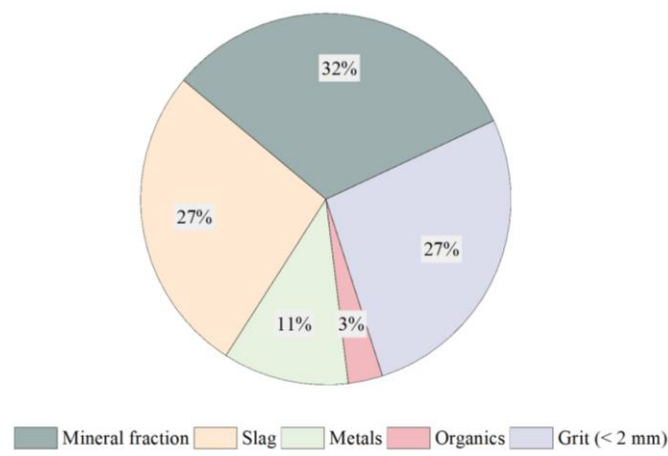


Figure 9. Bottom ash composition. Used with the permission of Bunge, 2019.

Jung & Osako 2009 performed water extraction tests on FA samples to remove undesired substances like chlorine and inorganic salts and to concentrate valuable rare metals. The study also determined the metal content and leaching behavior. Their results showed that some elements like Ag, Ga, Sn, and Sb presented the lowest leaching recovery at a neutral pH. At the same time, the major elements (Cl, Ca, Na and K) were leached regardless of the pH range. In contrast, Cu, Pb, and Zn were mainly insoluble at a neutral pH. Wang et al. 2021 also studied the variables that could contribute to the heavy metals leaching. Mn and Cr leaching behavior is associated with pH, chemical oxygen demand (COD), chloride ions and alkalinity. In contrast, the leaching behavior of Zn and Cu are mainly subjected to pH and

alkalinity variables. Some other variables that could affect the elements' leaching properties are waste content as organic matter, heavy metals species, and chemical bounds.

Nevertheless, studies like Šyc et al., 2018; Muchova et al., 2008; Morf et al., 2013; Funari et al., 2015, and Park et al., 2021 have found significant concentrations of valuable elements which generate a new perspective on MSW as a secondary source of these elements. In fact, Jung & Osako 2009 stated that Ag, In, Pd, Pb, and Zn contents in the FA samples are higher than the natural mineral occurrence. Park et al. (2021) established that BA and FA contain 185.80 mg/kg and 179.19 mg/kg of rare earth elements (REE), respectively. The results from a study conducted by Morf et al. (2013), showed an average concentration of 11 mg/kg, 120 mg/kg of Co and Ni, respectively, and 74 mg/kg of Sn, and 11 mg/kg of V in an MSW incinerator from Hinwil, Switzerland.

Funari et al. (2015) sampled untreated BA and FA residues to determine their elemental composition and major chemical compounds through the analytical techniques of inductively coupled plasma spectrometry (ICP-MS) and X-ray fluorescence spectrometry (XRF). The results showed that silica (SiO_2) and calcium oxide (CaO) are the main constituents for both by-products, with concentrations higher than 30g/100g and 20g/100g, respectively, for BA samples. On average, FA samples contain >30g/100g of CaO and about 10g/100g of SiO_2 . The iron content is about 10g/100g expressed as Fe_2O_3 and ~8 mg/kg of Al_2O_3 in the bottom ash samples. The titanium and magnesium content are present as oxides with an average concentration of 1.25 mg/100 mg and 5.16 mg/100 mg, respectively. As for the FA results, Al_2O_3 , MgO , and K_2O concentrations are around 5g/100g, while Fe_2O_3 and TiO_2 content are <3 g/100 g. The magnesium oxide (MgO) present in the by-products could be derivatives from metallurgical processes, electronic devices, and agricultural fertilizer.

1.7 Developments in Valuable Elements Recovery from MSWI by-products

In recent years, the increasing need, use, and production of modern high-tech has increased the demand for raw materials and the production of metals. However, natural resources and mineral deposits are limited, which have led to an expanded search for resources that can meet the world's demand for valuable elements. In addition, the circular economy is a model of production and consumption in which alternative sources are the main focus, reducing material use and being less natural resource intensive. The goal would be to make the mining supply chain more sustainable. Hence, energy recovery and valuable components recovery from MSW make it an integral part of the circular economy model. Figure 10 show the circular economy model applied to the MSW process.

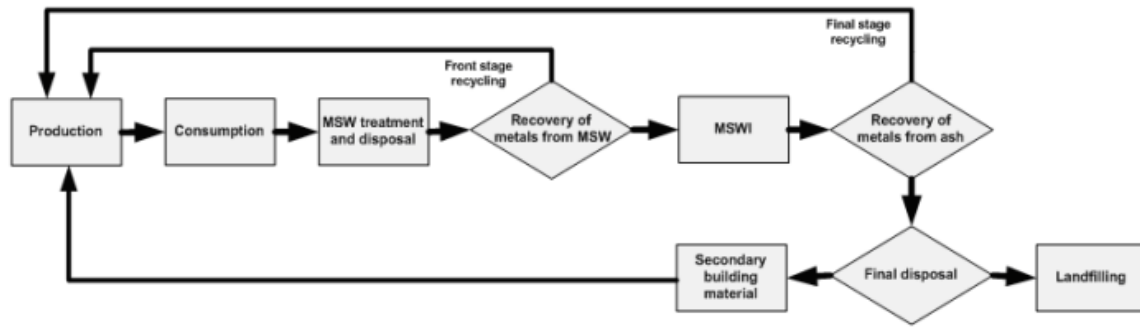


Figure 10. The circular economy model applied to the consumer goods lifecycle from MSW. Taken from Kinnunen, 2006. Used with the permission of Helsinki University of Technology.

Several studies have been conducted under the premise that MSWI contains potential economic levels of valuable elements and, therefore, would be considered an alternative source of such elements, like Funari et al. (2015) who concluded that the average elemental and chemical compounds concentration in MSWI is comparable to economic ore concentrations. Since the 1990s, several technologies and flowsheets for downstream processing to metal recovery (mainly for NFe metals) have been developed and some of them have been applied in WtE facilities on an industrial scale. The Šyc et al. (2020) article presented a comprehensive review of the different technological approaches for recovering valuable components from BA. Besides the overall mineral and elemental content, the particle size distribution and the liberation of the recoverable materials were the most determinant factors for the recovery efficiency. Mechanical processing and physical separation are widely used to process, concentrate and recovery metals from the bulk BA matrix (Bunge, 2019). Magnetic susceptibility, electrical conductivity, and density are the most prominent physical properties in metals in the BA matrix.

Many WtE facilities have been built up and developed in recent years, and each has its process. However, the pretreatment and separation principles are similar among them. Below, the most frequent pretreatment and treatment methods will be described.

1.7.1 Pretreatment methods

- *Comminution:* Besides reducing the average particle size and shape, the target of comminution is to reach the liberation of valuable and hazardous elements trapped in conglomerates and BA bulk matrix. Additionally, by reducing the particle size, a larger surface area will be available for chemical or physical interactions, thus increasing the recovery efficiency of following treatments (Kinnunen, 2006). The feed size distribution and the desired particle size are selected parameters to determine which comminution type is appropriate. The forces applied to achieve the size reduction could be provided by

crushing, using compression or impact forces, or by grinding, through attrition and abrasion (Wills & Finch, 2016a). When the liberation size of the particles is bigger than 10 mm, crushing is pertinent (Wills & Finch, 2016b). Nevertheless, Bunge 2019 mentions that the ductile oversize material like steel sheets and the unburnt material like wood and paper in the BA could clog the crusher, limiting the compression crushers' ability to process BA. If the particle size needs to be smaller than 1 mm to achieve the liberation size, grinding will be better suited (Wills & Finch, 2016c).

- *Classification:* The most common treatment limitation is the particle size, thus in order to obtain homogeneous and narrow- size fractioned material flows, the comminution product is separated by size fraction. In conventional MSW processing facilities, the material classification is often carried out on screens, which allow for the removal of the contaminants and classify the material in two or three streams (Šyc et al., 2020). The oversized items, like large pieces of iron and metal scrap, are usually removed by a finger sieve or bar sizer (Bunge, 2019). The intermediate size fraction is classified through a drum or trommel, and the fine fraction is commonly classified by vibrating screens, where the vibration reduces the blinding phenomenon, in which the screen apertures are plug with pieces of material (Wills & Finch, 2016d).

1.7.2 Treatment operations

- *Magnetic separation:* This technique works according to the material's magnetic susceptibility. The treatment classifies the particles as ferromagnetic or paramagnetic depending on if the particles have strong or weak magnetic properties. Due to the high magnetic susceptibility, low-intensity magnetic separation (LIMS) is mainly used for ferromagnetic particles. In contrast, paramagnetic materials, such as iron oxides and stainless steel, are concentrated through high-intensity magnets (HIMS). Materials like glass and non-ferrous metals not recovered by the HIMS process are classified as non-magnetic. In the MWS processing, magnetic separation is often carried out after BA is discharged. In advanced treatment plants, multi-step magnetic separation is employed for different size fraction streams. Magnetic separation is regularly used to recover large pieces of Fe scrap, steel cans, and fine magnetic particles of iron oxides and agglomerate (Kinnunen, 2006). Figure 11 illustrates the working principle of magnetic separation where the feed material goes on the conveyor belt; When a material with magnetic properties passes by it is attracted to the magnet, which is usually located at the top. After being drawn and separated from the feed stream, the magnetic tape transports it to the concentrate container.

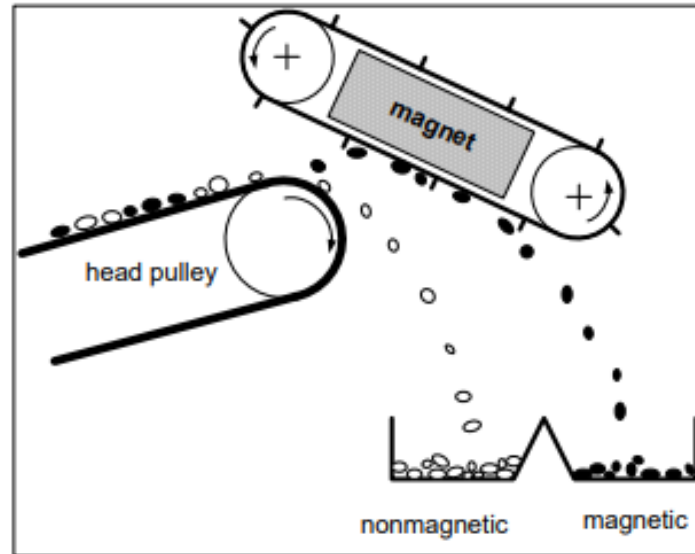


Figure 11. Scheme of the magnetic separation's working principle. Used with the permission of Bunge, 2019.

- *Eddy Current Separation (ECS)*: It is usually applied after the magnetic separation over the non-magnetic stream to recover non-ferrous metals like Al, Cu, and stainless steel, based on the conductive properties. This equipment generates an alternating magnetic field caused by loops of electrical current induced by conductors (Ramachandra Rao, 2006). The input material enters to the magnetic field and if particles contain metal, the metal containing material will be accelerated and deflected at a specific force, which is accordance to the magnet strength, particle mass, density, and electrical conductivity. In contrast, the non-conductive particles will be unaffected on their regular trajectory. Figure 12 shows the ECS working principle.

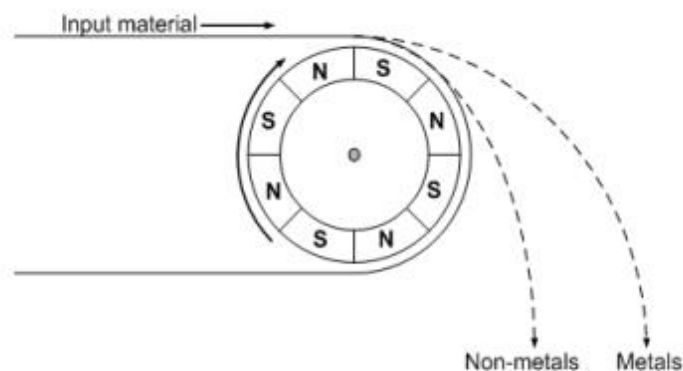


Figure 12. Eddy current separation working principle scheme. Used with the permission of Bunge, 2019.

Smith et al. 2019 and Bunge, 2019 assert that particles and alloys of Al, Mg, Cu, Ag, Au, and Zn are effectively extracted by the ECS process; however, small particle size (> 1 mm) and geometry are the main limitations, because it implies that higher excitation frequencies will be required (about three orders of magnitude higher frequency). Particles larger than 10 mm subjected to an electromagnetic field can reach different deflection trajectories, facilitating their separation (Kinnunen, 2006). The ECS design regarding the number of poles, the permanent magnet's strength, and the rotation speed will determine the magnetic flux density and frequency. These variables will determine its capacity to recover small non-ferrous particles, the thickness of the feed layer on the belt, and the ECS capacity (t/h) (Smith et al., 2019). Other technologies based on ECS principles have been developed focusing on smaller size distribution (from 500 microns to 10 mm), like wet eddy current separators, Magnus ECSs, and backward operating ECSs. Nevertheless, none have been performed at full scale (Settimo et al., 2004).

- *Sensor-Based Sorting* is mainly used to separate metal and glass particles. Its working principles are illustrated in Figure 13. The instrument is equipped with a sensor (usually a metal detector), which detects when a piece of metal passes over the conveyor belt and sends a signal to the computer, which calculates the parabolic trajectory of the particle and sends an air nozzle to divert it to the other side of the splitter (Bunge, 2019). The metal detector can achieve a grade and recovery index of over 90% to identify metals in particles larger than 4 mm (Šyc et al., 2020). It facilitates the recovery of all metals even if they are enclosed or trapped in a mineral matrix, regardless of their magnetic force magnitude.

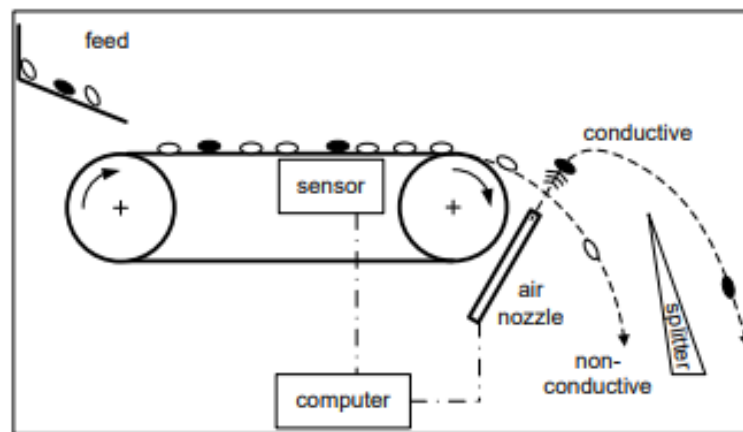


Figure 13. Sensor sorters working principle. Used with the permission of Bunge, 2019.

X-ray fluorescence and optical sensor have been applied and studied to detect and distinguish materials based on their physical properties (e.g., color, shape). However, because of the system's complexity

and the associated cost, the sensor system is suitable for materials with high economic value (Šyc et al., 2020).

- *Density Separation:* This process is based on the different specific gravities between two or more elements or components. In terms of MSWI ash, the alloys and the valuable metals, such as gold, copper, and brass have a specific gravity between 3.2 – 4, while the bulk ash fraction density is usually about 2.6 kg/dm³ (Holm et al., 2017; Šyc et al., 2020). The separation process can be carried out either dry or wet; however, both scenarios have some limitations. When processing MSWI ash, the density separation can be performed right after the extraction from the incinerator. In this scenario, the particles will be liberated but wet and clogged. Alternatively, after waiting until the material is dry, the BA will have gone through a solidification process (Bunge, 2019). Ramachandra Rao, 2006 asserts that a wet density separation will facilitate and increase the separation efficiency and valuable metals recovery. Some techniques apply water as the aqueous medium to carry out density separation; however, air and another aqueous medium with a known specific gravity can be used. Equipment widely used in mineral processing and, nowadays, in metallurgical waste processing for density separation are the shaking tables, pneumatic tables, and Jigs. Šyc et al., 2020 mentioned some studies that have determined that 10 to 20% of the elemental metals are enriched in the fine fraction (0.5 - 2 mm) and could be recovered through density separation. The gravity separator has shown significant recovery values for non-ferrous (NFL) metals; however, using natural force to separate them can take longer. A centrifugal concentrator has been implemented to enhance these factors and has achieved enrichment factors up to 10 (Holm et al., 2017).

1.8 Aims and objectives of the research

As the literature revealed several studies have been conducted in order to determine the MSWI by-products composition and their main characteristics, most of them motivated by environmental concerns. Likewise, significant advances and technological developments have been carried out using incineration by-products from different WtE facilities across the world to determine the best way to treat, remove or recover the potential toxic elements. However, a comprehensive characterization and a thorough overview of the physical, chemical, and mineralogical characterization of the valuable elements in the MSWI by-products is not yet available in the literature recovery. Therefore, this study aims to enhance the understanding of the MSWI by-products by carrying out a systematic characterization in order to determine the most suitable mineral concentration method. The specific objectives of this research are:

- Determine the physical, chemical, and mineralogical characteristics of the valuable elements and their distribution among the MSWI by-products.

- Carry out a systematical physical concentration study of the valuable elements in the MSWI by-products based on their density, size distribution and magnetic susceptibility.
- Subject the samples to different grinding residence times to evaluate the intra-particle heterogeneity and its effect in the physical properties of the valuable metals in MSWI by - products.

Chapter 2 Materials and methodology

2.1 Materials

2.1.1 *Sample collection and preparation*

The BA and FA samples used in this study were collected from a waste-to-energy facility located in New Jersey, U.S. Every year, this WtE facility processes over 540,000 tons of solid waste and produces about 500 pounds of ashes for every ton of waste incinerated (Olsen, 2006). The annual electricity generated is 42 MW. All the samples were transported and delivered to the Mineral Processing Laboratory at Virginia Tech in closed plastic buckets. Before analysis, the BA sample was placed on a flat surface in an approximately 3 cm thickness layer and subjected to 5 to 7 days of air-drying at room temperature to reduce mineralogical changes that could be induced by drying the sample in an oven at higher temperatures. Once the sample was dry, coarse objects and materials like iron, glass, ceramic, and non-mineral materials were sorted by hand. On the other hand, the FA sample did not require preparation prior to the following tests. Each sample was coning and quartering. In total, four subsamples were taken and analyzed. It is worth noting that in the present research, the elements association, distribution and mineralogical arrangements will be referred to as minerals, although it does not meet the conditions of its strict definition.

2.2 Methodology

MSWI ash samples were fractionated based on differences in physical properties, such as particle size, magnetic susceptibility, and density. The wet sieving method was used to assess the particle size distribution, which was performed according to the ASTM C92 standard. Sieves of different apertures were used to separate the samples into different size fractions. The wet magnetic separation was carried out using a high-intensity magnet to separate the magnetic material from each sample. Float-sink test was performed using a heavy liquid medium to separate the particulate materials based on the specific gravities. A comprehensive mineralogical characterization study was accomplished. The dominant mineral phases from the MSWI ash samples were determined through XRD, while the mineral phases of trace elements were characterized by SEM-EDX. Complementary information was obtained using XRF. To identify the chemical nature of the MSWI samples, elemental analysis, and leachability tests were performed, while the loss on ignition and the occurrence modes of the valuable elements were determined. Figure 14 sum the systematic characterization methodology design for the MSWI samples.

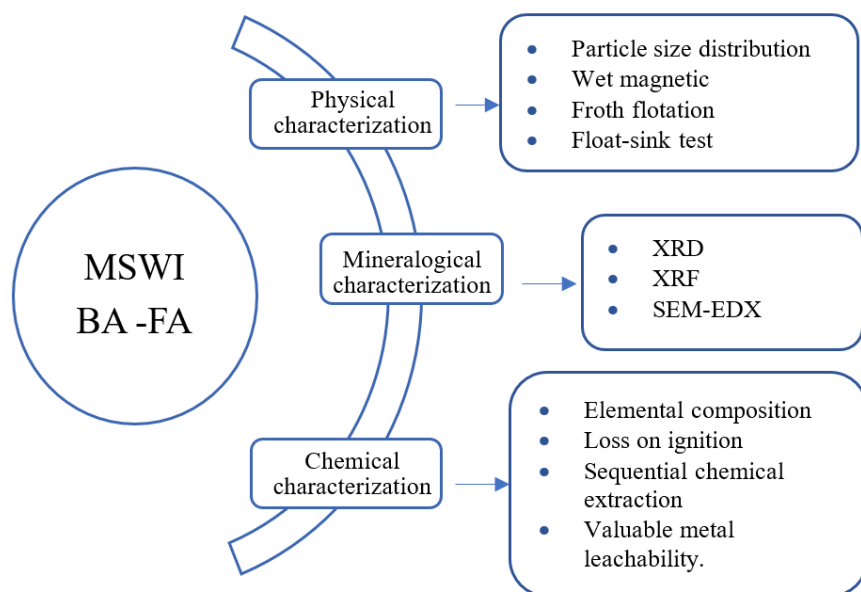


Figure 14. MSWI systematic characterization plan.

2.2.1 Physical characterization

2.2.1.1 Particle size distribution:

The BA subsamples were pulverized in an electric mill for a residence time of 2 min, while a non-mechanical comminution process (mortar and pestle) was used for the FA subsamples. Figure 15(a) shows the BA sample condition before and after being pulverized in the electric mill, while Figure 15(b) shows the FA sample non-mechanical comminution. The products generated were used to determine the particle size distribution through wet sieving, according to the ASTM C92 standard method. The entire samples were sieved on screens with mesh sized 75 (0.2mm), 100 (0.15mm), 150 (0.1 mm), 200 (0.074 mm), 325 (0.045 mm) and 400 (0.0385 mm), generating 7 different size fractions. The sieving products were dried in a furnace at 60 °C, and then subjected to further compositional and chemical analyses.



Figure 15. Comminution process (a) BA sample pulverized in an electric mill, b) FA non-mechanical comminution.

2.2.1.2 Wet magnetic separation:

Magnetic separation tests were performed using a neodymium bar magnet. A certain amount of the samples was mixed with tap water in a polypropylene beaker. The slurry was agitated using an overhead stirrer to suspend the particles. The bar magnet was placed on the outside wall of the beaker, and under the function of magnetic force, magnetic particles were attached to the wall. After that, the slurry containing the material without magnetic susceptibility was poured out from the beaker and recorded as the non-magnetic fraction. The bar magnet was removed from the outside wall, and the particles on the wall were collected as the magnetic fraction.

The performance of the test was evaluated based on enrichment ratio and recovery. The enrichment ratio (ER) represents the metal content in the fractionation products in the metal content in the feed, and it is calculated following the equation (1); where c_i , and f_i represent the assay of the i element in the magnetic stream and in the feed, respectively.

$$ER = c_i / f_i \quad (1)$$

While the recovery (R_i) index represents the proportion of a metal in the feed that is recovered into the fractionation products, and it calculated using the equation (2); where Y represent the mass yield of the magnetic fraction, and c_i , and f_i represent the assay of the i element in the magnetic fraction and in the feed.

$$R_i = Y \times (c_i / f_i) \quad (2)$$

Before determining the elemental composition of the fractioned products to calculate the enrichment ratio and recovery index, it was necessary to remove the organic matter due the metals encapsulated in organic matter cannot be digested and quantified, causing unreliable results. Therefore, the by-products were ashed at 750 °C for an hour using a muffle furnace, according to the standard test method described in BS ISO 1171:2010.

2.2.1.3 Float-Sink test

The float-sink test separates the particulate materials based on the specific gravities' differences in a heavy liquid medium, relying on a function of the density's differences regardless of the particle size. Considering the MSWI, the valuable metals or alloys have a specific gravity between 3.2 – 4 (Holm et al., 2017), while the matrix ash fraction density is about 2.6 kg/dm³ (Šyc et al., 2020). The density separation test was carried out using lithium metatungstate (LMT) as the heavy liquid (2.95 specific gravity) in a

centrifuge tube. A small amount of the sample was added to the heavy liquid and dispersed carefully by slow stirring with a spatula. Then, the tube was placed in a high-speed centrifuge for 10 min at 3000 rpm, where the centrifugal force accelerated the particles' separation according to their specific gravities. The lighter particles floated on the liquid surface were collected, whereas the particles of higher specific gravity sank. Subsequently, a small amount of raw sample was re-added to the heavy liquid. The procedure was repeated until the particles of higher specific gravity were enough to further tests. Float and sink by-products were rinsed several times with hot tap water to remove the residual LMT. Figure 16 illustrate the filtration step from the float-sink test and the overall experiment set up.



Figure 16. Float- Sink test set up.

2.2.2 Mineralogical characterization

2.2.2.1 X-ray Diffraction (XRD)

As part of the mineralogy characterization the X-ray diffraction analysis was conducted using a Bruker D8 Advance Twin diffractometer with Ni-filtered Cu-K α radiation ($\lambda = 0.154$ nm) generated at a voltage of 40 kV and a current of 40 mA. The patterns were recorded over a 2θ range of 7° to 69° with a step size of 0.05° . MDI Jade 6.5 software was used to determine the structural and phase identification from the XRD patterns.

2.2.2.2 X-ray fluorescence spectrometry (XRF)

The samples were analyzed to determine major ($> 1\%$), and minor ($0.1 - 1\%$) element composition using a Niton XL2 handheld X-ray fluorescence (XRF) analyzer equipped with a 10 kW Ag tube anode, located at the Mineral Processing Laboratory of Virginia Tech. To conduct the test, the samples were

comminuted by hand using a mortar and pestle until a powder material was obtained, and then placed as loose powder into an XRF sample cup previously assembled.

2.2.2.3 Scanning electron microscopy with energy dispersive X-ray spectroscopy (SEM/EDX)

Scanning electron microscopy (SEM) coupled with energy-dispersive X-Ray spectroscopy (EDX) analyses were performed to create a comprehensive elemental map and determine the samples' mineralogical characteristics. Before SEM-EDX analysis, samples were sprinkled on a double-sided carbon tape mounted on an SEM aluminum stub coated with a 15 nm thick layer of Pd/Pt using a desktop sputter coater (208 HR, Cressington Scientific Instrument, England, UK). The SEM-EDX analysis was performed using a JSM-IT500HR SEM (JEOL, MA, U.S.) equipped with an Ultim Max EDX detector (Oxford Instruments, Abington, U.K.). The spectrum showed values between 10,000 and 100,000 cps and the accelerating voltage used was between 15 kV and 20 kV. The EDX data was analyzed using AZtech software (Oxford Instruments, Abington, U.K.). Utilizing AZtech, a 'Map' mode was employed over a selected area to identify the distribution of elements of interest using elemental maps of the area. In contrast, 'Point & I.D.' (P&ID) mode was used in AZtech to determine the elemental composition at a specific point or particle across a region of interest.

2.2.3 Chemical characterization

To chemically characterize the by-products of MSWI, it was necessary to perform a series of tests and experiments for which reagents were used. Table 1 lists the chemicals, their grade, concentration, supplier, and the section that describes the test in which it was used.

Table 1. List of chemicals used and related information.

Chemical name	Chemical formula	grade	Concentration	Purchase from	Section
Hydrochloric acid	HCl	Trace metal	37 wt%	Thermo Fisher Scientific, U.S.	2.2.3.1, 2.2.3.3, 2.2.3.4
Nitric acid	HNO ₃	Trace metal	67 wt%	Thermo Fisher Scientific, U.S.	2.2.3.1, 2.2.3.3, 2.2.3.4
Hydrofluoric acid	HF	Trace metal	50 wt%	Thermo Fisher Scientific, U.S.	2.2.3.1, 2.2.3.3, 2.2.3.4
Magnesium chloride	MgCl ₂	Pure	> 99 wt%	Thermo Fisher Scientific, U.S.	2.2.3.3
Acetic acid	CH ₃ COOH	Certified ACS	> 99.7 wt%	Thermo Fisher Scientific, U.S.	2.2.3.3
Hydroxylammonium chloride	NH ₂ OH·HCL	Pure	> 99 wt%	Thermo Fisher Scientific, U.S.	2.2.3.3
Hydrogen peroxide	H ₂ O ₂	Certified ACS	30 wt%	Thermo Fisher Scientific, U.S.	2.2.3.3
Ammonium acetate	CH ₃ COONH ₄	Pure	97 wt%	Thermo Fisher Scientific, U.S.	2.2.3.3, 2.2.3.3

2.2.3.1 Elemental composition - Inductively coupled plasma spectrometry (ICP-MS)

In order to determine the total elements composition and valuable metals content in the MSWI by-products, the inductively coupled plasma spectrometry (ICP-MS) analysis was used. The solid samples were ashed in a furnace at 750 °C for 2 h to remove the unburnt organic material; then, the after-ashed material was digested. 9 mL of hydrochloric acid (37 wt% concentration), 3 mL of nitric acid (67 wt% concentration), and 2 mL of hydrofluoric acid (50 wt%) of trace metal grade were added to 0.100g of the solid sample in a digestion vessel. The digestion procedure is explained in Figure 17. The procedure of microwave-assisted digestion used to determine the BA and FA samples' elemental composition., which was carried out in a closed microwave digestion system (Multiwave GO Plus, Anton Paar, USA). The vessels were placed and subjected to 185 °C for 35 min. Microwave-assisted digestion is an efficient sample dissolution method for obtaining metal concentrations from incinerator ashes because the elevated temperatures increase the acids' oxidative potential, accelerating the sample decomposition. It prevents the volatilization and atmospheric contamination generated by an open system and dissolutions

methods (Jung et al., 2004). Once the process was complete, the samples were diluted 100 times in 5% HNO₃ solution and analyzed for metals concentrations using a Thermo Electron iCAP-RQ inductively coupled plasma mass spectrometer (ICP-MS) per Standard Method 3125-B (APHA, AWWA, and WEF, 1998) at Materials Characterization Lab of Virginia Tech. Samples and calibration standards were prepared in a matrix of 2% nitric acid by volume.

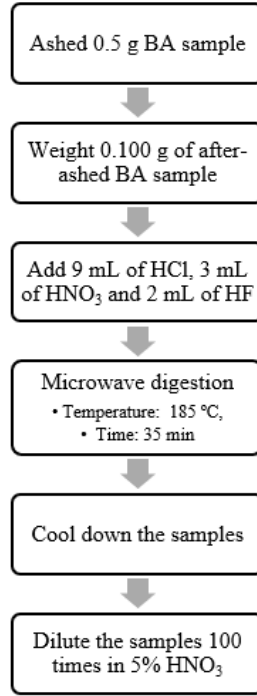


Figure 17. The procedure of microwave-assisted digestion used to determine the BA and FA samples' elemental composition.

2.2.3.2 Loss of ignition (LOI)

The loss on ignition refers to the total amount of material lost, including organic matter content and the CO₂ lost from carbonates. To carry out the procedure, the samples were split and placed in a ceramic crucible with known weight, and the sample dry mass was measured (m_1). Then the crucible was placed into a furnace at 750 °C for 2 h, once the crucible cools down, the sample was weight (m_2). The LOI content was calculated in % following the equation (3):

$$C = \frac{m_1 - m_2}{m_1} * 100 \quad (3)$$

2.2.3.3 Sequential chemical extraction (SCE)

Sequential chemical extraction tests were performed to identify the binding and leaching characteristics of metals from the MSW incineration by-products. The SCE is a widely used protocol, where the solid sample is tested in a stepwise manner utilizing a sequence of acid reagents at specific conditions to identify and quantify the metals leached under each step. Tessier et al. (1979) applied a 5 steps extraction method to quantify 5 fractions. The exchangeable fraction is quantified using magnesium chloride at pH 7.0 with continuous agitation, the carbonate- bound fraction is determine using sodium acetate at 1 M, the fraction bounded to iron and manganese oxides is quantified by continuous agitation of the solid residue from the carbonate-bound fraction in 20 mL of hydroxylammonium chloride in 25% of acetic acid (v/v). The organic-matter bound fraction is determined according to Gupta & Chen, (1975) method, in which the solid residue from the previous step is added to nitric acid and hydrogen peroxide at 30%, and occasionally stir for 2 h at 85 °C. Then, ammonium acetate at 20 % (v/v) was added to the previous mix and agitated for 30 min. The solid residue from the organic matter bound step is the final residue of the sequential extraction and is digested following the procedure explained in the section 2.2.3.1. Likewise, in 1982 Sposito published an article describing a sequential extraction protocol to identify and quantify the metals in 5 different fractions, (1) exchangeable, (2) sorbed, (3) organic, (4) carbonate, and (5) sulfide, using 0.5 M KNO₃, 0.5 M NaOH, 0.05M Na₂ EDTA, and 4 M HNO₃, respectively.

The protocol used in this study, presented in Figure 18 classified the major and trace elements into five different occurrence modes. At the beginning, 5.0 g of solid was weighted and leached with 70 mL of type I deionized water (DI) with a resistivity value of 18.0 MΩ·cm at room temperature for 1 h to determine the water-soluble fraction of metals (WL). The solid residue from the previous step was reacted with 1 M MgCl₂ and 0.11 M CH₃COOH at room temperature to extract the ion-exchange (IE) and acid soluble (AS) fractions, respectively. The fourth step used the solid residue obtained from the AS extraction step and added into 0.5 M NH₂OH·HCl to extract the reducible species (Re). The oxidable fraction (Ox) was quantified adding to the resultant solid fraction from the reducible step, 8.8 M H₂O₂ for 1h at room temperature, then at 85 °C for 1h. Once the time was over, a 1 M CH₃COONH₄ was added and stir for 16h at room temperature. The residual solid of the fifth step was weighted and digested by microwave digestion using HCl, HNO₃ and HF. The solution generated from the digestion process was collected for ICP-MS analysis to measure elemental concentration.

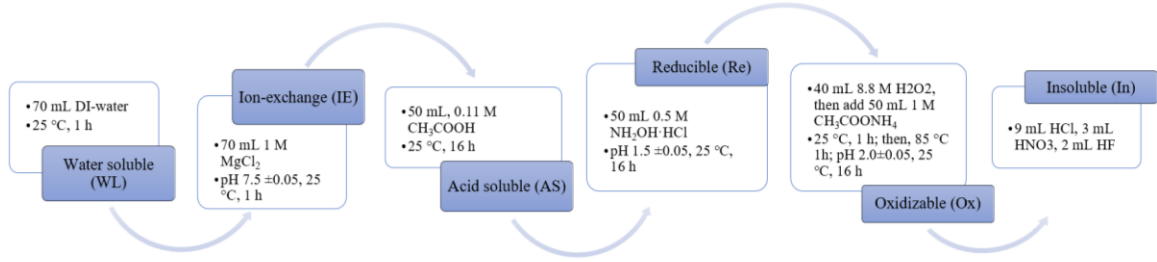


Figure 18. Sequential chemical extraction protocol used for this study.

After each step, the slurry was subjected to solid/liquid separation. The leachate was collected for elemental composition analysis using ICP-MS, while the solid was rinsed using deionized water and dried at 60 °C for 12 h before initiating the next step. The total amount of valuable elements in the feed (E_f) material was back-calculated using the expression (4):

$$E_f = \left((C_{i,WL} \times V_{WL}) + (C_{i,IE} \times V_{IE}) + (C_{i,AS} \times V_{AS}) + (C_{i,Re} \times V_{Re}) + (C_{i,Ox} \times V_{Ox}) \right) + \left(\frac{C_{i,In} \times m_{In}}{m_m} \right) \quad (4)$$

where $C_{i,WL}$, $C_{i,IE}$, $C_{i,AS}$, $C_{i,Re}$, and $C_{i,Ox}$ (ppm, representing mg/L) represents the i element concentration in the leachate solution in the WL, IE, AS, Re, and Ox step, respectively, while V_{WL} , V_{IE} , V_{AS} , V_{Re} , and V_{Ox} (L) refers to the solution volume in the WL, IE, AS, Re, and Ox step, respectively; $C_{i,In}$ (ppm, representing mg/Kg) represents the i element concentration in the insoluble solid residue; m_{In} (kg) the weight of the insoluble solid residual, and m_m (kg) weight of the total solid sample used for the test. The valuable elements' concentration results from equation (4) were compared to those obtained from the elemental composition test measured with ICP-MS to reduce the statistical error propagation and confirm the results' reliability.

On the other hand, the valuable elements distribution in a specific occurrence mode (MO_f) was calculated following the equation (5), where the concentration of valuable element extracted in determined step ($C_{i,j}$, ppm) were multiply by the solution volume in the corresponding step, divided by the back-calculated element concentration in the feed material (E_f).

$$MO_f = \frac{C_{i,j} \times V_j}{E_f} \quad (5)$$

2.2.3.4 Acid leaching test

Acid leaching is a widely used metallurgical process for the dissolution of metals employing acid dissolution that can subsequently be treated through hydrometallurgical approaches to concentrate and

purify the dissolved metals. To evaluate the leachability of the valuable metals like Ni, Co, Ti, Fe, V, and Sn from the BA and FA, a series of acid leaching tests were performed in this study. The tests were performed in a three-neck round bottom flask made of borosilicate glass; the flask was immersed in a temperature-controllable water bath and placed on a multi-position magnetic stirrer with a heating function, and a reflux condenser was connected to the flask to avoid water loss due to evaporation. The experimental set up used for the acid leaching tests is shown in Figure 19.



Figure 19. Experimental set up used for the acid leaching tests.

The leaching conditions evaluated were acid types, acid concentrations and leaching temperatures. For each test, 5.0 g of solid sample was mixed with 100 mL of an acid solution at a specific concentration for 2 h. Representative samples were collected from the slurry at different reaction times (5 min, 15 min, 30 min, 90 min, 120 min) to evaluate the leaching kinetics. The liquid fractions collected were centrifuged at 4000 rpm for 3 min, and directly subjected to elemental analysis, while the solid fractions were dried at 60 °C for 12 h and digested using HCl, HNO₃ and HF to determine its elemental composition. The results were used to calculate leaching recoveries (R_i) of the valuable elements, according to the equation described in Zhang & Honaker (2020).

$$R_i = 100\% \times \frac{C_i \times V}{(E_f \times 0.01)} \quad (6)$$

where C_i (ppm) is the valuable elements concentration in the representative leachate sample taken during the process, V represents the volume of the feed solution (100 mL), and E_f (ppm) is the back-calculated total valuable elements concentration in the feed material, calculated using the equation (4).

2.2.4 *Statistical analysis*

The paired t-test was the statistical procedure used to develop a statistical analysis to determine the statically level of difference or associations between the elemental content among the pre-treated samples. Comparisons were made within the samples among six individual groups, labeled as MF1-5 and NF1-5, for the magnetic and non-magnetic fractions of the five sizes, respectively. 2.95FF1-5, and 2.95SF1-5, referring to the float and sink samples, from the density test performed to the five sizes at 2.95 SG, respectively; and 2.6FF1-5, and 2.6SF1-5, which stand for the float and sink by-products from density test conducted at 2.6 SG.

Chapter 3 Characterization results

3.1 Elemental composition

Elemental contents analyses reveal that the major elements in the BA sample are Si, Ca, Fe and Na, with 182.51 g/kg, 40.65 g/kg, 60.45 g/kg and 22.38 g/kg, respectively. Collectively, they account for 88% (w/w) of the total sample element content, which is coherent with the elemental compositions determined from MSWI bottom ash samples in previous studies (Muchova, 2010; Piantone et al., 2004; Blanc et al., 2018). Additionally, the XRD pattern of the MSWI-BA (Figure 20) shows that the predominant mineral phases identified were silica (SiO_2), calcite (CaCO_3) and anhydrite (CaSO_4). Some other phases identified as minor phases are gismondine ($\text{CaAl}_2\text{Si}_2\text{O}_8 \cdot 4\text{H}_2\text{O}$) and ettringite ($\text{Ca}_6\text{Al}_2(\text{SO}_4)_3(\text{OH})_{12} \cdot 26\text{H}_2\text{O}$). The sharp peaks of silicate phases identified by XRD (quartz and gismondine) are consistent with the elemental contents results from the BA, shown in Table 2, which indicates that Si is the most abundant element in the sample. Although the Fe content is relatively high based on the elemental content results, no Fe-bearing pattern was identified from the XRD spectrum likely due to the existence of iron in poorly crystallized, amorphous structures. According to Piantone et al., (2004) the dome shape in the XRD pattern between 10° and 15° (2θ) is due to the presence of a vitreous fraction in the sample.

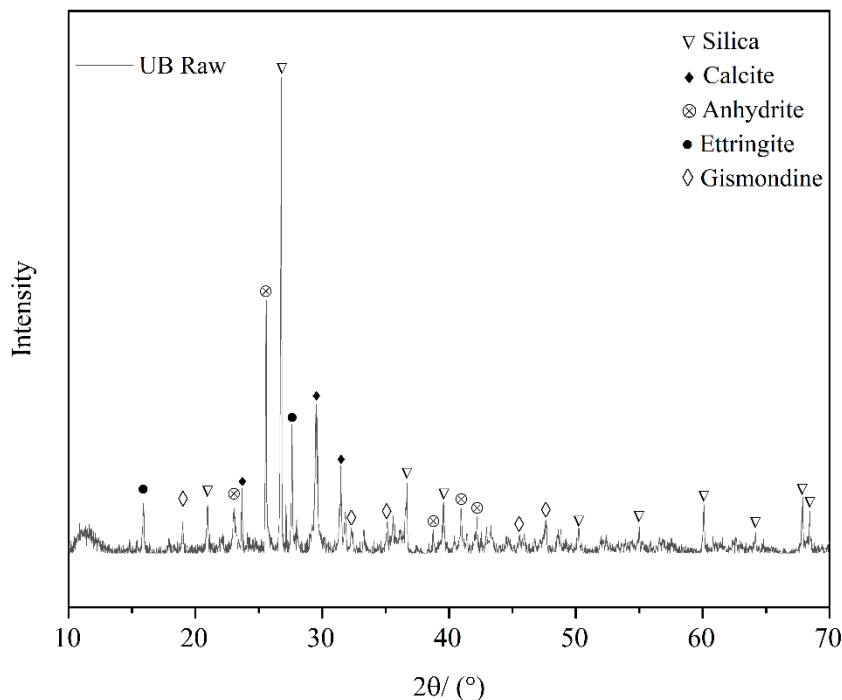


Figure 20. XRD pattern of the bottom ash sample.

The elemental composition analyses (Table 2) showed that the material also contained minor elements, such as Co, Ni, V, Mn, and Sn. The total rare earth elements (TREEs) content in the sample, calculated as the sum of the 15 lanthanides plus yttrium, was 28.56 mg/kg. Sc and Ce were the primarily constituents of the TREE content in the sample (15.89 mg/kg and 4.60 mg/kg, respectively).

As for the elemental composition of the MSWI-FA, the analyses reveal that 71% (w/w) of the sample is comprised by Si, Ca, Na and Zn, with 56.17 g/kg, 13.25 g/kg, 27.06 g/kg, and 14.39 g/kg, respectively. Compared to the BA, the major elements have an overall lower concentration in the FA; however, the Zn content in the FA is about 4 times higher, due to the formation of $ZnCl_2$ formed during the combustion, which is easily volatilize and absorb on the fly ash (Pan et al., 2013). Ni and V content in the FA, as trace elements were nearly an order of magnitude lower than the those in the BA sample, while Sn and Ag concentration are slightly higher than the BA results, with 630.3 mg/kg and 16.0 mg/kg, respectively. Due to the refractory materials resistance to decomposition by heat, they are collected and concentrated in the BA, which increases the Fe content in the BA stream. The Sc concentration results were not included because the data was not reliable, causing statistical differences in the TREE results between the duplicates. Pan et al. (2013); Wan et al. (2006); Piantone et al. (2003) studies found similar FA elemental compositions as the results obtained in this study and presented and compared to the MSWI-BA composition in the Table 2.

Table 2. Elemental contents of major elements, minor elements, and main rare earth elements in the MSWI BA and FA samples.

Major elements (g/kg)									
	Si	Ca	Fe	Na	Mg	Ti	P	Zn	Cu
BA	182.51	40.66	60.45	22.38	7.52	9.22	5.05	3.91	2.15
FA	56.17	13.25	4.15	27.06	4.38	3.14	2.42	14.39	0.57

Minor elements (mg/kg)								
	Co	Ni	V	Mn	Sn	Sr	Ag	Mo
BA	42.67	122.06	129.29	871.01	178.50	252.20	7.91	15.31
FA	10.91	36.91	73.14	284.80	630.30	153.66	16.00	13.93

Rare earth elements (mg/kg)									
	TREE	Sc	Y	La	Ce	Nd	Sm	Eu	Gd
BA	28.56	15.89	0.46	3.71	4.60	2.14	0.36	0.20	0.31
FA	12.84	-	0.50	3.81	4.68	2.15	0.34	0.13	0.31

The XRD results of the ground FA sample show the appearance of large amounts of highly soluble inorganic salts, like halite (NaCl) and sylvite (KCl). Other mineral phases identified in the XRD spectrum, shown in Figure 21, were calcite (CaCO_3), anhydrite (CaSO_4), and gypsum ($\text{CaSO}_4 \cdot 2\text{H}_2\text{O}$), portlandite ($\text{Ca}(\text{OH})_2$) and Silica (SiO_2). The dome-shape at the beginning of the spectrum reveals a prominent presence of amorphous or poorly crystalized phases. These crystalline structures have been observed in MSWI-FA samples in previous studies (Wan et al., 2006; Piantone et al., 2003), and are consistent with the elemental composition results obtained in the current study. It is important to mention that a carbonates component decompose at a temperature close to 700°C , suggesting that after the incineration process, CaO is added to the fly ashes to control pH and promote the PTE dissolution, causing the formation and presence of carbonates components in the final stream of the FA.

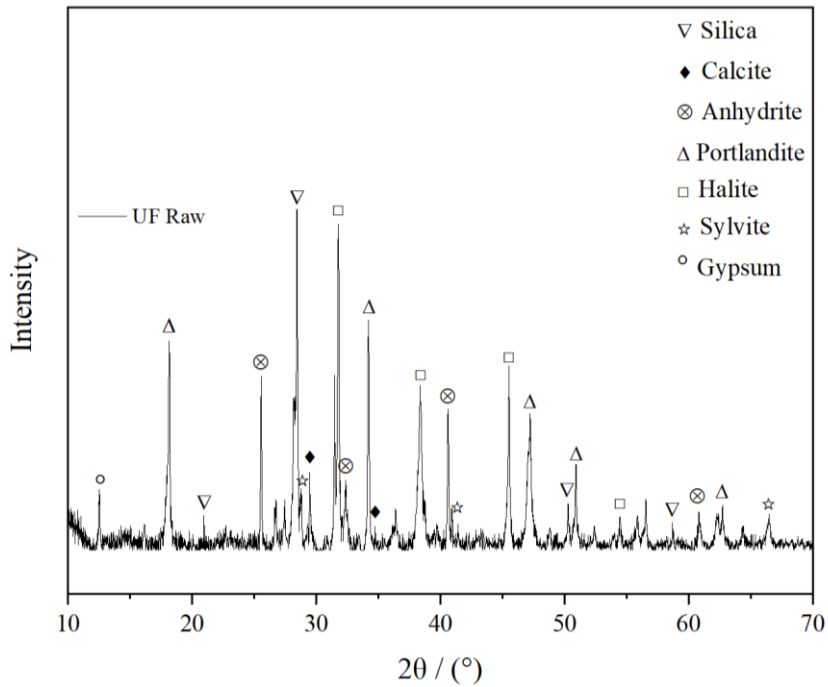


Figure 21. XRD pattern of the fly ash sample.

Some of the elements detected in the samples, such as Zn, Mn, V, Co, Ni, Ti, Sn, and REE, have been defined as critical elements by the US Department of the Interior based on their importance for the development and the high risk associated with its supply chain (Department of the Interior, 2022). However, studies have been carried out to determine the concentration and leaching characteristics of heavy metals, precious elements, and other elements due to environmental concerns about MSW, but little has been studied on the concentration, distribution, and benefit of valuable elements. (Šyc et al., 2018; Muchova et al., 2008; Morf et al., 2013; Funari et al., 2015; Park et al., 2021; Jung and Osako 2009 and Morf et al. 2013). The distribution of critical and valuable elements between the grain size fractions and the by-

products of physical fractionation has not been thoroughly investigated. Additionally, the valuable elements content shown in Table 2 was compared with the natural occurrence of the elements in the earth crust. The ore grade of Ti is 0.75% (Force et al., 1977), while for Cu is between 0.5-3% (British Geological Survey, 2007) and for Mn is 0.1% (Emsley et al., 2001). The grade of these elements in the BA by-product are 6.02%, 1.41%, and 0.56%, respectively. Likewise, from the FA sample the Zn and Sn content represent 20.38% and 0.89%, while the natural occurrence of these elements has a grade of 5-15% for Zn (Wang, 2016) and 0.5% for Sn (Elliott et al., 1997). As for the Fe, although natural occurrences of hematite and magnetite can contain values greater than 60% of iron, some economically exploitable deposits have a grade in ranges between 11% to 33%, which can be compared with the 39.5% of Fe contained in the BA sample. Hence, a new perspective on MSW as a secondary source of valuable elements has sparked interest and research.

3.2 Transfer coefficients and elements distribution

To evaluate the distribution of the critical and valuable elements among the BA and FA, the transfer ratios (K) of each element were calculated. The methodology was adopted similarly by Zhang et al. (2008) to assess the distribution of heavy metals among the different types of residues, and by Funari et al. (2015) to determine raw materials distribution between solid residues from an Italian incinerator. For this study, the transfer ratios and enrichment ratios were calculated for the following critical and valuable elements: manganese (Mn), cobalt (Co), nickel (Ni), copper (Cu), zinc (Zn), titanium (Ti), iron (Fe), and tin (Sn). The transfer ratios of the elements previously mentioned in the BA (K_{BA}) and the FA (K_{FA}) samples were calculated by the following equations:

$$K_{FA} = \frac{FA(\%) \times C_{iFA}}{BA(\%) \times C_{iBA} + FA(\%) \times C_{iFA}} \quad (7)$$

$$K_{BA} = \frac{BA(\%) \times C_{iBA}}{BA(\%) \times C_{iBA} + FA(\%) \times C_{iFA}} \quad (8)$$

Where FA (%) and BA (%) represent the mass flow in percent of the fly ash and bottom ash after the incineration process, respectively. C_{iBA} and C_{iFA} are the i -element concentration in mg/kg in the corresponding by-product. To use the equations, it was necessary to make assumptions based on the literature and information provided by the WtE facility operator. According with a database obtained, there are 74 WtE facilities across the U.S. with a total average processing capacity of 1272.43 ton/day, and based on several studies (Kaza & Bhada-Tata, 2018; Wang et al., 2021; Wiles, 1996; Tang et al., 2015) BA represent 30 % by weight of the total incinerated MSW, while the FA accounts 5% by weight of the MSW processed, which is consistent with the BA to FA ratio presented by Dou et al. (2017) as 6:1. In this manner,

BA and FA total production were determined and their percentages from the total ash production, the results reveals that BA represents 85.71 %, while FA is 14.29 %. Variations between $\pm 5\%$ were conducted to determine how susceptible the results were regarding the element distribution among the by-products. However, there were no significant variations in the elemental distribution.

Figure 22 and Figure 23 illustrate the transfer coefficients of selected elements to determine their distribution among the BA and FA samples and identify the most useful residue for the recovery of the valuable elements. The analysis reveals that volatile elements, like Zn and Sn are scattered in the MSWI by-products, whereas Co, Mn, Ti, Fe, and basic metals, such as Cu, and Ni are primarily found in the BA stream. This type of elemental distribution has been observed before by Astrup et al. (2011), Funari et al. (2015), and Morf et al. (2013). Due to the lack of reliable results for the Sc concentration in the FA stream, its distribution cannot be determined; however, based on the literature, a higher concentration of Sc has been found in the BA stream. (Funari et al., 2015).

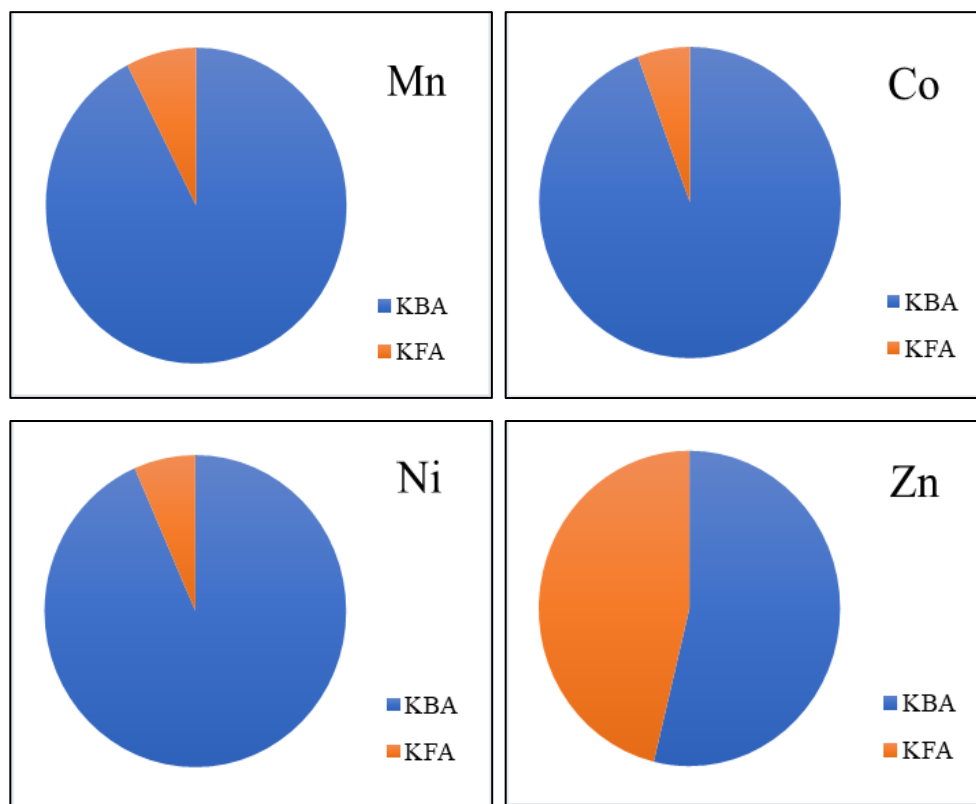


Figure 22. Mn, Co, Ni, and Zn distribution between BA and FA samples calculated following the expressions (7) and (8).

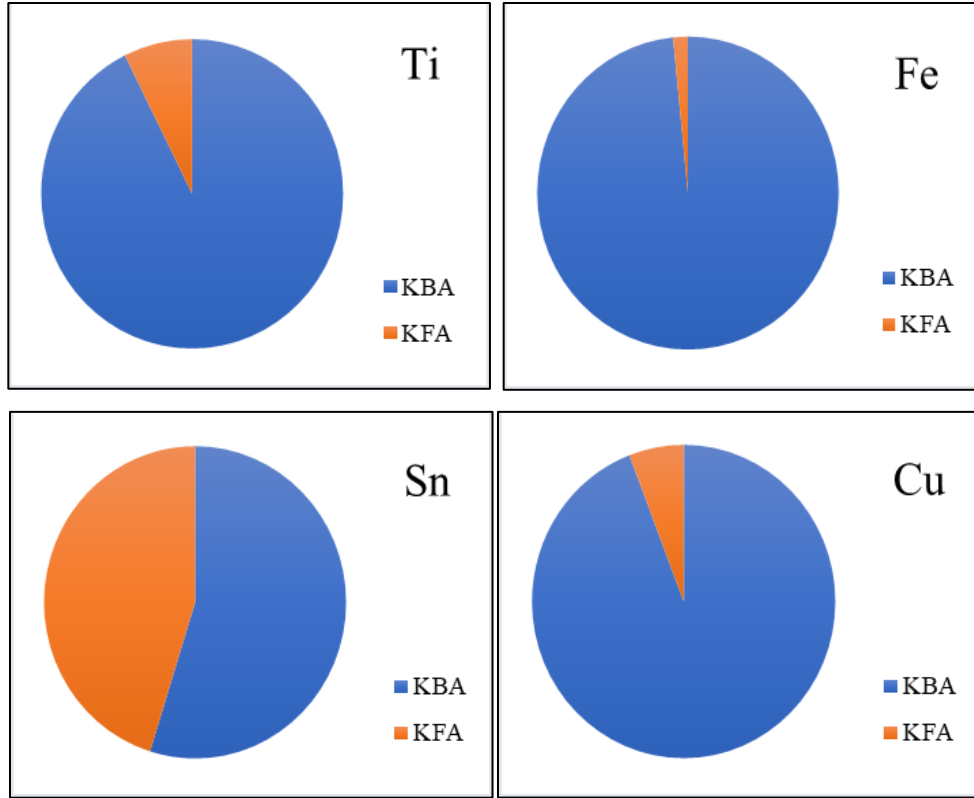


Figure 23. Ti, Fe, Sn, and Cu distribution between BA and FA samples calculated following the expressions (7) and (8).

Based on the transfer coefficients and the mass balance of the BA and FA production from the MSW incineration process, it can be determined that the most useful residue for the recovery of valuable elements is BA. Therefore, the results presented hereinafter will be focused on BA.

3.3 Leachability of the valuable metals

A series of acid leaching tests were conducted under different experimental conditions to determine the BA valuable metals' recovery and leaching kinetics. The acids used in this study were HNO_3 and HCl , and each acid was tested at 0.5 M, 1 M, 1.5 M, and 2 M, and the temperature was set up at 75 °C. Dou et al. (2017) describes that acidic conditions can greatly enhanced the valuable elements mobilization and lead to higher recovery values, which is consistent with most of the results obtained as shown in Figure 24 (a). It summarizes the effect of the HCl concentration on the valuable elements' recovery from the BA sample. The leaching recoveries of Cu and Fe from the BA samples were 23% and 28%, respectively, when using 0.5M HCl , while their recovery was 89% and 92% when increasing the HCl concentration to 1 M, respectively. Sc, Fe, Cu, Zn, and Mn could be released by 1 M HCl , and further elevations in acid

concentration had negligible recoveries' improvements. In contrast, the leaching recoveries of Co and Ni when 0.5 M HCl was used as lixiviant were 75% and 52%, respectively; nevertheless, by increasing the acid concentration up to 2 M, the highest recovery values were achieved. Whereas Figure 24 (b) summarized the effect of the HNO₃ concentration on the leaching characteristics of the valuable elements in the BA samples, which shows a similar pattern as that of the HCl concentration, where the leaching recoveries of the valuable metals increased when increasing the acid concentration. For example, the leaching recovery of Ti, Cu and Sn was increased significantly when increasing HNO₃ concentration from 0.5 M to 1 M; their recovery increase by 20, 35, and 32 absolute percentage, respectively. Some elements, such as Sc, V, Fe, Mn, and Zn, were extracted when using HNO₃ at 0.5 M, and further recovery increment was minimal when increasing the lixiviant concentration. As for Co and Ni, similar leaching behavior was observed when using HNO₃, where the recovery reached 80% and 83%, respectively, at the highest acid concentration, at 2M.

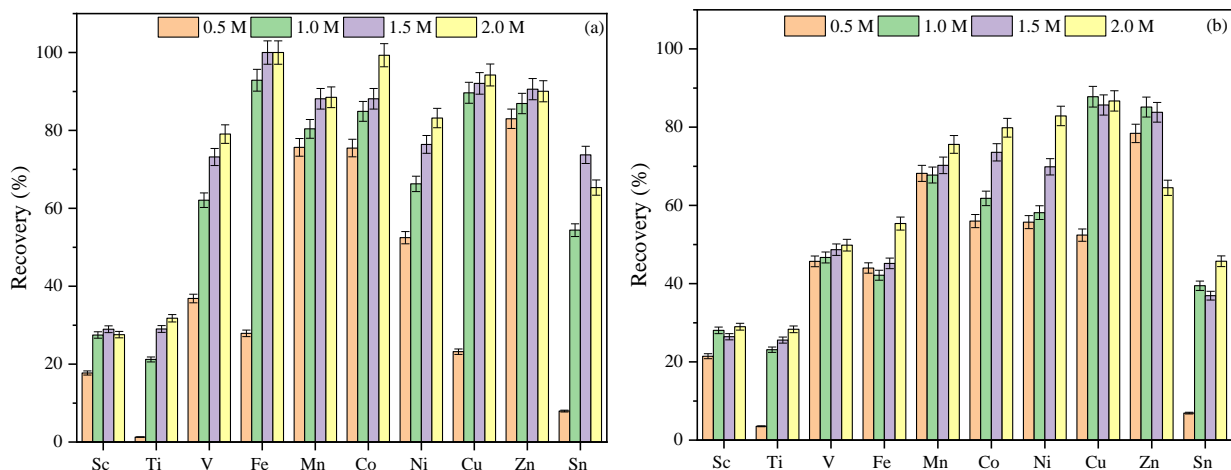


Figure 24. Effect of the acid concentration on the valuable elements' recovery from the BA sample with (a) HCl and (b) HNO₃.

Additionally, the leaching kinetics of the valuable elements from the BA sample were evaluated. The tests were carried out under similar conditions for a period of 120 min at 75 °C to compare the valuable elements leaching behavior at 1 M, 1.5 M, and 2 M HCl. Figure 25 (a) reveals that Zn, Co, Mn, Cu, and Fe present high leachability characteristics because recoveries closer or greater than 80% were achieved within the first 30 min using HCl at 1 M. While Sc and Ti recoveries do not exceed 40% even using HCl at 2 M and after 120 minutes of reaction (Figure 25 (c)). In contrast, medium leachability characteristics were observed for Sn, V, and Ni, with recoveries of 75%, 76%, and 78%, respectively, under 1.5 M HCl, which are considerably higher than the recoveries obtained using 1 M HCl, of 59%, 68%, and 70%, respectively.

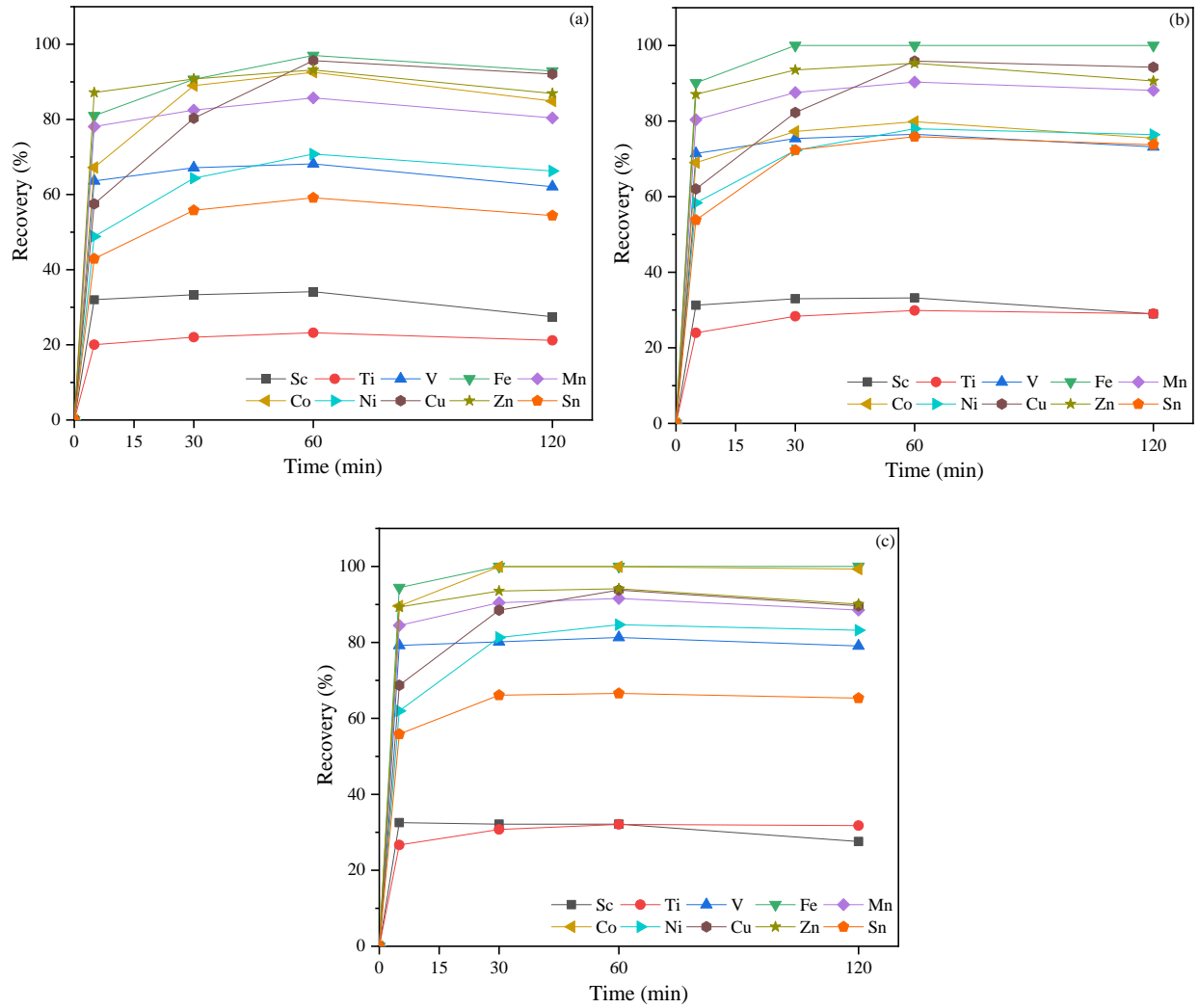


Figure 25. Leaching kinetics of the valuable elements from BA sample using (a) 1 M, (b) 1.5 M, and (c) 2 M HCl.

The effect of temperature on the leaching recovery of valuable metals was evaluated. The tests were performed by keeping all the leaching variables except temperature constant and using 2 M HCl as the lixiviant. The temperatures evaluated were 25 °C, 50 °C, 75 °C, and 90 °C, which were achieved by immersing the flask in a temperature-controllable water bath. As presented in Figure 26, higher leaching temperature had negligible effect on the leaching recoveries of Sc, Ti, V, and Fe. Whereas Zn, Sn, and Cu achieved the highest recovery under 75 °C. However, as for Co, Ni, and Mn, a significant improvement in their recoveries was noticed when increasing the temperature from 25 °C to 90 °C. For example, around 51% of Ni was extracted when the leaching test was carried out at 25 °C, while at 90 °C, the Ni recovery was increased up to 83%. Similar results were observed by Prameswara et al. (2022), where Ni recovery increased by 50% when increasing the leaching temperature from 30 °C to 90 °C. According to Fu et al.

(2018), this increment in the leachability results occurred because higher temperatures can encourage the oxidation and sulfuration of the material, causing a reduction in the pH, which will promote the realized and leachability of elements such as Ni and Co. This phenomenon indicates that the solubility of these valuable metals could be improved under higher leaching temperatures.

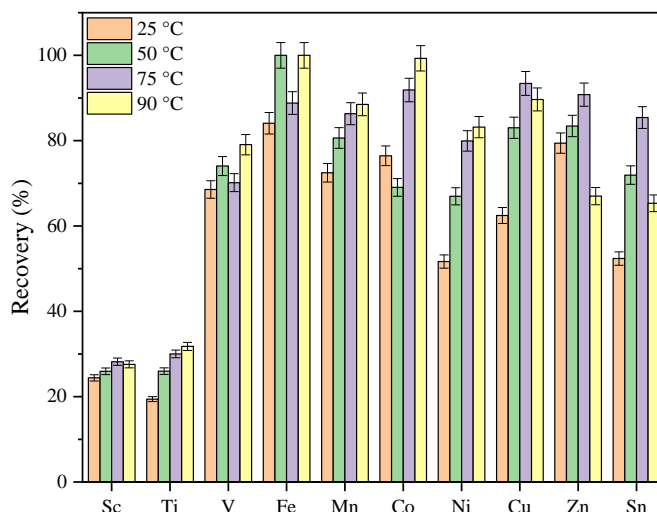


Figure 26. Effect of the temperature on the leaching recovery of the valuable metals from BA sample using HCl at 2 M.

In conclusion, most valuable metals, such as Fe, Mn, Co, Cu, and Zn, can be extracted from the BA sample using 1M HCl as a lixiviant, with recovery values greater than 80%. According to Figure 25, the leaching reaction is a fast process, and equilibrium can be achieved within the first 30 minutes. Likewise, the release of elements, such as Co, Ni, and Mn, is sensitive to the reaction temperature. A higher recovery value can be obtained when relatively higher leaching temperatures are used; nevertheless, the economic feasibility should also be considered.

3.4 Modes of occurrence and association of the valuable elements

As described in Section 2.2.3.3, the sequential chemical extraction (SCE) test was performed to identify the binding and leaching characteristics of the valuable metals from the BA sample, where the metals are extracted by reacting with a sequence of acid reagents at specific conditions. The valuable elements extracted were quantified and classified into six different occurrence modes, water-soluble (WL), ion-exchange (IE), acid-soluble (AS), reducible (Re), oxidable (Ox), and insoluble (In). Figure 27 shows the distribution of Fe, Ti, Zn, Cu, and selected trace elements in the different modes of occurrence in the BA sample. Around 83% of Ti and 82% of Sc occurred in an insoluble form, indicating that these elements will not dissolve under strong acidic and oxidizing conditions (e.g., 40-mL H_2O_2 plus 50-mL

CH₃COONH₄). These results are consistent with the low leaching recovery obtained for these elements under strong acid conditions and high temperatures (Figure 25 (c)). A minimal amount of the valuable elements was present as water soluble, ion-exchangeable, or acid soluble forms. As for the Zn, Co, and Mn, they present the higher reducible form content, which means that 49% of the Zn, 45% of the Co, and 30 % of the Mn are easier-to leach compared to the Ti and Sc that is mostly insoluble. The oxidizable distribution among the valuable elements is higher in Cu and Sn, with 57% and 46%, respectively, indicating that they can be extracted under oxidizing leaching conditions. The occurrence modes distribution observed in Cu, Zn, Ti, and Ni have been previously observed by Bruder-Hubscher et al. (2002) and Alam et al. (2019). From the elements' leachability characteristics is possible to infer that a concentration and liberation process previous to the leaching step can facilitate and improve the recovery of the valuable elements.

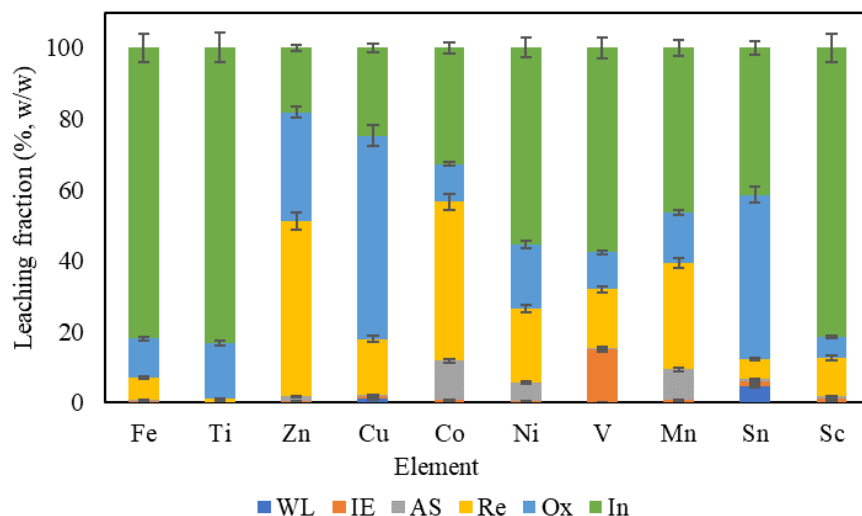


Figure 27. Distribution of the occurrence modes of the valuable elements from the BA sample.

3.5 Mineralogical characterization

The data generated from the SEM/EDX analysis carried out in the BA sample were collected based on the valuable elements selected for this study and previously mentioned in section 3.2. It is worth noting that the samples were sprinkled over a double-sided carbon tape and coated with a 15 nm thick layer of Pd/Pt. This suggests that measurements of C and Pd/Pt are likely due to the sample preparation. Additionally, based on the elemental composition characterization study done in the present study and literature review, Zr has not been associated with the MSWI-BA matrix. However, Zr content was identified when excluding the Pt from the EDX readings. The Zr content identified in the EDX analysis can result from the overlap peak identification of the EDX spectrum. The energy peak of the Zr energy peak is at

2.042 keV, while the Pt energy peak is 2.0488 keV (Liao, 2006), the element used to coat the samples, as described in section 2.2.2.3.

Based on the elemental composition and EDX spectra of particles 1 and 2 shown in Figure 28, it can be inferred that Fe can be found in the BA sample as iron oxides. These results are consistent with the section 3.1 findings, where it was determined that the MSWI ash was enriched in iron constituents. The different oxidation states (mainly 2+ and 3+) are suggested by the different elemental distribution and the Fe-O ratio shown in the EDX spectra in Figure 28. This premise is consistent with Rissler et al. (2020) study in which is concluded that the different oxidation state may be present due to the oxygen's variable presence and access in the fuel bed in the combustion chamber. However, the different elemental distribution can also be caused by the presence and increment of other elements in the particle, such as Ca and Si and their binding with O atoms. Additionally, as previously mentioned in the Section 3.1 regarding the elemental composition of the by-products, Zn tends to form $ZnCl_2$ formed during the combustion process as shown in the EDX spectra of particle 3 in Figure 29.

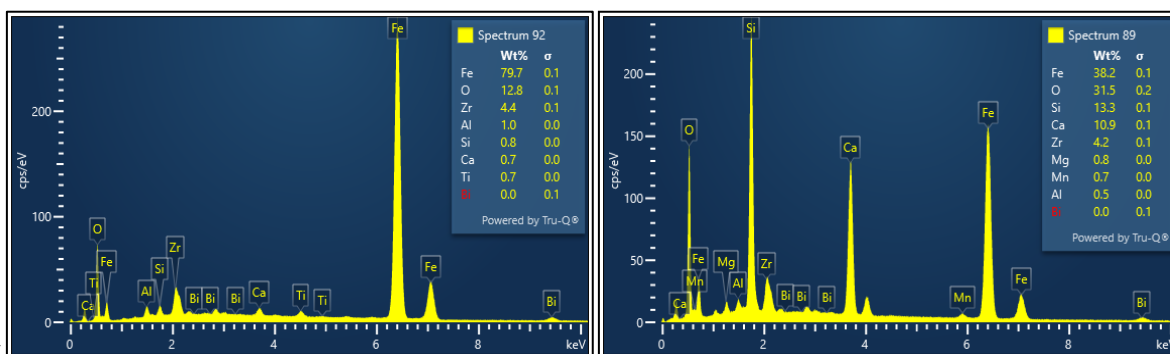


Figure 28. EDX spectra of Particle 1 (left) and particle 2 (right).

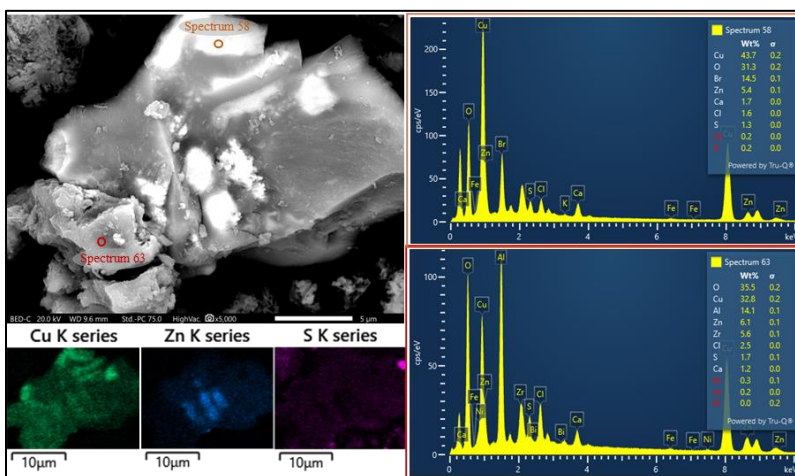


Figure 29. BSE image (top left), elemental maps (bottom left), and EDX spectra (right) of particle 3.

Other Fe- rich constituents were found as metallic inclusions, spinel in a series of Al-Ti substituted varieties, and secondary products, like the Fe-Si-rich gel phase. Figure 30 shows iron-phosphorus particle depleted of oxygen embedding in a calcium-silicate matrix. By merging the information provided by the diagram phase of the Iron-Phosphorus system, the P&ID analysis results, and the elemental content from the EDX spectra of the particle, which reveals a ~40 wt.% of P content, it is possible to conclude that the particle is likely a FeP metallic inclusion, formed in the combustion chamber at high temperatures (Okamoto, 1990).

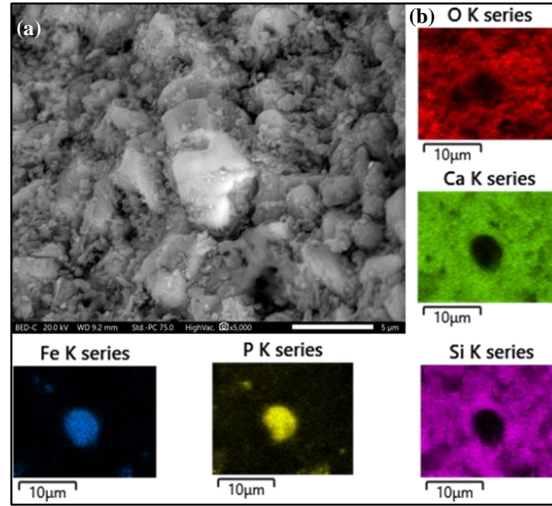


Figure 30. (a) BSE image and (b) elemental maps of a Fe-P metallic inclusion from the BA raw sample.

Previous studies (Wei et al., 2011; Mantovani et al., 2021) have identified spinel group minerals in the MSWI-BA. The general composition of the spinel groups is AB_2O_4 , where A represents metal with a valence plus two, commonly Fe, Mg, Zn, Ni or Mn, and B refers to metals with a valence of plus three, often Al, Fe, or Cr. In this study, aluminum-spinel, and magnetite-spinel series were found. Through the “Map” and “P&ID mode it was possible to demonstrate the existence of the Fe_3O_4 - $FeAl_2O_4$ system, which is the transition from magnetite (Fe_3O_4) to hercynite ($FeAl_2O_4$), through the octahedral substitution of Fe^{3+} by Al^{3+} and Si^{4+} (Figure 31(a, b))

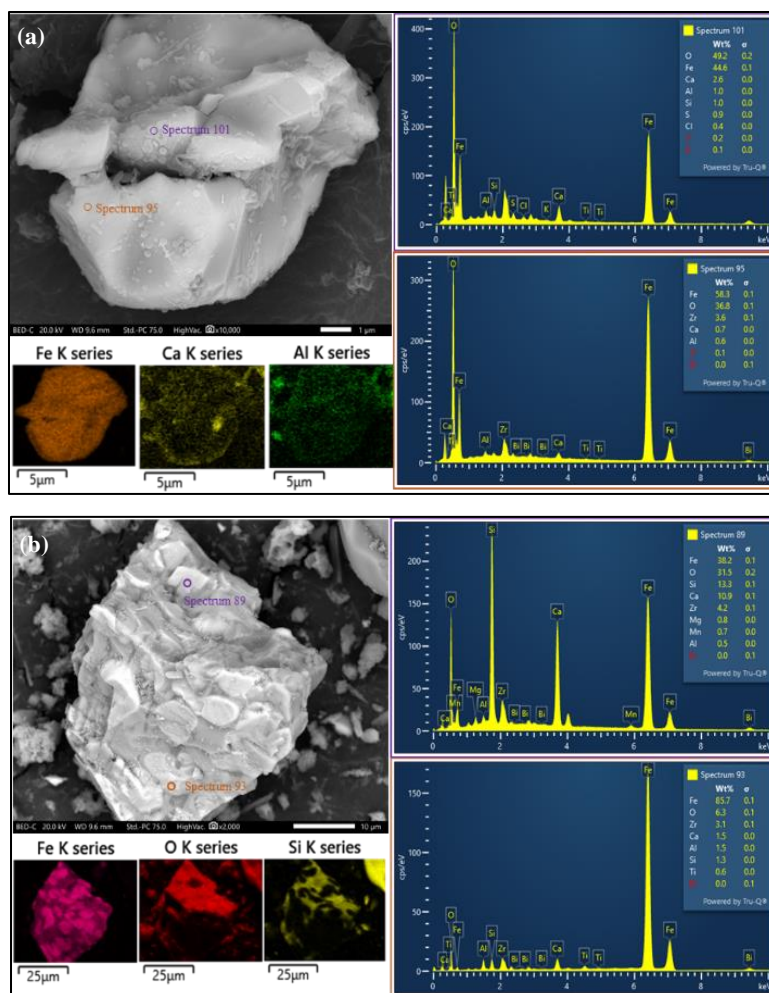


Figure 31. BSE image (top left), elemental maps (bottom left), and EDX spectra (right) of (a) octahedral substitution of Fe^{3+} by Si^{4+} and Al^{3+} , and (b) tetrahedral substitution of Fe^{2+} by Mg^{2+} , Ca^{2+} , and Mn^{2+} from the MSWI -BA sample.

Overall, the main findings from this chapter were that the BA was identified as the most valuable MSWI by-product due to its enrichment in critical and valuable elements, based on the results obtained through the transfer coefficients methodology. Furthermore, the leachability and reaction kinetics of the valuable elements from the BA sample were assessed and classified according to the recovery achieved and the acid conditions used. The SEM-EDX analysis was carried out in order to determine the valuable element association and chemical binding properties. The main Fe – bearing speciation was identified as iron oxides, spinel-group, in the transition from magnetite to hercynite and metallic inclusions.

Chapter 4 Physical concentration results

According to the results obtained in section 3.2, which concluded that the BA sample is enrichment in valuable elements, a systematic physical concentration was carried out using this sample. The sample with internal sample code, UB, was sorted by hand to remove the clastic rock particles and then classified into five-size fractions. The five size fractions generated were particles with a diameter between mesh sized -50/+100, -100/+170, -170/+200, -200/+325, and -325. A portion of each size subsample was collected for chemical and mineralogical characterization. As showed in Figure 32, the remaining portion of the sample was collected and used as the feed material for wet magnetic separation and density separation. The first density separation process was performed using the heavy liquid medium, LMT, at 2.95 specific gravity, and the procedure technique was done following the description from section 2.2.1.3. Once the float and sink material were collected, rinsed, and dried, the float material collected was used as a feed for a second-density separation stage performed using the LMT at 2.6 specific gravity.

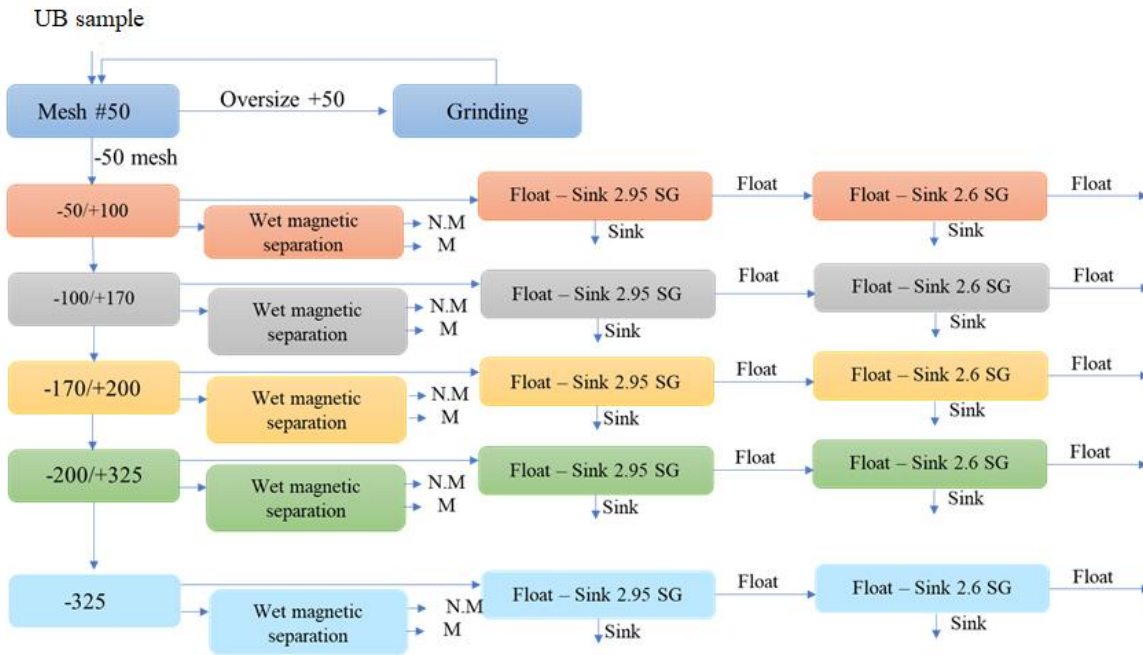


Figure 32. Systematic physical characterization flowsheet of the BA sample.

4.1 Wet Sieving

4.1.1 Size fractionation characteristics

Funari et al. (2015) and Naderizadeh et al. (2016) have reported that the accumulation of metals could be related to particle size. Therefore, size reduction and wet sieving tests were carried out to evaluate the

distribution of the valuable metals and determine which size fractions are dominant in valuable metals. Additionally, obtaining a homogeneous stream in terms of particle size provides narrow-fractionated material to optimize the efficiency of the coming concentration process (Šyc et al., 2018). A wet sieving test was performed in order to reduce stickiness and the obstruction of the mesh with particulate material (Born, J. P., 2018).

As Figure 33 shows, the enrichment ratio of the Zn was close to 1.25 in the particles with a diameter smaller than 45 μm (minus 325 mesh) and less than 1.0 in the middle and coarse size fractions. This indicates that Zn is enriched in the finer fraction of the sample. In contrast, elements such as Fe and Sc tend to decrease their concentration as the BA particle size is reduced. The Fe enrichment ratio was below 1.0 in the fractions of particles with a diameter below 74 μm (minus 200 mesh), while for the Sc, a similar result was observed in particles in the minus 325 mesh fraction. These results suggest that Fe and Sc are enriched in the coarse fraction of the BA sample. Takayuki Shimaoka (2014) found coarse unburned iron pieces from the MSWI feedstock originated from the iron containers and thin sheets. At the same time, Xia et al. (2017) concluded that the primary mineral for Fe is hematite due to the metal oxidation in the combustion process. However, Cu, Mn, Co, Ni, Sn, and V distributions showed an even enrichment in coarse and fine fractions, most likely due to the low concentration of the mentioned elements in the middle-size fraction. Researchers like Yao et al. (2010), Xia et al. (2017), and Chimenos et al. (1999) have found that valuable elements, such as Sn, Cu, and Zn, are concentrated in fine particle size fractions because they trend to form pure solid melts in small particles during the combustion process. As for the Ti distribution and enrichment, it did not vary considerably in the different size fractions. This is shown in Figure 33, where all the enrichment ratios are close to 1 regardless of the particle size.

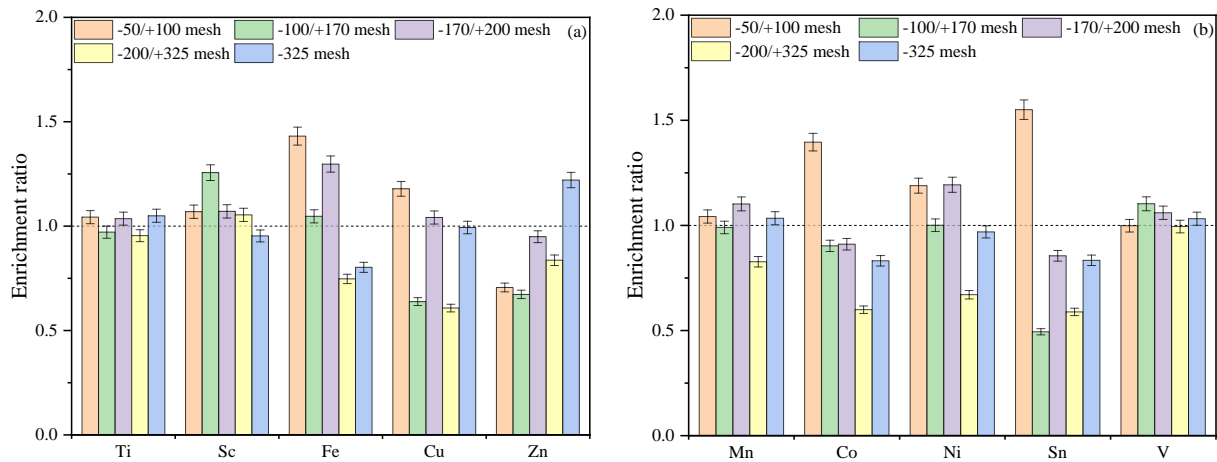


Figure 33. Valuable elements' enrichment ratios per size fraction in the BA sample for (a) Ti, Sc, Fe, Cu, and Zn and (b) Mn, Co, Ni, Sn, and V.

Regarding the mass yield as a function of the size fraction, Figure 34 shows that the particle sizes with a diameter bigger than 150 μm , labeled as the coarse fraction, represents 24% (w/w) of the BA sample. In comparison, the particles with a diameter between 150 μm and 45 μm , considered the middle fraction, accounts for 38% (w/w) of the BA sample. The remaining 38% comprises fine fractions with particles smaller than 45 μm . By merging the enrichment ratios and the mass yield results, it can be concluded that classifying the ash into the coarse, middle, and fine-size fractions could lead to better metal concentration yields during processing for the different size fractions and optimization of the recovery test.

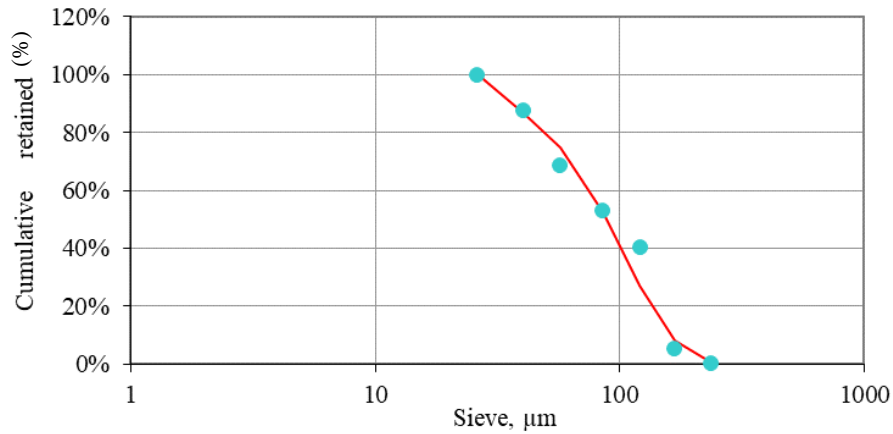


Figure 34. Cumulative particle size distribution pattern of BA sample using Rosin Rammler Regression.

4.2 Magnetic separation

4.2.1 Magnetic separation performance indicators

After determining the valuable and critical mineral distribution in the MSWI-BA sample among the size fraction, magnetic separation was conducted to increase the recovery of ferrous metal and other magnetic elements. According to Yin et al. (2021), the magnetic separation performance and enrichment are a function of the bound of multi-metallic oxides fractions (e.g., Fe-Mn; Fe-Ti), morphology, mineralogy, and elemental distribution per size fraction. Figure 35 (a, b) shows a significant concentration of Fe, Cu, and Co in the magnetic fraction. The overall enrichment ratios of these elements were 1.92, 1.51, and 1.66, respectively. These results indicate that these valuable elements are associated with paramagnetic or ferromagnetic minerals and can be recovered through magnetic separation. According to statistical analysis, Yin et al. (2021) concluded that magnetic separation changes the element distribution, especially for Fe, Co, Ni, Sn, and V.

However, when analyzing by size fraction, particles from the fine fraction may have a higher surface area to volume ratio, which increases the interaction in the magnetic field. Nevertheless, in small particles, the centrifugal force exerted by the agitator is greater than the magnetic force exerted by the magnet. This decreases the concentration of the material with magnetic susceptibility. For example, Co, Ni, Zn, Ti, and V recovery gradually decreased (Figure 36) when the particle size was reduced. These results are consistent with Yin et al. (2021) who concluded that sizes significantly affect the valuable element concentration through wet magnetic separation. Regarding the remaining valuable elements (Fe, Sc, Cu, Mn, and Sn), which showed a size-independence behavior, these may be attributed to higher Fe- containing mineral phases. These mineral phases will likely be stable complexes with strong magnetic properties that neutralize the size effect (Caviglia et al., 2019).

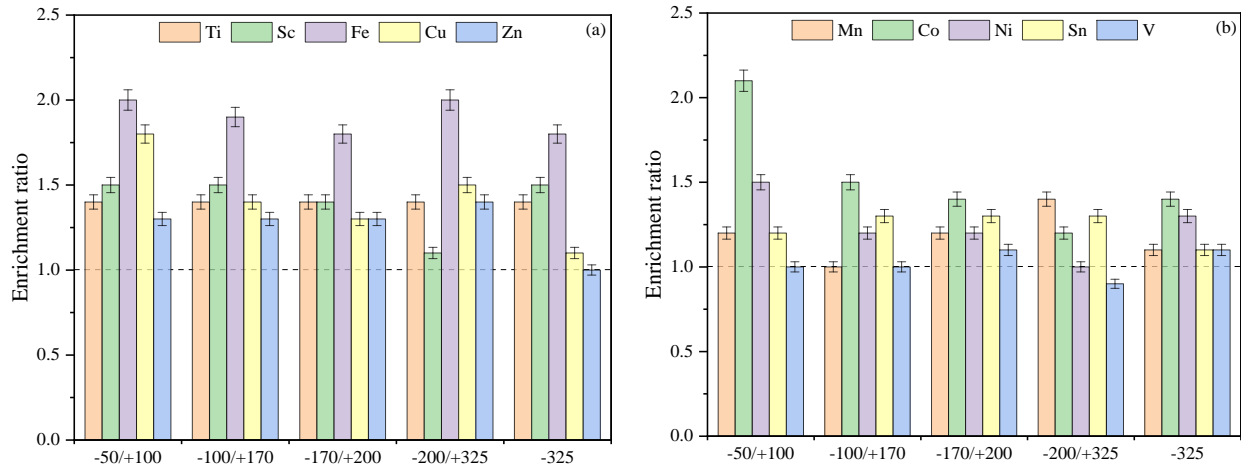


Figure 35. Magnetic separation enrichment ratio for (a) Ti, Sc, Fe, Cu, and Zn and (b) Mn, Co, Ni, Sn, and V

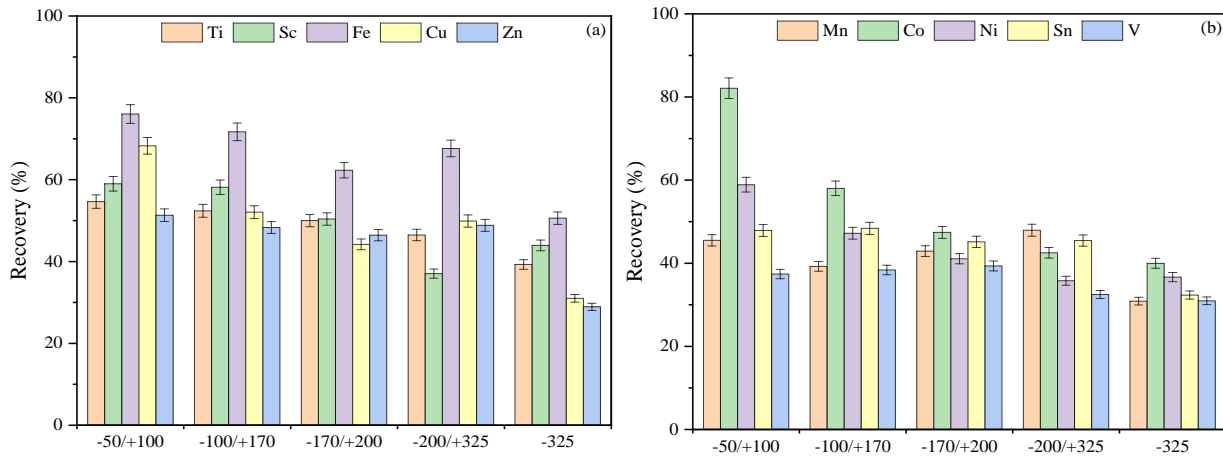


Figure 36. Magnetic separation recovery for (a) Ti, Sc, Fe, Cu, and Zn and (b) Mn, Co, Ni, Sn, and V of the MSWI bottom ash sample per size fraction.

4.2.2 Mineralogical characterization of the magnetic fraction

From the mineralogical characterization results of the BA raw sample, described in section 3.5, it was possible to conclude that the main Fe-rich constituents existed in chemical forms of iron oxides, such as magnetite, hematite, and its transition and substituted varieties (hercynite), spinel group, and metallic inclusions. As previously shown in Figure 36 (a, b), Ni, Mn, Cu, and Co presented an enrichment. These results are likely due to the electron configuration of the elements mentioned above, which have an unpaired electron in the *d* orbital allowing them to exhibit magnetic properties or affinity for Fe. SEM/EDX results from the magnetic fraction showed that Mn, Cr, and Ni were associated with the iron-bearing particles, indicating their affinity with Fe (Figure 37). The previous statement can be linked to the geochemical classification by Goldschmidt (1937). The author classified Ni and Mn as highly siderophile elements, while Cr is considered moderately siderophile.

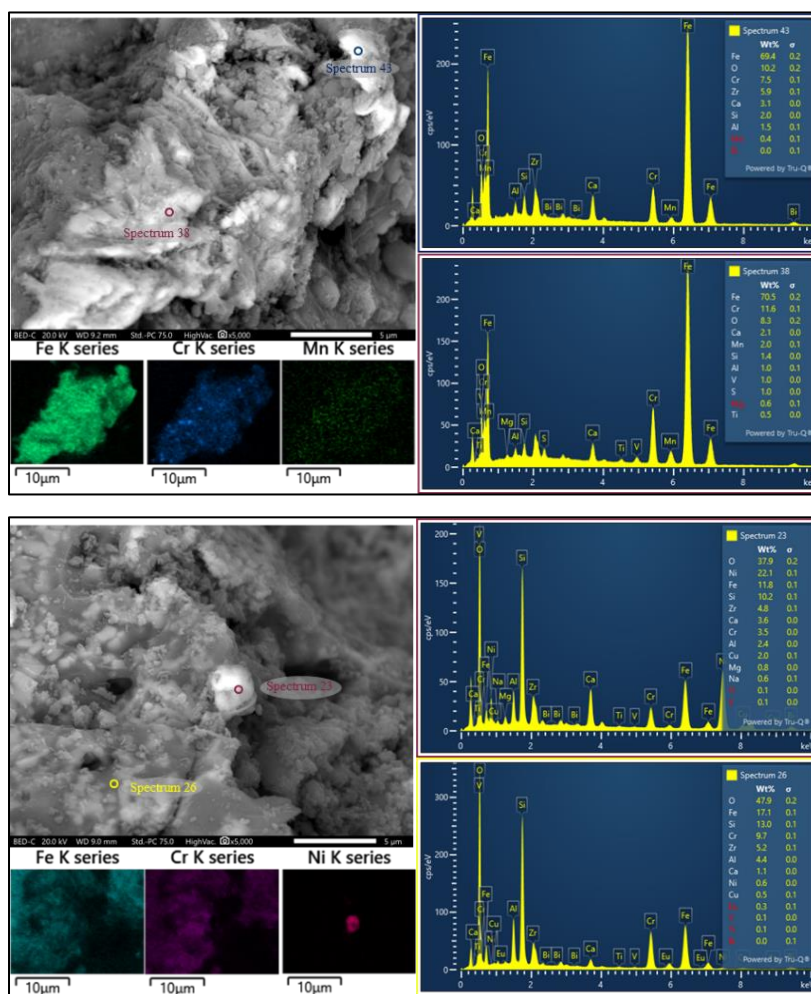


Figure 37. BSE image (top left), elemental maps (bottom left), and EDX spectra (right) of a Fe-rich constituent from the magnetic fraction enriched with (a) Mn and Cr, and (b) Ni, and Cr.

Although Cu, in its natural state, is not attracted by magnet forces, Cu was slightly enriched, mainly in the coarse fraction of the magnetic stream. It can be attributed to the previously described metallic inclusions (section 3.5) of Fe-Cu particles and the formation of CuFe_2O_4 clustered in Fe oxides, as shown in Figure 38. Rissler et al. (2020) identified CuFe_2O_4 as one of the Cu chemical forms in four of six MSWI-BA samples and quantified that this inverse spinel (also called Cuprospinel) accounts for up to 16% of the Cu occurred chemical forms. Cuprospinel is characterized by its magnetic properties, which according to Zhang et al. (2017) study, decrease by reducing the particle size. It explains the decrease in the enrichment ratio results observed in the section 4.2.1, when reducing the grain size.

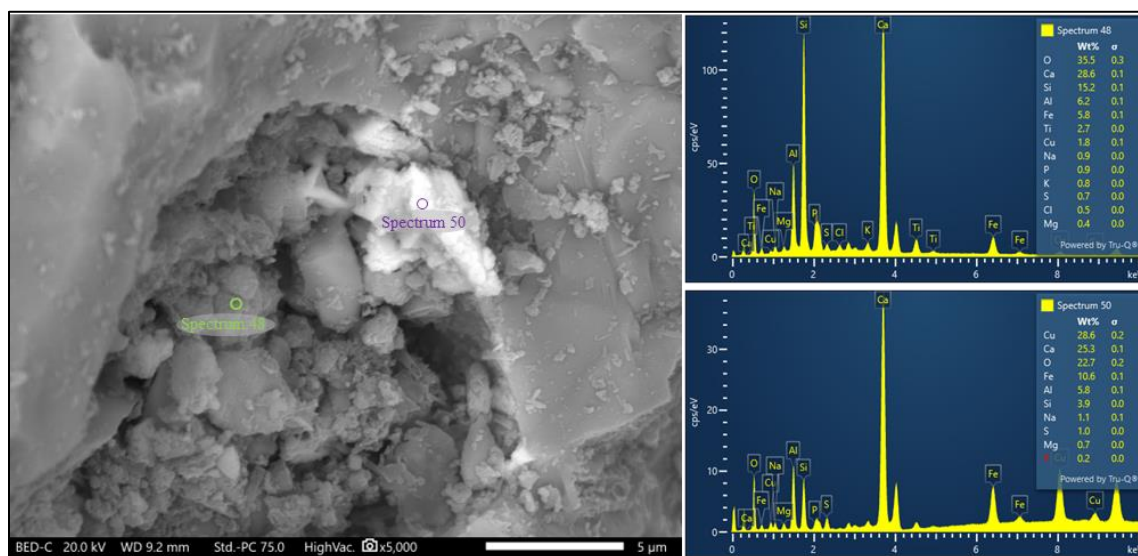


Figure 38. BSE image (left) and EDX spectra (right) of a possible Fe-Cu metallic inclusion, surrounded by Ca – Si matrix from the magnetic fraction of the BA sample.

Other non-targeted elements were found in the magnetic fraction mineralogical characterization performed using SEM/EDX, such as Si, Al, and Ca. These can be attributed to the Fe-rich minerals likely being embedded in amorphous siliceous glass or in a partially crystallized aluminosilicate matrix. Figure 39 displays the elemental map of an iron spinel in a series of Al^{3+} and Ti^{4+} substituted varieties embedded in a Ca-Si enriched matrix. In another study (Wei et al., 2017), it was concluded that even after a two-step magnetic extraction of a WtE BA sample, high Ca and Si content were found in the magnetic stream. These outcomes and findings suggest that longer comminution times could liberate the minerals and particles that contain the valuable elements and increase the selectivity of the process.

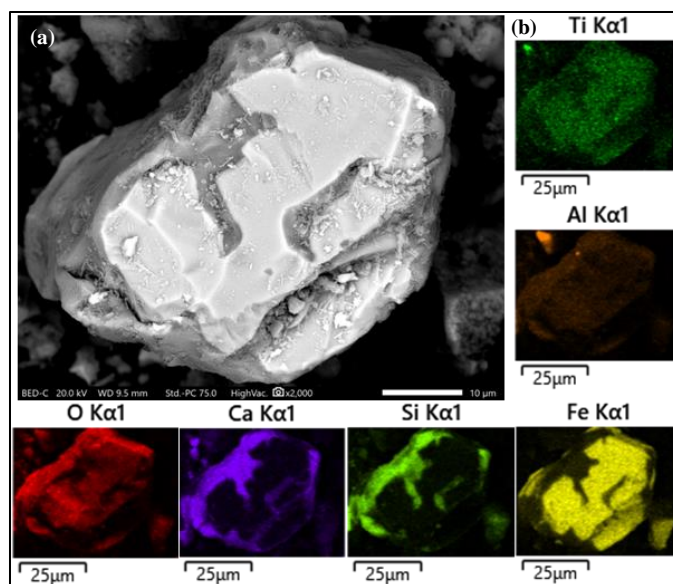


Figure 39. (a) BSE image and (b) elemental maps of a Fe-rich particle embedded in Si-Ca enrich matrix from the magnetic fraction of the BA raw sample.

On the other hand, as expected, the diamagnetic mineral phases, which were determined by XRD analyses in section 3, such as Silica, Calcite, Anhydrite, Ettringite, and Gismondine, were observed in the non-magnetic fraction of the BA sample. Likewise, Figure 40 shows the SED/EDX results of a Cu-S-O particle (most likely CuSO_4) and a Zn-S-O particle (likely ZnSO_4) observed in the non-magnetic fraction. Results published by Tuan et al. (2010) indicated that CuO and CuSO_4 dominated the Cu speciation in the BA, while a study by Zhang et al. (2020) showed that Zn speciation was mainly Zn_2SiO_4 and ZnSO_4 in fresh MSWI-BA from China. Although CuSO_4 exhibits paramagnetic properties, the particle size is about 25 microns, which could cause the centrifugal force exerted by the agitator to be greater than the magnetic force exerted by the magnet.

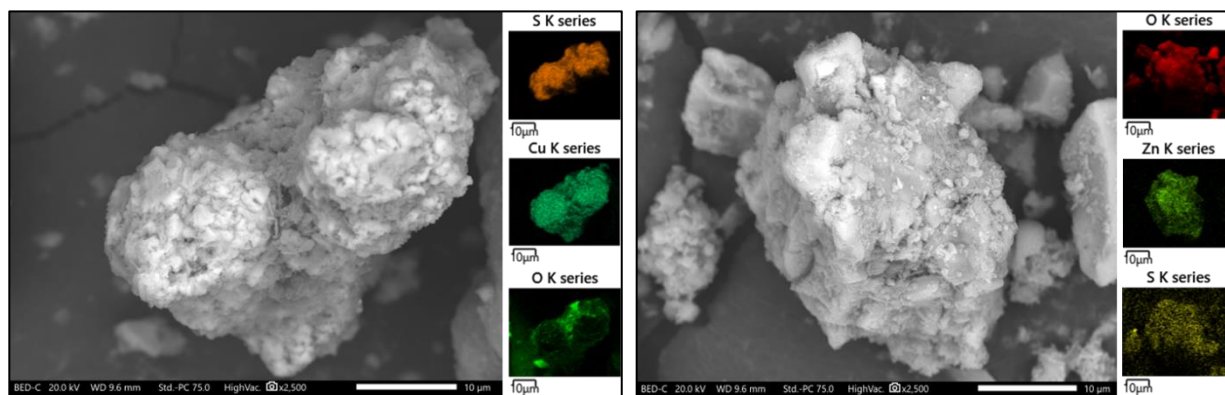


Figure 40. BSE image (left), and elemental maps (right) of (a) Cu-S-O particle, and (b) Zn-S-O particle from the non-magnetic fraction of the BA sample.

4.3 Density separation

4.3.1 Density separation performance indicators

To address the limitations that magnetic separation has with small particle sizes, current MSWI-BA treatment plants operate under several steps including a mechanical separation process. Based on a study by Šyc et al. (2020), around 10-20% of valuable elements in the MSWI-BA are present in the fine fraction, which cannot be efficiently concentrated through sensor-based sorting or magnetic separation. In some WtE facilities, after concentrating the ferrous metals and other magnetic elements through magnetic separation, the non-magnetic stream frequently goes under an extra step of comminution and sieving processes. The passing material from the sieving process feeds the density separation process, usually done using centrifugal concentrator equipment such as a jigger, hydrocyclone, and/or air table sorting.

Hwang et al. (2008) estimated the bulk density of the MSWI ash using the results of XRD analysis and the elemental content of single elements. Then, they compared the composition based on a series of float-sink separations. The medium was prepared using DI water and CaCl_2 at 95% purity at different medium densities (1.0 g/cm^3 , 1.2 g/cm^3 , and 1.4 g/cm^3) and liquid-to-solid volume ratios (L/S) of 30, 40, and 60. However, from the extensive literature review, the density separation process has not been scaled up to an industrial scale. The most common aqueous medium used in the industry to perform a density separation test is water, which presents small particle size restrictions and selectivity limitations. This study used LMT at 2.95 SG and 2.6 SG as the medium liquid to evaluate the recovery of the valuable elements. The results of XRD analysis, SEM/EDX from the raw sample, and the metal content determined using the digestion system and ICP-MS analysis provided valuable information about the MSWI composition, valuable elements content, and their mineral phases. Table 3 summarizes the estimated MSWI-BA main mineral phases, elemental composition, and density reported in the literature.

Table 3. Estimated minerals in MSWI-BA and density (g/cm³)

Mineral Phases / Elements	Formula	Density (g/cm ³)	Reference
Anhydrite	CaSO ₄	2.31-2.97	Hudson Institute of Mineralogy, 2019
Ettringite	Ca ₆ Al ₂ (SO ₄) ₃ (OH) ₁₂ ·26H ₂ O	1.8	Hudson Institute of Mineralogy, 2019
Gismondine	CaAl ₂ Si ₂ O ₈ ·4H ₂ O	2.26	Hudson Institute of Mineralogy, 2019
Hercynite	FeAl ₂ O ₄	3.82	Hudson Institute of Mineralogy, 2019
Magnetite	Fe ₃ O ₄	7.87	Hwang et al., 2008
Quartz	SiO ₂	2.70	Hwang et al., 2008
Calcium carbonate	CaCO ₃	2.71	Hwang et al., 2008
Calcium titanate	TiCaO ₃	3.98	Hudson Institute of Mineralogy, 2019
Cobalt oxide	CoO	6.44	PubChem, 2021
Copper (II) oxide	CuO	6.31	PubChem, 2021
Copper sulfate	CuSO ₄	3.6	PubChem, 2021
Cupric sulfide	CuS	4.76	PubChem, 2021
Iron chromite	FeCr ₂ O ₄	4.97	Hudson Institute of Mineralogy, 2019
Iron Phosphide	FeP	6.74	PubChem, 2021
Manganese iron oxide	MnFeO ₃ -MnFeO ₄	3.6 - 4.74	PubChem, 2021
Manganese oxide	MnO	5.37	PubChem, 2021
Titanium dioxide	TiO ₂	4.23	PubChem, 2021
Zinc chloride	ZnCl ₂	2.91	PubChem, 2021
Zinc oxide	ZnO	5.61	PubChem, 2021
Copper	Cu	8.93	Hwang et al., 2008
Zinc	Zn	7.12	Hwang et al., 2008

As shown in Table 3, the valuable elements and their mineral phases have a higher density than the non-targeted minerals phases. The 2.95 SG density test, illustrated in Figure 41, showed enrichment ratios higher than 2.0 in Fe, Cu, Co, and Ni in the coarse fraction of the BA fraction, which decreases when decreasing the size fraction. As for Sc and V, their enrichment ratios are reasonably constant regardless of the size fraction. While Zn, Ti, Mn, and Sn, although their enrichment ratios are below 2.0, their enrichment tendency decreases with the size fraction reduction. Similar behavior is observed in the valuable elements' recovery in Figure 42, where valuable elements and their mineral phases with significant density differences, such as Fe, Fe-rich constituents, Cu speciation, and Co-minerals, had recovery over 80%.

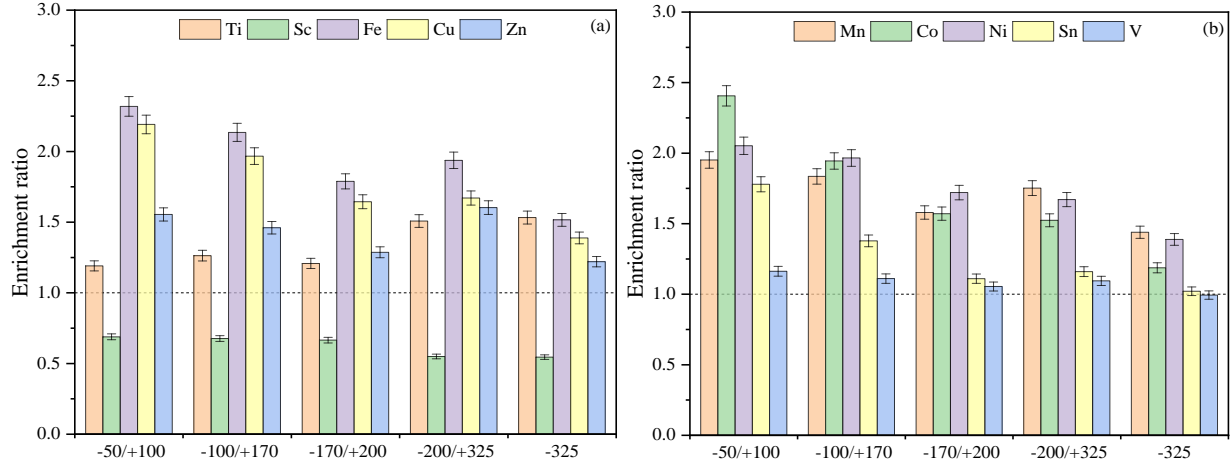


Figure 41. Density separation enrichment ratios for (a) Ti, Sc, Fe, Cu, and Zn and (b) Mn, Co, Ni, Sn, and V at 2.95 specific gravity of the MSWI-BA sample per size fraction.

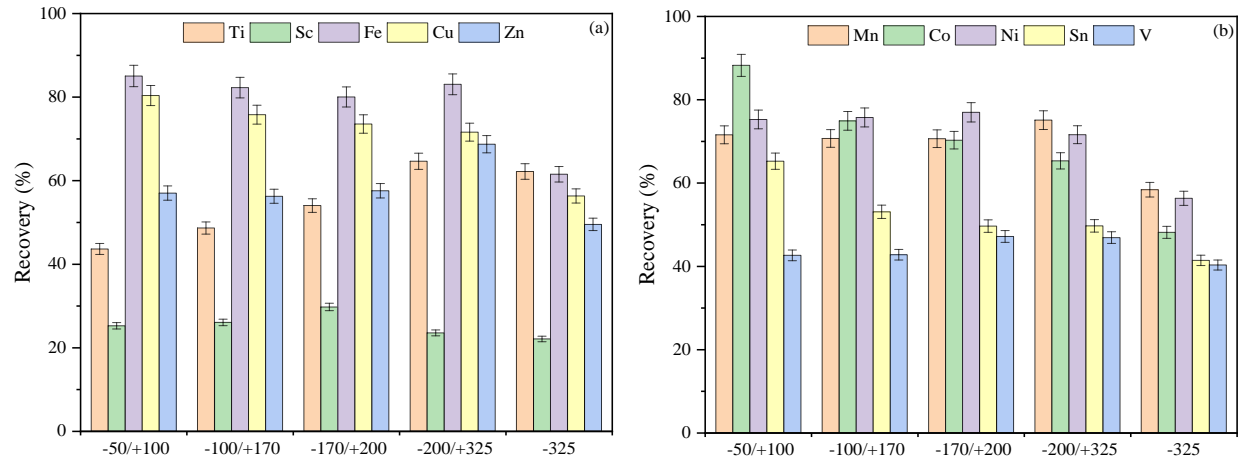


Figure 42. Density separation recovery for (a) Ti, Sc, Fe, Cu, and Zn and (b) Mn, Co, Ni, Sn, and V at 2.95 specific gravity of the MSWI-BA sample per size fraction.

Like Hwang et al. (2008) study, different cutting densities were evaluated. The float material from the 2.95 SG test was collected, rinsed, and dried and then used as a feed for a second-density separation stage at 2.6 S.G. The second stage aims to work as a scavenger process and recover the valuable particles that did not sink in the first stage. As expected, the sink fraction yield increased as the medium density decreased. From Figure 43 (b), it is observed that by decreasing the cutting density, the enrichment ratios of the minor elements (Mn, Co, Ni, Sn, and V) were similar across the different size fractions. It is worth noting from Figure 43 (a) that the enrichment ratio of Fe was slightly higher in the fine fraction than in the coarse fraction. This observation could be associated with the minor Fe enrichment achieved in the fine fraction in the first float-sink test stage. Although most of the valuable elements' recovery from the float-sink test at 2.6 SG was above 80%, as shown in Figure 44, the enrichment ratios were low.

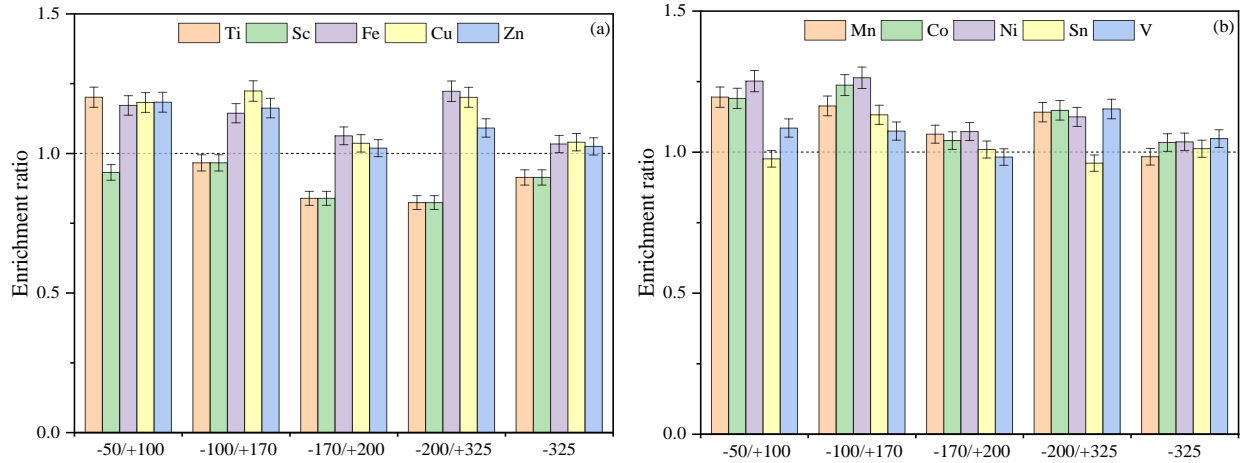


Figure 43. Density separation enrichment ratio for (a) Ti, Sc, Fe, Cu, and Zn and (b) Mn, Co, Ni, Sn, and V at 2.6 specific gravity of the MSWI-BA sample per size fraction.

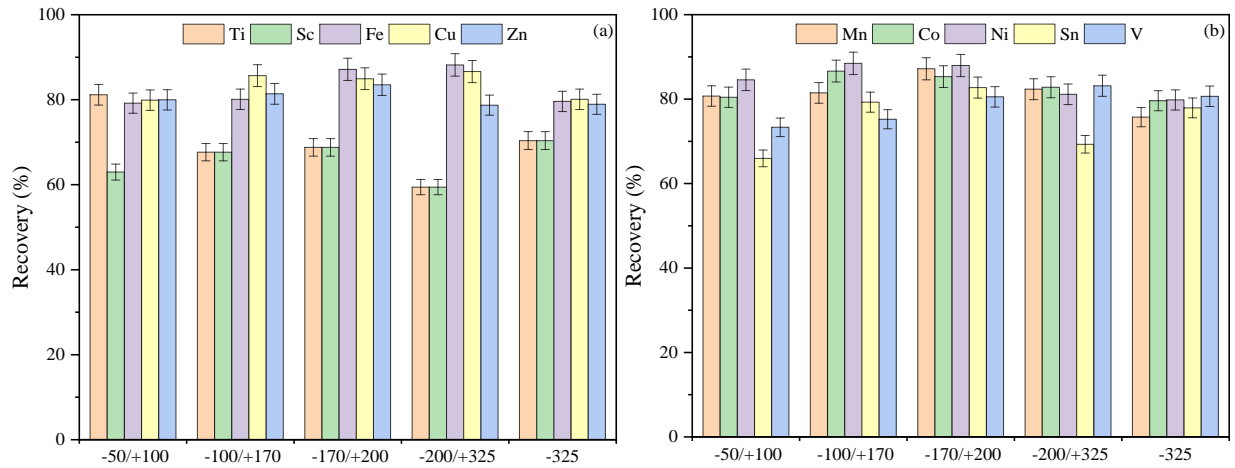


Figure 44. Density separation recovery for (a) Ti, Sc, Fe, Cu, and Zn and (b) Mn, Co, Ni, Sn, and V at 2.6 specific gravity of the MSWI-BA sample per size fraction.

From the results and the metallurgical indexes from the density separation, it can be concluded that most elements were considerably enriched with a 2.95 SG cutoff density, except for the Sc and V, which enrichment ratios were closer to 1.0 regardless of the size fraction. As for the 2.6 SG test performed as a scavenger process to recover the remaining valuable elements of the float material from the first stage of the density test, no noticeable enrichment and selectivity were observed.

4.3.2 Mineralogical characterization of the Sink fraction

Based on the MSWI-BA mineral phases and the estimated minerals existing in the BA sample summarized in Table 3 and the metallurgical indicators described in section 4.3.1, enrichment in the valuable elements was observed in the sink fraction due to their specific gravities. To estimate the mineral

phases concentrated in the sink fraction, SEM/EDX analysis was performed. Fe-rich constituents such as iron oxides (Figure 45), most likely magnetite with a specific gravity of 7.87 (Hwang et al., 2008), were identified. However, the EDX spectra (Figure 45, bottom right) revealed a minor content of Mn, Al, Ca, and Si (0.3 wt.%, 0.2 wt.%, 0.2 wt.%, and 0.2 wt.%, respectively), indicating the association of aluminum/calcium-silicate mineral phases. Likewise, Figure 46 depicts the BSE image and the elemental maps of a Fe-spinel group particle with Cr^{3+} partial substitution, which has an approximate specific gravity of 4.97 (Hudson Institute of Mineralogy, 2019).

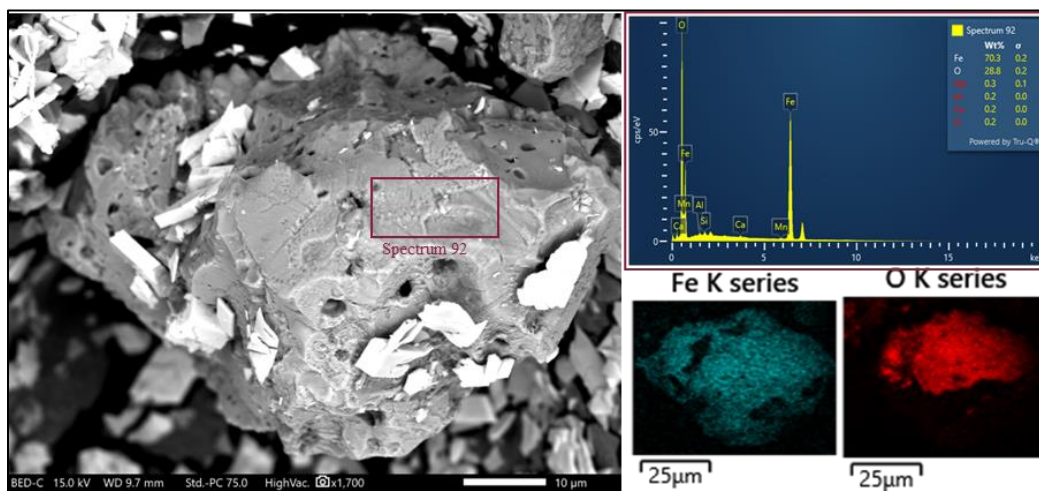


Figure 45. BSE image (left), EDX spectra (top right), and elemental maps (bottom right) of most likely magnetite with aluminum/calcium-silicate mineral phases association from the sink fraction of the BA density test.

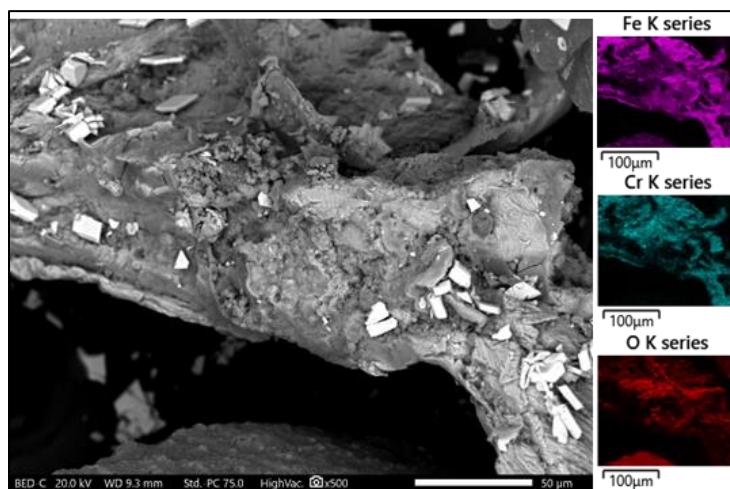


Figure 46. BSE image (left), and elemental maps (right) of a Fe-spinel group with Cr^{3+} substitution (iron chromite) from the sink fraction of the BA density test.

On the other hand, the Cu enrichment in the coarse fraction through density separation was higher than the magnetic separation. It could be justified by the relatively high specific gravity of its mineral phases, like copper oxide, copper sulfate, and cupric sulfite, with specific gravities of 6.31, 3.6, and 4.76, respectively. Figure 47 depicts a copper oxide particle clustered in a calcium-silicate matrix. Nevertheless, according to Rissler et al. (2020), the Cu can be present in diverse oxidation states (0, 1+, and 2+) in the MSWI-BA due to the variation in the presence and access of oxygen in the fuel bed in the combustion chamber.

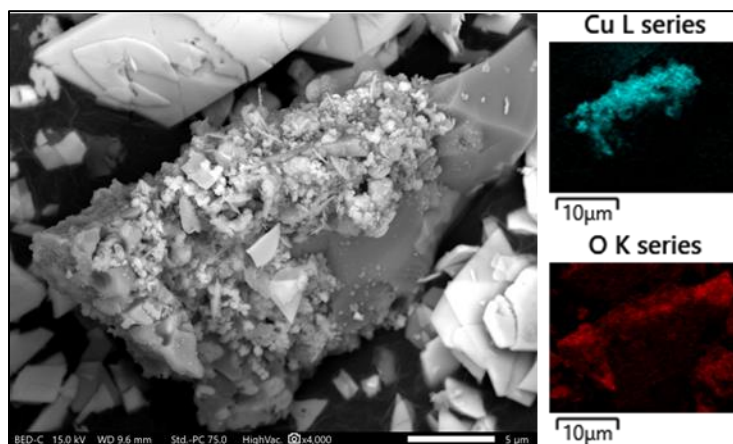


Figure 47. BSE image (left) and elemental maps (right) of a copper oxide particle from the sink fraction of the BA density test.

As previously mentioned, copper sulfide was also identified as one of the mineral phases of copper. Through the mineralogical analysis done using the SEM/EDX results in the sink fraction of the density test, an enriched area of copper sulfide was identified (Figure 48). The particle is likely associated with calcium oxide (CaO) and calcium titanate (CaTiO_3), based on the EDX spectra elemental content results depicted in Figure 48 (left). These findings and associations have been previously observed and described by Arickx et al. (2008), who studied the speciation of Cu in the MSWI-BA through optical microscopy and electron microprobe (WDX/EDX). This study concluded that metallic Cu, Copper oxide, and Cu_2O were the most abundant Cu speciation. Likewise, it concluded that copper mineral phases were frequently together with Ca, Cl, and S.

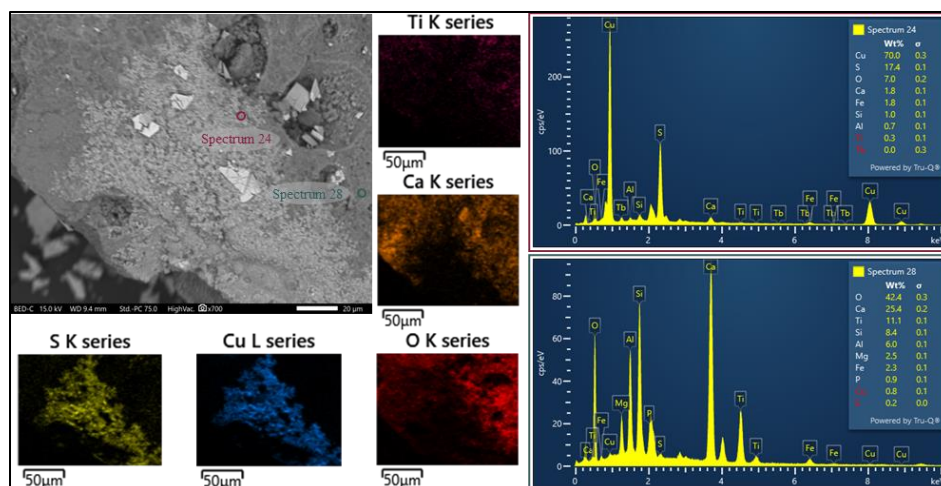


Figure 48. BSE image (left), elemental maps (middle and top left), and EDX spectra (right) of a Cu-S metallic inclusion, surrounded by CaO and CaTiO₃ from the sink fraction of the BA density test.

As observed in section 4.3.1, Ti was slightly enriched through the float-sink test at 2.95 cutoff density. According to the SEM/EDX results, the main Ti speciation enriched in the sink fraction was calcium titanate (CaTiO₃), as shown in Figure 49. This mineral phase deduction of the Ti is consistent with Ilyushechkin et al. (2020) characterization study of inorganic matter of Australian MSWI, in which it was concluded that calcium titanate (CaTiO₃), calcium oxide (CaO) and calcium silicate (Ca₂SiO₄) were the major calcium-rich phases in the MSWI ashes. Additionally, the enrichment of Ti in the sink fraction is consistent, considering that this mineral phase has a specific gravity of 3.98 (Hudson Institute of Mineralogy, 2019), which is a higher density than the aqueous medium used (2.95).

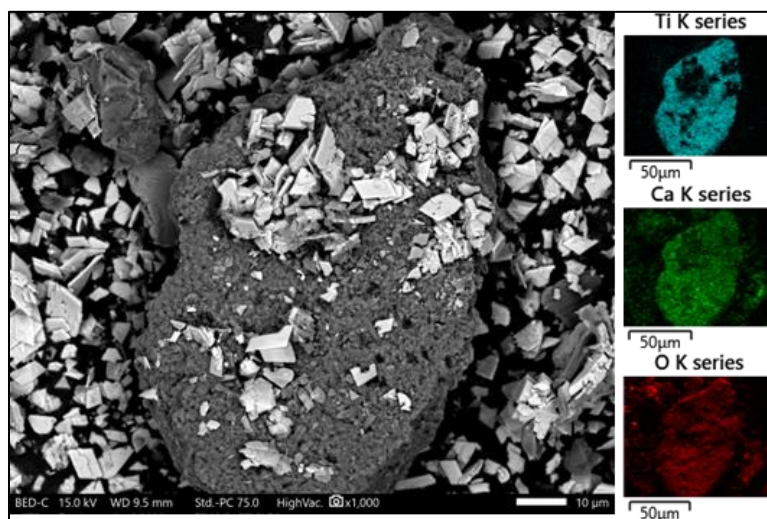


Figure 49. BSE image (left) and elemental maps (right) of a calcium titanate particle from the sink fraction of the BA density test.

4.4 Statistical analysis

To determine whether there is a statistical difference in element distributions in the by-products generated from each separation process, a paired t-test was performed. The comparisons were made within the samples among six individual groups of samples, with a total of 5 samples each group ($n=5$). Groups one and two refer to the magnetic separation by-products labeled MF 1-5 (magnetic fraction) and NF1-5 (non-magnetic fraction). Groups three and four stands for the density test performed at 2.95 SG, labeled as 2.95 FF1-5, and 2.95 SF1-5, referring to the float and sink samples, respectively. The float and sink fraction from the density test carried out at 2.6 SG constitute groups five and six, marked as 2.6 FF1-5 and 2.6 SF1-5, respectively. Significant differences were considered when the calculated p -value was less than 0.05. The p -values calculated from the paired t-test for the content of the valuable element are presented in Table 4.

Table 4. p -values of paired t-test for valuable elements content among magnetic, non-magnetic, float fraction, sink fraction at 2.95 and 2.6 specific gravity of the BA sample.

<i>p - values</i>	<i>Total elemental content (ppm)</i>		
<i>(n= 5)</i>	MF vs. NF	SF vs. FF (At 2.95 SG)	SF vs. FF (At 2.6 SG)
<i>Sc</i>	✓ 5.66×10^{-3}	✓ 2.56×10^{-4}	✓ 8.00×10^{-3}
<i>Ti</i>	0.215	✓ 0.016	✓ 0.029
<i>V</i>	0.247	0.340	0.095
<i>Fe</i>	✓ 2.57×10^{-3}	✓ 6.42×10^{-3}	✓ 0.017
<i>Mn</i>	✓ 0.039	✓ 2.50×10^{-3}	✓ 3.11×10^{-3}
<i>Co</i>	✓ 0.044	✓ 0.047	✓ 0.029
<i>Ni</i>	✓ 0.036	✓ 5.19×10^{-4}	✓ 6.71×10^{-3}
<i>Cu</i>	0.440	✓ 3.99×10^{-3}	✓ 9.45×10^{-3}
<i>Zn</i>	0.067	✓ 0.027	✓ 0.015
<i>Sn</i>	✓ 1.36×10^{-3}	0.110	0.088

MF refers to the magnetic fraction of the BA sample.

NF refers to the non-magnetic fraction of the BA sample,

SF stands for the sink fraction from the density tests of the BA sample,

FF stands for the float fraction from the density tests of the BA sample,

SG stands for the specific gravity,

✓ refers to the p -value < 0.05 .

The results unveiled significant differences in the distribution of Sc, Fe, Mn, Co, Ni, and Sn between MF and NF. The test indicated that the elemental distribution mentioned above did change through magnetic separation. Regarding the float-sink separation at 2.95 SG and elemental redistribution, results shown that a total of 8 elements, Sc, Ti, Fe, Mn, Co, Ni, Cu, and Zn, are statistically different between the FF and SF. These outcomes are consistent with the enrichment ratio indicator calculated in section 4.3.1 where most elements were enriched. Sc, Ti, Fe, Mn, Co, Ni, Cu, and Zn distribution was changed through the density test performed 2.6 SG. However, the statistical analysis unveils differences in the distribution, but it is limited to determining the enriched fraction. For example, the p-value for the Sc distribution after the density test at 2.95 was 2.56×10^{-4} , indicating a significant difference between the sink (SF) and float fraction (FF). However, the enrichment ratio index from section 4.3.1 was slightly over 0.5 among the different particle size fractions.

To address this limitation and evaluate the influence of the size fraction in the redistribution of the elements after each separation process (magnetic separation and density test), a parameter previously used by other researchers (Kukier et al., 2003; Lu et al., 2009; Wei et al., 2017), named “enrichment coefficient” (EC) was used. This parameter indicates the presence of an element in the concentrate stream compared to the tailing stream. It is calculated following the equation (9); where c_i represent the assay of concentrate of the i element, in the j size fraction in the magnetic stream or sink fraction and t_i represents the from non-magnetic stream or float fraction, according to the test being evaluated.

$$EC = c_{i,j}/t_{i,j} \quad (9)$$

The relative enrichment coefficient of valuable elements from the magnetic separation and density separation at 2.95 SG and 2.6 SG are shown in Table 5 and Table 6 (a, b), respectively. Coefficients greater than 1.0 for a specific element in a determined size fraction indicate that it is enriched in the magnetic fraction or the sink material, according to the corresponding process. Overall, Fe had the highest EC value, followed by Co and Cu in the magnetic fraction, indicating the effectiveness of the process to concentrate these elements and their mineral phases. Likewise, there is a decreasing tendency in the EC values when reducing the particle size, suggesting a correlation between the particle size fraction and valuable elements' concentration.

Table 5. Relative enrichment coefficient of valuable elements in the magnetic material per size fraction of the UB sample.

Elements	Enrichment coefficient (EC) by size fraction					
	-50/+100	-100/+170	-170/+200	-200/+325	325	Average
Ti	1.91	1.79	1.86	1.67	1.63	1.77
Sc	2.28	2.27	1.88	1.13	1.98	1.91
Fe	5.03	4.13	3.07	4.02	2.59	<u>3.77</u>
Cu	3.41	1.77	1.47	1.92	1.13	<u>1.94</u>
Zn	1.67	1.52	1.61	1.84	1.03	1.53
Mn	1.32	1.05	1.39	1.77	1.13	1.33
Co	3.20	2.25	1.67	1.42	1.68	<u>2.05</u>
Ni	2.27	1.46	1.29	1.07	1.46	1.51
Sn	1.45	1.53	1.53	1.60	1.21	1.46
V	0.95	1.02	1.20	0.93	1.13	1.04

The relative EC from the float-sink at 2.95 SG presented in Table 6 suggests a high processing efficiency to concentrate Fe, Cu, Mn, Co, and Ni, with average values of 5.65, 3.97, 3.01, 4.97, and 3.92, respectively. However, a significant variance can be observed in the enrichment coefficients of the Mn and Ni in the coarse fraction of the sample compared to the fine fraction. The comparison between the EC in the coarse and the fine fraction, showed a reduction of 79, 80, 68, 75, and 64 absolute percent change in Fe, Cu, Mn, Co, and Ni, respectively. These outcomes indicate a correlation between the elements' enrichment through the density separation and the particle size, similar to the phenomenon described in the magnetic separation section. As for the 2.6 density separation process fed with the float fraction from the 2.95 SG density test, the overall EC values are considerably lower than the EC values obtained through the other separation methods, most likely due to the low assay of the valuable elements in the feed stream. Likewise, as previously concluded in section 4.3.1, the Sc cannot be efficiently enriched by float-sink regardless of the cutoff density used.

Table 6. Relative enrichment coefficient of valuable elements in the sink material from the density test at (a) 2.95 SG and (b) 2.6 SG per size fraction of the UB sample.

(a) Elements	Enrichment coefficient (EC) by size fraction					
	-50/+100	-100/+170	-170/+200	-200/+325	325	Average
Ti	1.34	1.51	1.45	1.18	0.99	1.29
Sc	0.58	0.56	0.52	0.41	0.42	0.50
Fe	9.82	7.40	4.95	4.02	2.05	<u>5.65</u>
Cu	7.07	4.99	3.44	2.93	1.44	<u>3.97</u>
Zn	2.29	2.05	1.68	1.37	0.86	1.65
Mn	4.35	3.85	2.97	2.51	1.36	<u>3.01</u>
Co	5.97	4.77	2.92	2.76	1.47	<u>4.97</u>
Ni	5.25	4.98	4.13	3.36	1.89	<u>3.92</u>
Sn	3.24	1.81	1.22	1.05	1.04	1.67
V	1.28	1.19	1.10	0.87	0.80	1.05
(b) Elements	Enrichment coefficient (EC) by size fraction					
	50/+100	-100/+170	-170/+200	-200/+325	325	Average
Ti	2.07	2.10	1.10	1.91	1.25	1.68
Sc	0.82	0.90	0.48	0.57	0.71	0.69
Fe	1.83	1.72	1.49	1.80	0.93	1.55
Cu	1.91	2.56	1.24	1.43	1.12	1.65
Zn	1.92	1.87	1.11	1.41	1.18	1.50
Mn	2.01	1.88	1.50	1.86	1.17	1.68
Co	1.97	2.78	1.28	1.66	1.18	1.77
Ni	2.63	2.97	1.61	2.50	1.20	<u>2.18</u>
Sn	0.93	1.64	1.05	1.27	1.12	1.20
V	1.32	1.30	0.94	1.05	1.01	1.12

The main findings from the physical concentration study were that classifying the sample into the coarse, middle, and fine-size fractions could lead to better metal concentration yields. Likewise, the magnetic separation results showed that its performance and enrichment of the valuable elements is a function of the bound of multi-metallic oxides fractions and the metals affinity for Fe-rich particles. The mineralogical characterization of the magnetic fraction concluded that the main Fe-rich constituents existed

in chemical forms of iron oxides, such as magnetite, hematite with substituted varieties, spinel group, and metallic inclusions. However, non-targeted elements, such as Si, Al, and Ca, were also enriched because the Fe-rich minerals were likely embedded in amorphous siliceous glass or a partially crystallized aluminosilicate matrix. As for the 2.95 SG density test, enrichment ratios higher than 2.0 were obtained for Fe, Cu, Co, and Ni in the coarse fraction of the BA fraction, which decreases when reducing the size fraction. The SEM-EDX analysis carried out using the sink material from the density test revealed that magnetite, iron chromite, copper oxide, copper sulfate and calcium titanate are the main valuable elements' speciation with a specific gravity higher than 2.95.

Chapter 5 Evaluation of the effect of the particle size reduction

The evaluation of the effect of the particle size was performed to assess the intraparticle heterogeneity of MSWI BA. The evaluation consisted of particle size reductions by crushing and grinding for different residence times. By reducing the particle size, the free specific surface area increases, leading to the release of valuable metals associated with coarse particles. Veasey & Wills (1991), states that the critical function of the comminution process is to liberate the minerals from each other. Deficient mineral comminution can lead to higher energy consumption costs and the generation of ultra-fine material that may be lost or unrecoverable in the subsequent mineral processing (Somasundaran, 1986).

As previously described in section 3.5, some of the major and minor mineral phases are embedded in the molten matrix and in the Si-Ca enriched matrix, which binds the crystalline and metallic fractions according to the findings from Mantovani et al. (2021). Hence, in order to determine the intraparticle heterogeneity and resources potential, the BA sample was ground for different time intervals under the same conditions. After each comminution process, the ground material was collected, and prepared for the physical characterization tests and elemental composition determination through ICP-MS analysis after being digested.

5.1 Materials and methods

5.1.1 *Materials*

The BA sample used for the evaluation of the particle size was collected from a Waste-to-Energy (WtE) facility in New Jersey, U.S. The sample was transported and delivered on May 24th, 2021, to the Mineral Processing Laboratory at Virginia Tech in closed plastic buckets. Before analysis, the BA sample was placed on a flat surface in an approximately 3 cm thick layer and subjected to 5 to 7 days of air-drying at room temperature. Once the sample was dry, coarse objects and materials like iron, glass, ceramic, and non-mineral materials were sorted by hand. Subsequently, the sample was piled into a cone-shaped heap, and then the top of the cone was flattened by pressure. Further, the flattened sample was split into four portions, and the opposite portions were mixed and split again to ensure homogeneity. In total, two subsamples were taken and analyzed.

5.1.2 *Physical characterization*

In order to determine the effect of the particle size evaluated as a function of the grinding residence time, on the physical properties and valuable elements recovery from the BA sample, a sequence of physical

separation tests were performed after the comminution process. These tests included particle size distribution, magnetic separation, and froth flotation. The physical tests were carried out to evaluate the samples' particle size, magnetic susceptibility, density, and surface hydrophobicity properties and how they correlated with the different total grinding times. The magnetic separation test was performed following the conditions previously described in section 2.2.1.2.

5.1.2.1 Particle size reduction by grinding

The comminution process was performed in a Wet Batch Laboratory Mills Series 01-HD attrition mill (Union Process Inc., Ohio, U.S.). The grinding process was carried out with the samples at 25% solid concentration with a total of 2.8 kg of Type 52100 Chrome Steel Balls (Union Process Inc., Ohio, U.S.) of 1/4" diameter at a rotational speed of 400 rpm. The residence time chosen to perform the particle size reduction is shown in Table 7. After each comminution process, the samples were collected for the following tests.

Table 7. Grinding residence time used.

Test	Internal sample code	Residence time (min)
1	UB-1	10
2	UB-2	30
3	UB-3	60
4	UB-4	90

5.1.2.2 Flotation tests

The flotation test was carried out using a 1-L bench-scale Denver flotation machine. The slurry was brought to a solid concentration of 5% and thoroughly mixed using a high-speed overhead stirrer. Then, a pH regulator was added followed by 5 min of conditioning time. Subsequently, diesel was added as the collector, and five more min of conditioning time was taken. The pH was monitored and adjusted during the conditioning time as needed. Once the desired pH was reached and stabilized, one drop of methyl isobutyl carbinol (MIBC) was added into the slurry to promote bubble generation. Following another 5 min to float the slurry, the concentrate, and the tailings (non-floated material) were then collected, labeled, filtered, and dried for further analyses. The froth flotation experiment set up is illustrated in Figure 50. It is worth noting that the purpose was to evaluate whether flotation is viable, not to optimize flotation performance; thus, only a few tests were conducted. Table 8 lists the experimental conditions used for the froth flotation tests.



Figure 50. Froth flotation experiment set up.

Table 8. Experimental conditions used for the froth flotation tests.

Test No.	Conditions
1	0.168 g/ton Diesel, pH 8.8 (pH was adjusted with HCl)
2	0.338 g/ton Diesel, pH 9 (pH was adjusted with HCl)
3	0.084 g/ton Diesel, pH 9 (pH was adjusted with HCl)
4	0.168 g/ton Diesel, pH 12 (no pH adjustment)

Diesel is a non-polar hydrocarbon oil widely used as collector in coal and organic matter separation through flotation test because of its capacity to extend the hydrophobic effect (Mulleneers, 2001). In this study, the collector (diesel) was added to the system before the frother (MIBC), to facilitate the dispersion of the insoluble oily collector. The collector dosage (diesel) was selected based on the literature review and adjusted according to the results and flotation kinetics evaluated in preliminary results. As for the pH, previous studies (Kemal, 2007; Carlson & Kawatra, 2013) have concluded that higher organic matter removal can be obtained under slightly basic values.

5.1.2.3 Acid leaching test

A series of acid-leaching tests were performed to determine the effect of particle size on the valuable elements' leachability. The test setup was previously shown in Figure 19, and the test conditions were setup based on the sample characterization and valuable elements' leachability determined and described in section 3.3. The leachability and recovery of the valuable elements was evaluated at different lixiviant concentrations to determine the acid concentration influence and the effect of particle size as a function of the grinding time. Likewise, to evaluate the valuable elements leachability kinetics, 5.0 g of solid sample was mixed with 100 mL of HCl at 1.0 M. Representative samples were taken from the slurry at 5, 30, 60, and 120 min for a total leaching duration of 2 h. The liquid fractions collected were centrifuged at 4000 rpm for 3 min, and directly subjected to elemental analysis, while the solid fractions were dried at 60 °C for 12 h and digested using HCl, HNO₃ and HF to determine its elemental composition, according to the equations (4) and (6) described in Section 2.2.3.3 and 2.2.3.4, respectively.

5.1.2.4 Elemental composition - Inductively coupled plasma spectrometry (ICP-MS)

The total elements composition and valuable metals content in the by-products generated from the different residence grinding times of the BA sample were determined by inductively coupled plasma spectrometry (ICP-MS) analysis. The solid samples were ashed in a furnace at 750 °C for 2 h to remove the unburnt organic material. Then, the ashed material was digested using a closed microwave digestion system (Multiwave GO Plus, Anton Paar, USA). The sample preparation consisted of adding 9 mL of hydrochloric acid, 3 mL of nitric acid, and 2 mL of hydrofluoric acid of trace metal grade to 0.100 g of the solid sample in a digestion vessel. For this procedure, the vessels were heated to 185 °C for 35 min. Once the process was complete, the samples were diluted 100 times in 5% HNO₃ solution and analyzed using a Thermo Electron iCAP-RQ inductively coupled plasma mass spectrometer (ICP-MS) per Standard Method 3125-B (APHA, AWWA, and WEF, 1998) at Materials Characterization Lab of Virginia Tech. Samples and calibration standards were prepared in a matrix of 2% nitric acid by volume.

5.2 Results and discussions

5.2.1 Size fraction characterization and elemental composition

The particle size characteristics and the valuable elements redistribution caused by ball milling were evaluated on the MSWI-BA sample. The particle size distribution was measured after 10, 30, 60, 90 min of grinding, and results are presented in Figure 51. The distribution was linearized assuming a Rosin-Rammler distribution. The parameters and calculation for each data set from the sieve analysis are presented in Appendix A. From the figure it can be noted that after 60 min of grinding more than 90% of the particles in the BA sample have a diameter below 38 microns. Furthermore, most of the size reduction comes from

the particles below 200 mesh, which on average sharply increased about 30% of the total distribution. A study conducted Bond (1953) called the third theory of comminution, concluded that as for grinding, small particles require more energy for particle breakage than large particles due to interparticle heterogeneity and conglomerations. This could represent a limitation because 70% of the BA sample are particles that belong to a size fraction below 100 mesh, which could imply a higher energy consumption to comminute and reach the liberation particle size.

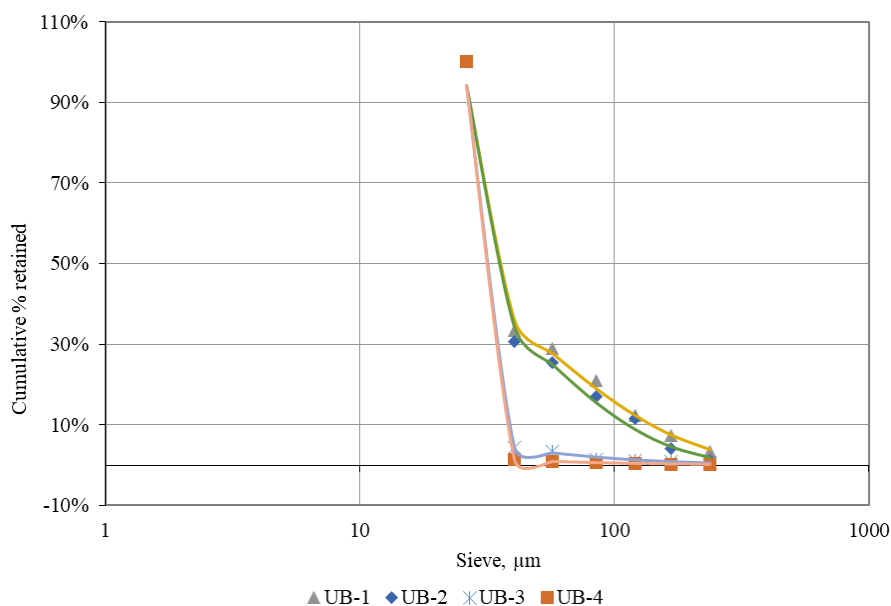


Figure 51. Particle size distribution of the BA sample subjected to different grinding times.

The redistribution of the valuable elements in the BA sample was evaluated after 10 and 30 min of grinding time and then compared with the elemental composition and valuable elements distribution from the raw sample described in section 4.1.1. The results shown that Zn was enriched in the finer fraction in the raw BA sample (Figure 52(a)), but when grinding the sample for up to 30 min, an even redistribution among the particle sizes can be observed (Figure 54(a)). According to Loginova et al. (2019) this phenomenon can be explained by the increment of the specific surface area generated by the grinding process that promotes the adherence of Zn compounds. Additionally, based on the elemental composition and speciation, it is worth considering the formation of Zinc hydroxide as a result of the interaction of the Zn compounds from the BA sample and the water added to perform the comminution process. According to the Standard molar Gibbs energy of formation ($\Delta_f G^0$) of the Zinc Hydroxide (-555.9 kJ/mol) reaction is spontaneous, and likely to coat the new fine particles generated by the grinding process (Russian Anatolievich Kiper, n.d.). The Fe content in the BA raw sample tends to decrease with the particle size, suggesting that the Fe is enriched in the coarse fraction. This tendency continues after 10 min of grinding

time, as shown in Figure 53(a). However, after increasing the grinding time to 30 min, the Fe distribution in the sample exhibits a normal distribution, with the highest enrichment ratio in the -150/+200 mesh size fraction. Similar results were previously obtained by Yao et al. (2014), who concluded that the particle size reduction caused by the abrasion-compression mechanisms involved in the ball milling, favors the mobility and redistribution of the heavy metal and rare earth elements among the different particle size intervals in the BA sample. In contrast, Ti and Sc content and distribution showed insignificant variance when comparing the particle size fraction in the raw BA sample, shown in Figure 52(a), the 10 min ground by-product presented in Figure 53(a), and the 30 min ground by-products shown in Figure 54(a).

As for the minor elements in the raw BA sample shown in Figure 52(b), Mn, Co, Ni, Sn, and V distributions showed an even enrichment among the size fractions. This was most likely due to the low concentration of the mentioned elements in the middle-size fraction. However, after 30 min of grinding, Mn, Sn, and V showed an even redistribution in the different particle sizes, with slight fluctuations among the +75 and -150/+200 mesh size fractions (Figure 54(b)). These results are consistent with the Loginova et al. (2019) study, in which a comprehensive characterization of the particle size fractions of the MSWI-BA was carried out. Likewise, it is worth noting possible sources of contamination introduced during the grinding process caused by the used of stainless-steel balls that could increase or modify the V content and distribution in the BA samples. Regarding the contents of Co and Ni in the raw BA sample, there was a smooth content increment in the coarse fraction (Figure 52(b)). Enrichment that after 10 min of grinding is redistributed in the different particle sizes (Figure 53(b)). This could be caused by the low content of these elements in the original sample. Similar results were previously observed by Yao et al. (2014), who concluded that the comminution process, either through continuous fluidization or ball milling, does not impact the mobility and redistribution of elements present at the ppm level.

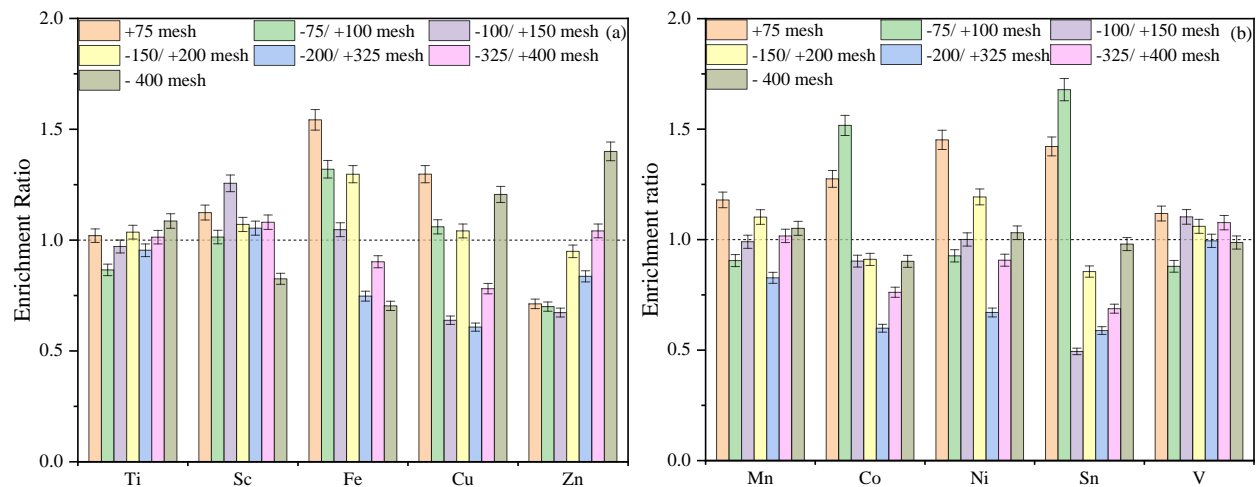


Figure 52. (a) Major and (b) minor elements distribution per size fraction from the BA raw sample.

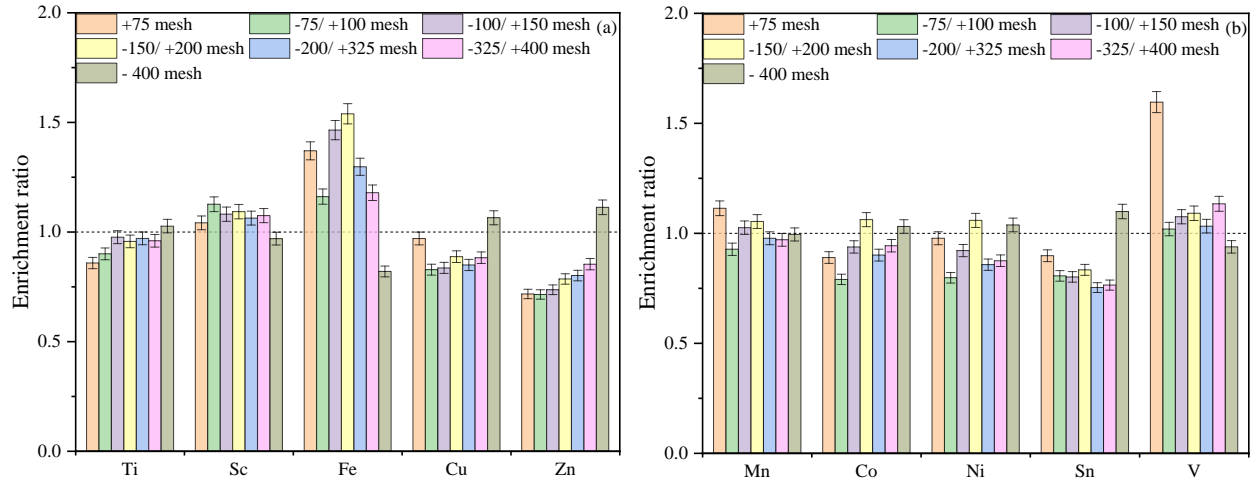


Figure 53. (a) Major and (b) minor elements distribution per size fraction from the BA sample after 10 min grinding time.

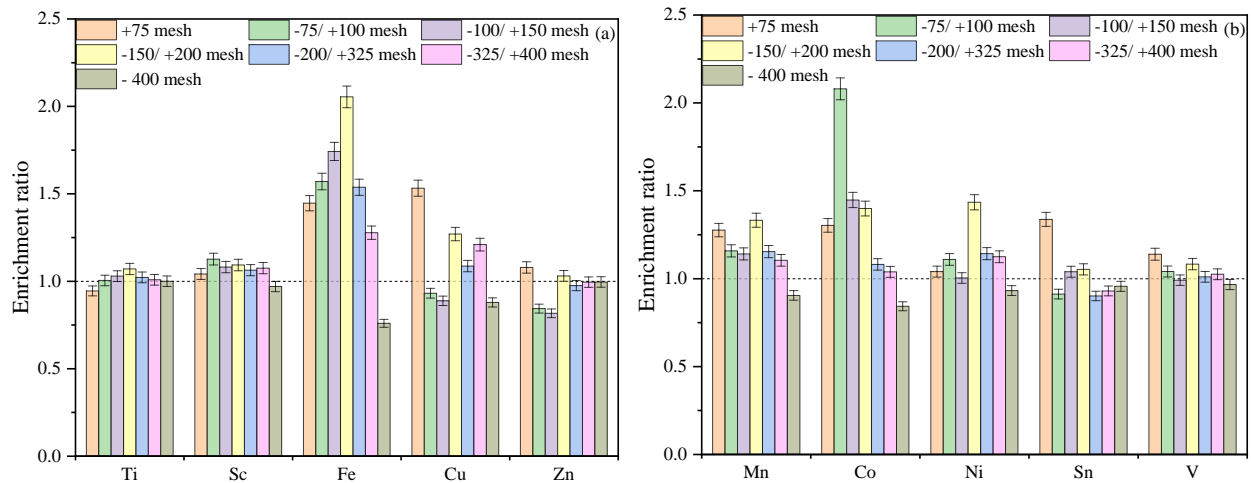


Figure 54. (a) Major and (b) minor elements distribution per size fraction from the BA sample after 30 min grinding time.

5.2.2 Flotation test

The flotation tests were conducted to determine whether the remaining organic matter in the BA sample could be removed and therefore improve the valuable elements' concentration and recuperation without optimizing flotation performance; thus, only a few tests were conducted. Likewise, the correlation between the froth flotation recovery, the unburned carbon removal, and the particle size of the sample were assessed. The flotation performance was evaluated under four test conditions based on two parameters, the valuable elements recovery and the loss of ignition of the samples subjected to a different grinding time as described in Table 8. The loss of ignition refers to the total amount of material lost, including organic matter

content and the CO₂ lost from carbonates. The LOI was calculated following equation (3) described in section 2.2.3.2. The results of the loss of ignition calculated for the concentrate stream according to the different grinding times and test conditions are presented in Table 9. The raw BA sample, which is the feed material, has an average of 14.73% loss of ignition. Nevertheless, Table 9 revealed a considerable reduction in the organic matter content under Test 2 and Test 3 conditions. In contrast, the loss of ignition of the concentrate by-products from the froth flotation obtained under the Test 4 condition were lower than the raw material but higher than the results obtained following the Test 2 and Test 3 conditions. These results suggest a correlation between the test efficiency in removing the organic matter and the pH of the slurry.

Table 9. Loss of ignition of the concentrate stream generated by the forth flotation tests.

	Test 1	Test 2	Test 3	Test 4
UB-1	6.63 %	5.23 %	3.23 %	11.10 %
UB-2	6.55 %	4.25 %	4.13 %	7.10 %
UB-3	7.72 %	6.45 %	6.43 %	9.13 %
UB-4	11.87 %	10.38 %	10.42 %	12.38 %

As for the valuable elements' recovery, Figure 55 (a-e) presents the enrichment ratio of the major elements (Ti, Sc, Fe, Cu, and Zn), achieved after the organic matter removal and the likely liberation of the element associated and embedded in it. The graphs are presented by valuable elements and each line color represent the results obtained under different test conditions, while each axis refers to the different grinding times. The literature review states that longer grinding times expose the organic matter and liberate the elements associated with it. This phenomenon benefits the interaction between the reagents and the solid material, favoring the valuable elements concentration. Valuable elements, such as Ti and Fe (Figure 55 (a, c)), were slightly enriched when the sample was ground for 60 min and the slurry was floated under Test 2 and Test 3 conditions, which reduced the organic matter to 6.45% and 6.43%, respectively. The results for Sc, Cu and Zn (Figure 55 (b, d, e)) exhibited higher enrichment ratios when the sample was ground for less than 60 min. These results indicate that efficient organic matter removal and short grinding times can contribute to the liberation of these elements. Among all the conditions used to conduct the flotation tests, the lowest loss of ignition percentage and highest enrichment ratios were obtained in the Test 2 conditions and under shorter grinding times. This suggests that the generation of fine particles could worsen the flotation performance.

Regarding the test conditions, the lowest organic matter content and highest enrichment ratios were achieved in most valuable elements when the pH was stabilized between 8.8 to 9.2 and controlled throughout the test. For example, the enrichment ratios achieved for Fe when the pH was not adjusted (Test

4) were below 1.0 regardless of the grinding time. These results can be explained by the electrostatic force changes caused by the shifts of the zeta potential led by the pH affecting the dispersion and particles' aggregation (Kemal, 2007; Carlson & Kawatra, 2013). Concerning the collector dosage, 0.338 g/ton used in Test 2 (depicted in blue in Figure 55), appears to favor the organic matter removal but saturated the slurry because it does not significantly improve the overall major elements concentration compared to the results obtained using 0.168 g/ton of collector (depicted in red in Figure 55).

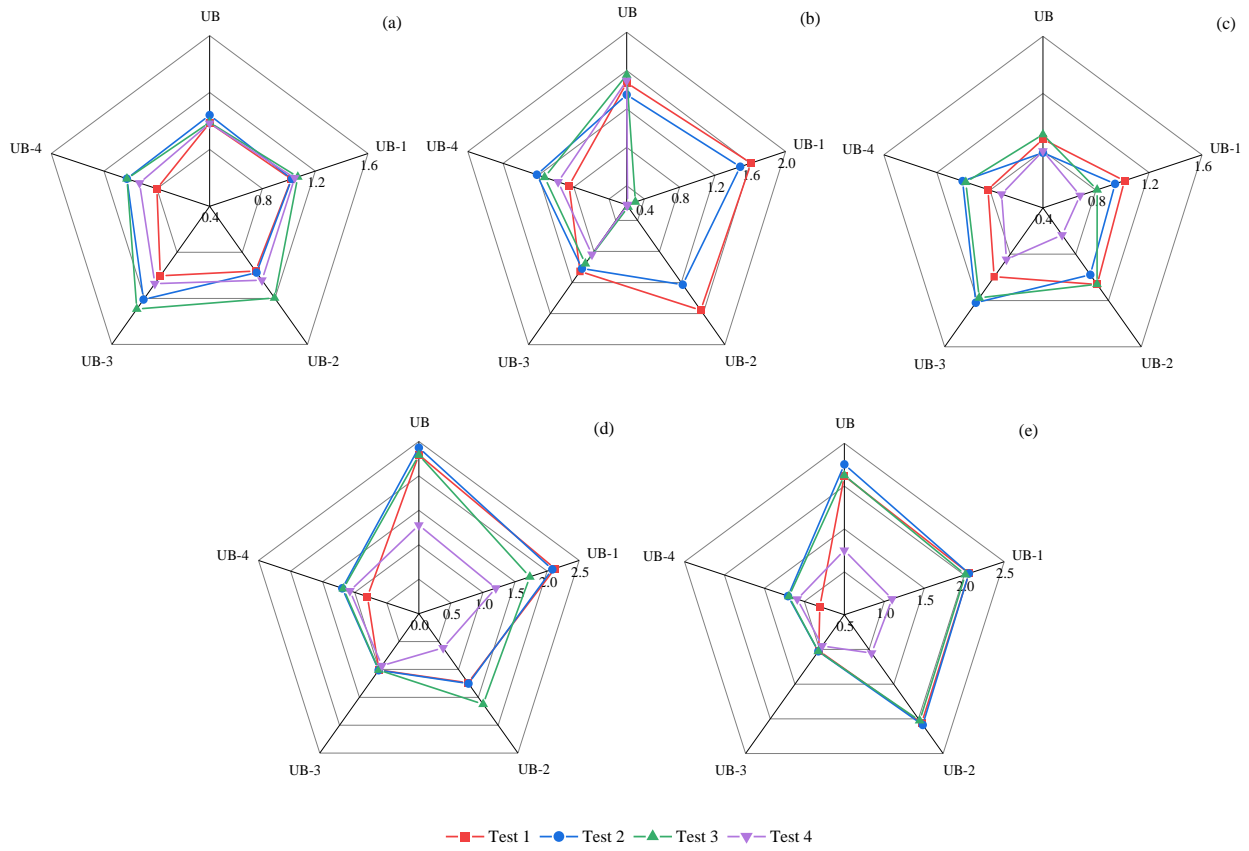


Figure 55. Effect of the grinding residence time of the BA sample in the enrichment ratio of (a) Ti, (b) Sc, (c) Fe, (d) Cu, and (e) Zn from a forth flotation carried out under different set up conditions described in Table 8.

The enrichment of the minor elements (Mn, Co, Ni, Sn, and V) achieved through the froth flotation tests are shown in Figure 56 (a-e). It can be observed from Figure 56 (a-e) that the pH strongly correlates with the overall performance and valuable elements concentration. Similar results were observed with the major elements and previously described in Figure 55 (a-e). Breitenstein et al. (2016) determined that slightly alkaline values favor the valuable elements' recovery, especially Cu and its mineral phases and

alloys. Additionally, when the sample was subjected to less than 60 min of grinding time, lower organic content and higher enrichment ratios were achieved for Co, Sn, and V (Figure 56. b, d, and e, respectively), suggesting that the presence of fine particles could decrease the valuable elements' recovery through flotation. Several studies (Arnold & Aplan, 1986; Yu et al., 2017; Norori-McCormac et al., 2017) agreed that the presence of fine particles could generate a layer of slime that may coat the particles. This could obstruct the interaction between the particles and the reagents, ultimately resulting in increased collector consumption.

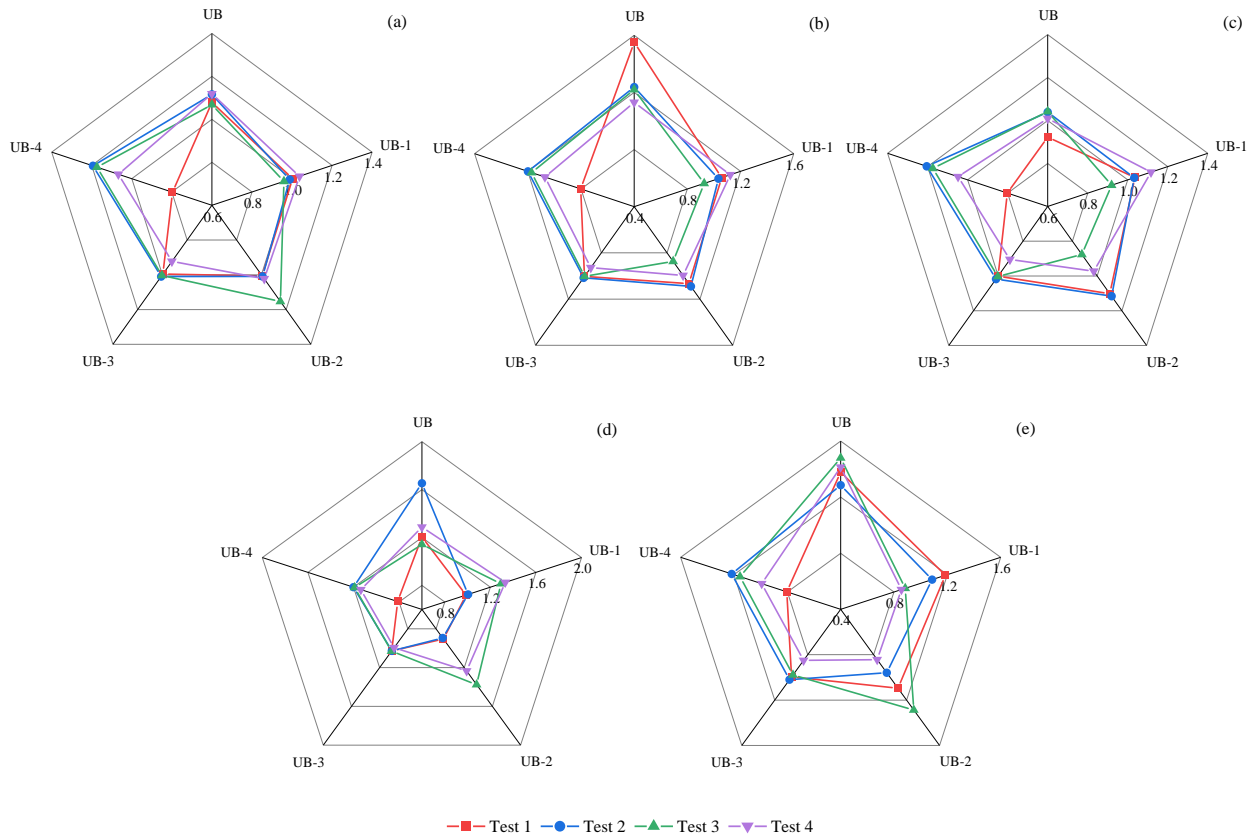


Figure 56. Effect of the grinding residence time of the BA sample in the enrichment ratio of (a) Mn, (b) Co, (c) Ni, (d) Sn, and (e) V from a froth flotation carried out under different set up conditions described in Table 8.

5.2.3 Magnetic separation

After determining the redistribution of the valuable elements after 10-, 30-, 60-, and 90-min grinding times, a magnetic separation test was performed to establish the correlation between the grinding time and the recovery of the valuable elements through wet magnetic separation. According to a study developed by Youcai, Z. (2017), the recovery rate of Fe could be increased from 6.4% to 7.6% and up to

15% when reducing the particle size from 300-100 mm to 100-80 mm and 70-25 mm, respectively. Figure 57 (a, b) reveals significant Fe, Mn, Co, and Ni enrichment in the magnetic fraction after 10 min of grinding time. The enrichments ratios reached were 1.97, 1.57, 1.50, and 1.64, respectively. The high Fe recovery achieved after 10 min of grinding could be explained by Del Valle-Zermeño et al. (2017) who inferred that a ferrous oxide layer coats the small ferrous particles in the MSWI-BA, causing the obstruction of the magnetic properties of the particles. Overall, smaller particle sizes, as a result of longer grinding times, tend to decrease the recovery of valuable elements. This could be caused by the centrifugal force exerted by the agitator being greater than the magnetic force exerted by the magnet.

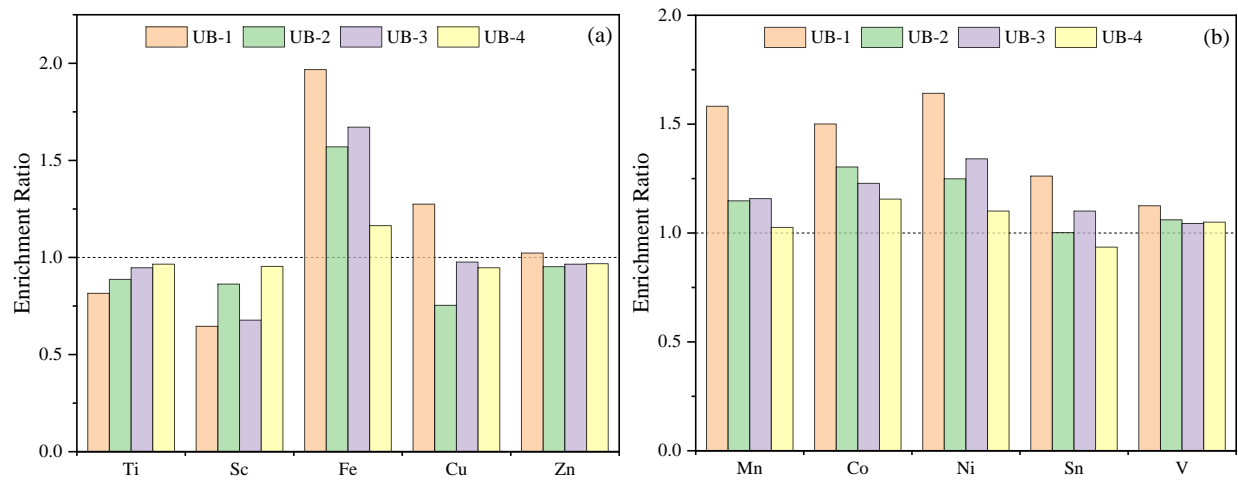


Figure 57. Effect of the grinding time of the BA sample on the (a) major elements and (b) minor elements recovery after a wet magnetic separation.

5.2.4 Leachability of the valuable metals

In order to evaluate the effect of particle size reduction on the valuable elements leaching behavior and kinetics, a series of acid-leaching tests were conducted under different experimental conditions. To assess the valuable elements' leachability, recovery, and their correlation with the particle size as a function of the grinding time, the tests were carried out using HCl as a lixiviant at 0.5 M, 1 M, 1.5 M, and 2 M. The results are illustrated in Figure 58 (a-d). Overall, the figure reveals negligible fluctuations in the leaching behavior of the valuable elements when the sample is subjected to longer grinding time, suggesting a low correlation between these two variables. Contrary to this proposition, the lixiviant concentration significantly affected the recovery of some valuable elements. For example, Fe, Co, Mn, Ni, and Sn increased their leachability by 28%, 10%, 11%, 19%, and 21%, respectively, when using HCl at 2.0 M (Figure 57 (d)) rather than HCl at 0.5 M (Figure 57 (a)) as a lixiviant. These results are coherent with Dou et al. (2017) conclusion that acidic conditions can lead to higher recovery values. On the other hand, Cu and Zn showed a high leachability capability, reaching recoveries greater than 80% when using 0.5 M HCl

(Figure 57 (a)). Meanwhile, V, Ti, and Sc were observed to have low leachability capabilities because they did not exceed 40% recovery even when using strong acid conditions such as HCl at 2.0 M (Figure 57 (d)).

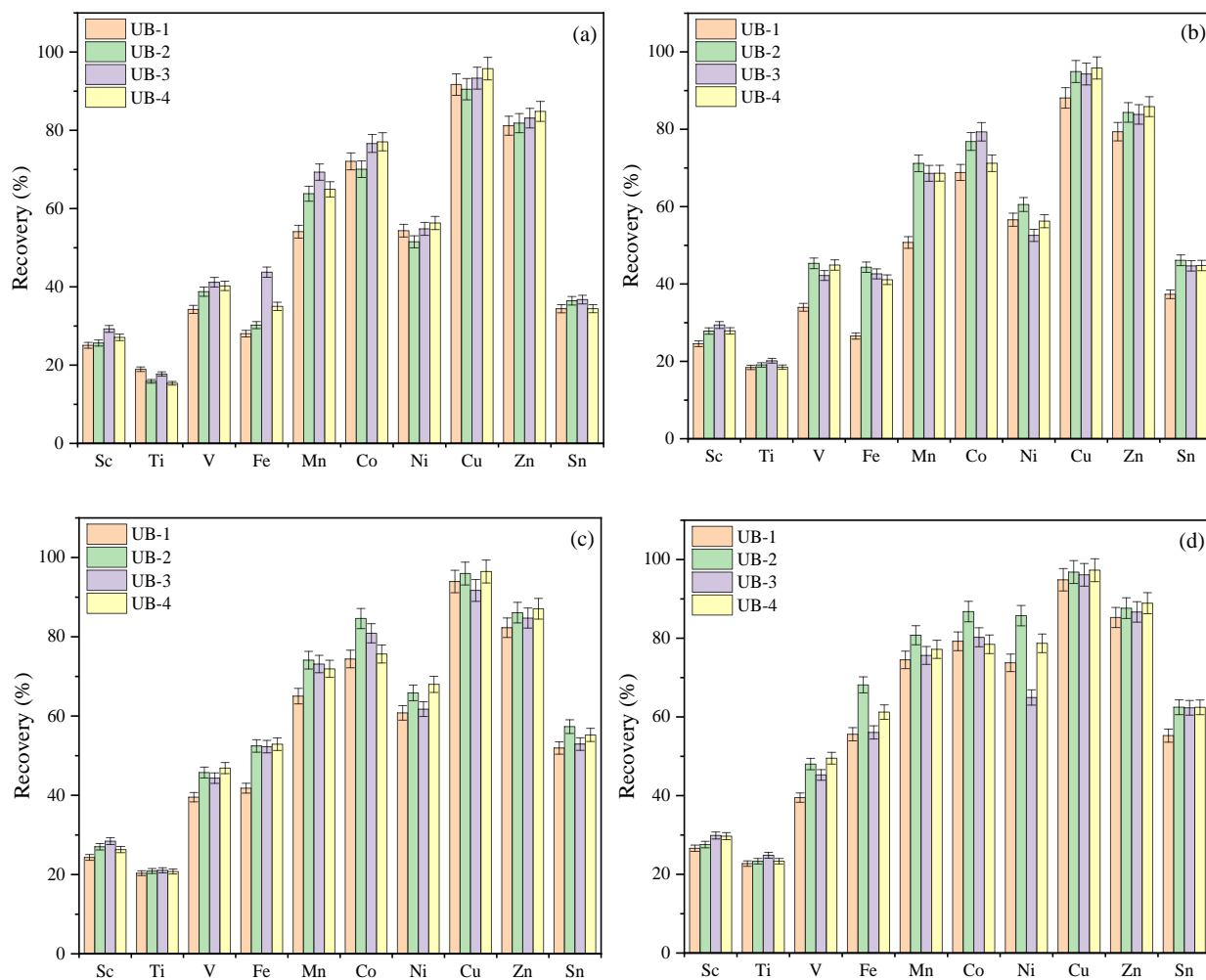


Figure 58. Valuable elements leachability at (a) 0.5 M HCl, (b) 1.0 M HCl, (c) 1.5 M HCl, and (d) 2.0 M HCl as a function of the grinding time.

Likewise, the effect of the particle size, as function of the grinding time on the leaching kinetics of the valuable elements, was assessed using HCl at 1.0 M as a lixiviant. The tests were conducted for a period of 120 min at 75°C. Representative samples were taken from the slurry at 5, 30, 60, and 120 min. Figure 59 (a-d) shows the leaching kinetics results after 10, 30, 60, 90 min of grinding, respectively. The results from the 10 min ground sample (Figure 59 (a)) suggest that Ti, Sc, V, Sn reach equilibrium in the first 5 min of leaching, while Mn, Ni, Co, and Zn take 60 min of leaching to achieve the maximum recovery and the reaction equilibrium. As for the Fe and Cu, after 60 min of reaction still present considerable fluctuations in their recovery values. However, Cu, Zn Co, Ni and Mn can be considered metals with high leachability properties because they achieve a recovery greater than 70%. The leachability kinetics of Ti, Sc, and Sn

remained the same when the BA sample is ground for 30 min (Figure 59 (b)). However, the recovery of V, Zn, Ni, and Co increased 41%, 77%, 74%, and 70%, respectively after 5 min of reaction, indicating that grinding times between 10 to 30 min could favor their recovery. In contrast, results from longer grinding times, such as 60 and 90 min (Figure 59 (c-d)) have negligible effect in the recovery and the leaching kinetic of the valuable elements.

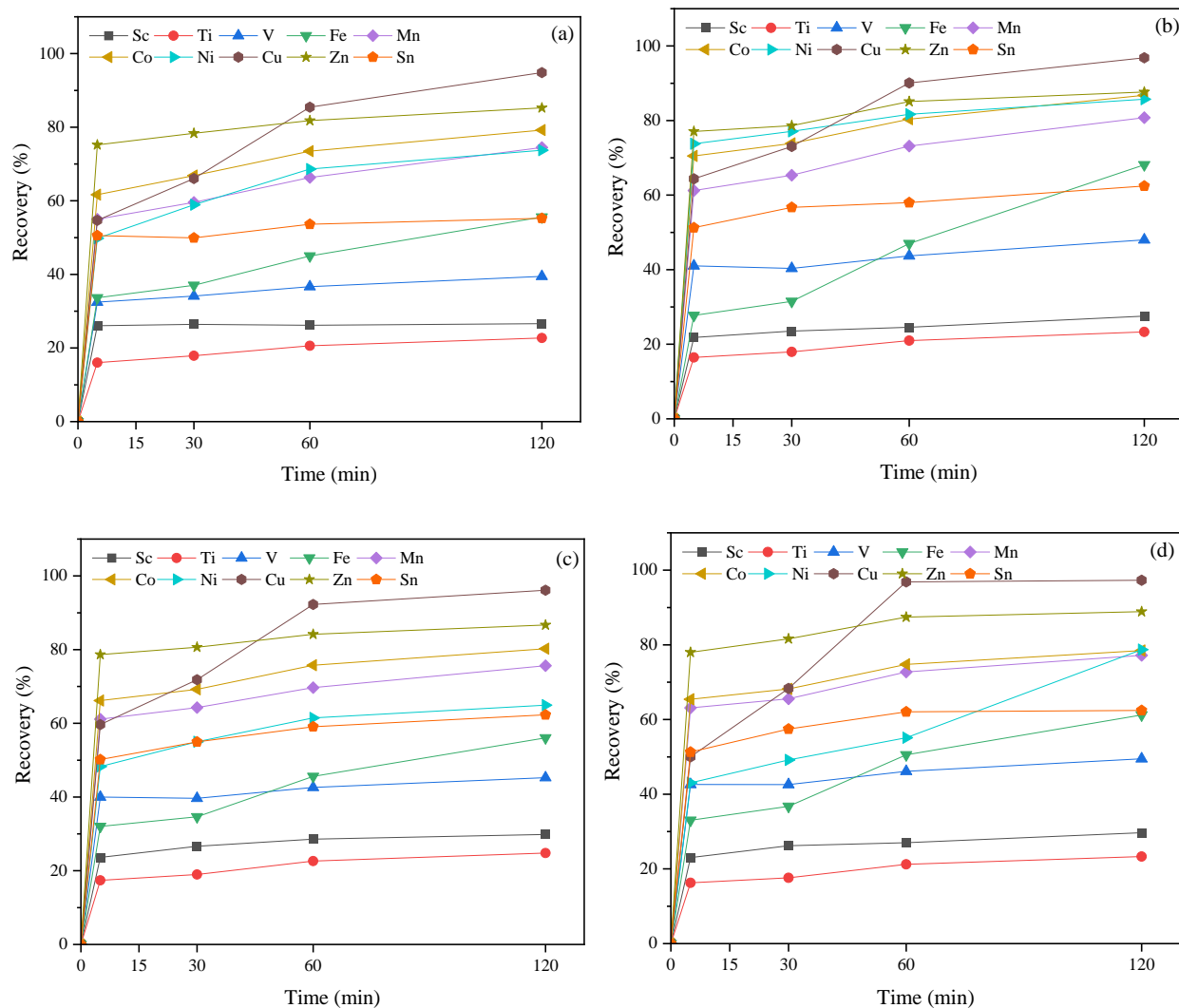


Figure 59. Effect of the (a) 10 min, (b) 30 min, (c) 60 min, and (d) 90 min grinding time on the leaching kinetics of the valuable elements using 1.0 M HCl.

5.3 Conclusions

A MSWI BA sample was subjected to an evaluation of the effect of the particle size reduction to understand the intraparticle heterogeneity and the effect of the particle size reduction on the physical properties, chemical properties, and the recovery indicators. After analyzing the particle size distribution

after grinding the sample for different residence times, it was determined that the fine particles require more energy to break. Most of the size fractions reach a steady state within the first 30 min of grinding. This represents a limitation because 70% of the BA sample are particles that belong to a size fraction below 100 mesh, which could imply a higher energy consumption to comminute. The elemental content revealed that the comminution process promotes the generation of a more specific surface area that enables the adherence of elements, such as Fe, Zn, and Cu, in the fine fraction.

In contrast, the minor elements showed an even enrichment among the size fractions. It is postulated that the comminution process does not impact the mobility and redistribution of the elements concentrated in a ppm level. From the concentration mechanisms used in this study, the froth flotation allowed Cu and Zn to be efficiently concentrated when the sample was ground for less than 30 minutes, reaching enrichment ratios of 2.41 and 2.25, respectively. Wet magnetic separation results revealed significant enrichment ratios of Fe, Mn, Co, and Ni after 10 min of grinding. However, the recovery of valuable elements decreased in the samples subjected to longer grinding times. This could be caused by the centrifugal force exerted by the agitator being larger than the magnetic force exerted by the magnet. These results suggest that combining subsequent beneficiation processes could lead to better valuable elements concentration yield and their recovery optimization.

Additionally, the effect of the particle size reduction, as a function of the grinding time on the leachability and valuable elements mobility was evaluated by acid leaching tests. The results showed negligible fluctuations in the leaching behavior of the valuable elements when the sample is subjected to longer grinding times. In contrast, the concentration of leached valuable elements varied significantly when using different lixiviant concentrations. The Cu, Fe, Zn, Co, and Ni leaching kinetics and recoveries in the leaching tests revealed that these metals are suitable for concentrating, enriching, and recovering through hydrometallurgical methods.

Chapter 6 Conclusions and recommendations for future work

6.1 Conclusions

The literature regarding the MSWI composition, behavior, and speciation is still limited. Previous characterization studies have quantified the potential toxic elements (PTE) and the heavy metal content in the incineration by-products driven by environmental concerns. However, a comprehensive characterization and a thorough overview of the physical, chemical, and mineralogical characterization of the BA in order to determine the most suitable mineral processing method is not yet available in the literature. In this work, one BA and one FA sample were analyzed to determine their elemental composition and distribution to select the most useful residue for recovering valuable elements. The elemental composition was determined by a combination of the digestion method, XRD and XRF tests. The transfer coefficient was calculated to evaluate the valuable elements' distribution among the MSWI by-products. The results revealed that the BA is a promising source of valuable elements, such as Ti, Fe, Zn, and Cu with a total concentration of 9.22, 60.45, 3.91, and 2.15 g/kg, respectively. Furthermore, the leachability and reaction kinetics of the valuable elements from the BA sample were assessed. Metals such as Fe, Mn, Co, Cu, and Zn were extracted using 1M HCl as a lixiviant, reaching recovery values greater than 80%. As for the kinetics of the reaction, equilibrium was achieved within the first 30 min. On the other hand, minor elements like Co and Ni were sensitive to the reaction temperature, suggesting that higher recoveries can be obtained by increasing the leaching temperature.

In order to assess the valuable elements' mobility and association characteristics, a sequential chemical extraction (SCE) semiquantitative test and SEM-EDX analysis were performed. The results showed that a minimal amount of the valuable elements was present as water-soluble, ion-exchangeable, or acid-soluble forms. 83% of Ti and 82% of Sc occurred in an insoluble form, indicating that these elements will not dissolve under strong acidic and oxidizing conditions, which is consistent with the leaching results obtained in this study. The oxidizable distribution among the valuable elements is higher in Cu and Sn. Additionally, about 10% of the Fe is present in reducible mode. This result is consistent with the information obtained by the EDX spectra. Fe was found in varieties of Fe-O ratios, indicating metal oxides in different oxidation states and structural arrangements. The SEM-EDX results revealed the presence of magnetite-spinel in transition to aluminum-spinel by octahedral substitution of Fe^{3+} by Si^{4+} and Al^{3+} and tetrahedral substitution of Fe^{2+} by Mg^{2+} , Ca^{2+} , and Mn^{2+} . These substitutions in the crystalline structure also explained

Mn, Cr, and Ni enrichment in the Fe-bearing particles. Metallic inclusions, such as Fe-S, Fe-Cu, Cu-S, and Fe-P, were also identified as the predominant metal speciation in the BA sample.

Once the chemical and mineralogical characterization of the BA sample was completed, the sample was divided according to its physical properties, such as particle size, magnetic susceptibility, and density. The sample was fractionated in 5 size fractions (50/+100 mesh, -100/+170 mesh, -170/+200 mesh, -200/+325 mesh, and -325 mesh) and subjected to a series of physical characterization tests. The elemental composition per size fraction revealed that Zn is enriched in the finer fraction, while Fe and Sc are enriched in the coarse fraction. From the particle size distribution and elemental enrichment per size fraction, it can be concluded that classifying the sample into the coarse, middle, and fine-size fractions could lead to better metal concentration yields.

Regarding the valuable elements' enrichment ratios and recovery achieved through magnetic separation, the valuable elements that exhibited affinity with Fe-bearing particles were efficiently concentrated and achieved higher enrichment ratios. The enrichment ratio of Fe was close to 2.0 among the different particle sizes, and recovery was nearly 80%. Metals such as Cu and Co were enriched by 1.51 and 1.66, respectively, suggesting that the magnetic separation performance and enrichment are a function of the bound of multi-metallic oxides fractions. However, when decreasing the size fraction, the centrifugal force exerted by the agitator was greater than the magnetic force exerted by the magnet causing a reduction in the concentration of the material with magnetic susceptibility. The mineralogical characterization of the magnetic fraction concluded that the main Fe-rich constituents existed in chemical forms of iron oxides, such as magnetite, hematite with substituted varieties, spinel group, and metallic inclusions. The enrichment ratios of Mn, Cr, Cu, and Ni obtained through magnetic separation can be explained by the presence of metallic inclusions, where these elements exhibit an affinity for the iron-bearing particles. Other non-targeted elements, such as Si, Al, and Ca, were enriched because the Fe-rich minerals were likely embedded in amorphous siliceous glass or a partially crystallized aluminosilicate matrix.

In comparison, the 2.95 SG density test reached enrichment ratios higher than 2.0 in Fe, Cu, Co, and Ni in the coarse fraction of the BA fraction, which decreases when reducing the size fraction. Subsequently, the float material from the 2.95 SG test was collected, rinsed, dried and then used as a feed for a second-density separation stage at 2.6 S.G. The results from this test showed that the sink fraction yield increased as the medium density decreased, and the enrichment ratios of the minor elements (Mn, Co, Ni, Sn, and V) were similar across the different size fractions. Complementary information was obtained by the mineralogical characterization of the sink fraction. The Cu enrichment, which was higher than the magnetic separation results, can be justified by the relatively high specific gravity of its mineral phases,

like copper oxide, copper sulfate, and cupric sulfite, with specific gravities of 6.31, 3.6, and 4.76, respectively. The slight enrichment of Ti when using a 2.95 cutoff density could be attributed to its predominant speciation as calcium titanate (CaTiO_3), considering that this mineral phase has a specific gravity of 3.98.

Finally, in this study, the BA sample was subjected to an evaluation of the effect of the particle size reduction to understand the intraparticle heterogeneity and determine the effect of the particle size reduction on the physical properties and recovery indicators. Most of the particles reached a fine size fraction, defined as a diameter below $45\mu\text{m}$ after 60 min of grinding. The elemental content revealed that the comminution process promotes the interaction of Fe, Zn, and Cu, in the fine fraction, by generating more surface area. In contrast, the minor elements were not significantly enriched by reducing the size fraction, suggesting that the comminution process does not impact the mobility and redistribution of the elements in low concentrations. From the beneficiation methods used in this section, the froth flotation using 0.338 g/ton Diesel as a collector and adjusting the pH between 8.8 to 9.2 and controlled throughout the test can efficiently reduce the organic matter content in the BA sample from 14.73% to 5.23%, 4.25%, 6.45% or 10.38% according to the grinding time (10, 30, 60, 90 min, respectively). Slight enrichment ratios were observed in the concentrate stream of the froth flotation, suggesting that these elements exhibit an affinity and are associated with the organic matter in the BA sample. The wet magnetic separation results revealed significant enrichment ratios of Fe, Mn, Co, and Ni after 10 min of grinding. These results suggest that combining subsequent beneficiation processes could lead to better valuable elements concentration yield and recovery optimization. These results reinforce the opportunity to find and extract valuable elements from alternative sources, turn the mining industry into less natural resource intensive, and keep materials, energy, and resources in a lifecycle loop while reducing landfilling disposal.

6.2 Recommendations for future work

Throughout the development of this study a series of limitations, methodologies and information were collected and are summarized in this section as recommendations for future studies, research, and work related to the MSWI characterization and beneficiation.

1. The results presented in this study were obtained by using the MSWI by-products from only one Waste-to-Energy facility in the U.S and the results cannot be taken as a generalization of all MSWI by-products. As mentioned before, the composition and elemental distribution in the incineration by-product can vary depending on economic development, urbanization, economic activities, seasons, and combustion process. However, the key factor to determine the potential value in the ashes generated by the incineration of MSW, is the changes in the composition that the season

could cause. A more robust dataset of the valuable element content in the MSW as function of the season, can lead to a stockpile segregated based on their feed grades, hence the concentration process can be standardized and reduce redundant test. This information would also contribute to minimizing the sampling error that would enable the development of more accurate beneficiation models.

2. This study presented an alternative to recover valuable elements and with it, contribute to the circular economy. However, the final BA application would determine the need for specific treatment technologies, environmental requirements, and technical barriers to overcome.
3. The results presented in this research constitute a basis for defining specific physical properties concentration routes. However, the extraction and purification of the valuable elements concentrated is still under investigation and a technical evaluation will be needed.
4. The comminution process used in the evaluation of the effect of the particle size reduction was carried out using ball milling for grinding. However, it is necessary to investigate the effect of alternative or unconventional particle size reduction mechanism in order to reduce the fine particle generation which could hinder the beneficiation effectiveness.
5. As expressed in this study, valuable elements such as Mn, Cr, Cu, and Ni exhibit an affinity for the iron-bearing particles, which were not identified by XRD spectrum. This is likely due to the existence of iron poorly crystallized or embedded in amorphous siliceous glass or in a partially crystallized aluminosilicate matrix. To have a better understanding of the tendency of these elements to form a bond with the Fe-particles, their interaction and reactivity, further investigation regarding the amorphous phase is recommended.
6. The wet magnetic separation performed in this study was chosen over the dry magnetic separation to avoid the adherence of non-magnetic particles into the magnetic fraction caused by the strong electrostatic attraction between the pulverized ash particles. However, by performing a wet magnetic separation in a water medium, it cannot be ensured that the speciation remained the same through the process. Dissolution of soluble constituents and possible reactions can have taken place between the medium and the ash. Additional investigation is suggested to suppress chemical reactions and mineralogical changes in the sample.
7. The gravity separation test carried out in this study was performed using lithium metatungstate as a heavy liquid medium. By increasing the cutoff density, the valuable elements, with a specific

gravity above 2.95, were separated from the bulk ash fraction, with an approximate specific gravity of 2.6. However, further investigation is required to overcome the technical barriers and limitations to scale-up the concentration process.

References

- Alam, Q., Florea, M. V. A., Schollbach, K., & Brouwers, H. J. H. (2017). A two-stage treatment for Municipal Solid Waste Incineration (MSWI) bottom ash to remove agglomerated fine particles and leachable contaminants. *Waste Management*, 67, 181–192. <https://doi.org/10.1016/j.wasman.2017.05.029>
- Alam, Q., Schollbach, K., Rijnders, M., van Hoek, C., van der Laan, S., & Brouwers, H. J. H. (2019). The immobilization of potentially toxic elements due to incineration and weathering of bottom ash fines. *Journal of Hazardous Materials*, 379, 120798. <https://doi.org/10.1016/j.jhazmat.2019.120798>
- Alam, Q., Schollbach, K., van Hoek, C., van der Laan, S., de Wolf, T., & Brouwers, H. J. H. (2019). In-depth mineralogical quantification of MSWI bottom ash phases and their association with potentially toxic elements. *Waste Management*, 87, 1–12. <https://doi.org/10.1016/j.wasman.2019.01.031>
- Arickx, S., Van Gerven, T., Boydens, E., L'hoëst, P., Blanpain, B., & Vandecasteele, C. (2008). Speciation of Cu in MSWI bottom ash and its relation to Cu leaching. *Applied Geochemistry*, 23(12), 3642–3650. <https://doi.org/10.1016/j.apgeochem.2008.09.006>
- Arnold, B. J., & Aplan, F. F. (1986). The effect of clay slimes on coal flotation, part I: The nature of the clay. *International Journal of Mineral Processing*, 17(3), 225–242. [https://doi.org/10.1016/0301-7516\(86\)90058-X](https://doi.org/10.1016/0301-7516(86)90058-X)
- Astrup, T., Riber, C., & Pedersen, A. J. (2011). Incinerator performance: effects of changes in waste input and furnace operation on air emissions and residues. *Waste Management & Research: The Journal for a Sustainable Circular Economy*, 29(10_suppl), S57–S68. <https://doi.org/10.1177/0734242x11419893>
- Back, S., Ueda, K., & Sakanakura, H. (2020). Determination of metal-abundant high-density particles in municipal solid waste incineration bottom ash by a series of processes: Sieving, magnetic separation, air table sorting, and milling. *Waste Management*, 112, 11–19. <https://doi.org/10.1016/j.wasman.2020.05.002>
- Blanc, D., Gonzalez, L., Lupsea-Toader, M. *et al.* Mineralogical Evolution and Leaching Behaviour of a Heap of Bottom Ash as a Function of Time: Influence on Its

- Valorization. *Waste Biomass Valor* 9, 2517–2527 (2018). <https://doi.org/10.1007/s12649-018-0444-1>
- Bond, F. C. (1953, January 1). *Mineral Beneficiation - The Third Theory of Comminution - Discussion The Third Theory of Comminution*. OneMine. <https://www.onemine.org/documents/mineral-beneficiation-the-third-theory-of-comminution-discussion-the-third-theory-of-comminution>
- Breitenstein, B., Elwert, T., Goldmann, D., Haas, A., Schirmer, T., & Vogt, V. (2016). Froth Flotation of Copper and Copper Compounds from Fine Fractions of Waste Incineration Bottom Ashes. *Chemie Ingenieur Technik*, 89(1-2), 97–107. <https://doi.org/10.1002/cite.201600017>
- British Geological Survey. (2007). *Definition, mineralogy and deposits Definition and characteristics*. https://www2.bgs.ac.uk/mineralsuk/download/mineralProfiles/copper_profile.pdf
- Bruder-Hubscher, V., Lagarde, F., Leroy, M. J. F., Coughanowr, C., & Enguehard, F. (2002). Application of a sequential extraction procedure to study the release of elements from municipal solid waste incineration bottom ash. *Analytica Chimica Acta*, 451(2), 285–295. [https://doi.org/10.1016/s0003-2670\(01\)01403-9](https://doi.org/10.1016/s0003-2670(01)01403-9)
- Bunge, R. (2019). Recovery of metals from waste incinerator bottom ash. In *UMTEC*. Institut für Umwelt- und Verfahrenstechnik UMTEC. https://www.umtec.ch/fileadmin/user_upload/umtec.hsr.ch/Dokumente/Metals_from_MWIBA_6_2019.pdf
- Carlson, J. J., & Kawatra, S. K. (2013). Factors Affecting Zeta Potential of Iron Oxides. *Mineral Processing and Extractive Metallurgy Review*, 34(5), 269–303. <https://doi.org/10.1080/08827508.2011.604697>
- Caviglia, C., Confalonieri, G., Corazzari, I., Destefanis, E., Mandrone, G., Pastero, L., Boero, R., & Pavese, A. (2019). Effects of particle size on properties and thermal inertization of bottom ashes (MSW of Turin's incinerator). *Waste Management*, 84, 340–354. <https://doi.org/10.1016/j.wasman.2018.11.050>
- Chen, L., Liao, Y., Ma, X., & Lu, S. (2020). Heavy metals chemical speciation and environmental risk of bottom slag during co-combustion of municipal solid waste and sewage sludge.

- Journal of Cleaner Production*, 262, 121318.
<https://doi.org/10.1016/j.jclepro.2020.121318>
- Chimenos, J. M., Fernández, A. I., Miralles, L., Segarra, M., & Espiell, F. (2003). Short-term natural weathering of MSWI bottom ash as a function of particle size. *Waste Management*, 23(10), 887–895. [https://doi.org/10.1016/s0956-053x\(03\)00074-6](https://doi.org/10.1016/s0956-053x(03)00074-6)
- Chimenos, J. M., Segarra, M., Fernández, M. A., & Espiell, F. (1999). Characterization of the bottom ash in municipal solid waste incinerator. *Journal of Hazardous Materials*, 64(3), 211–222. [https://doi.org/10.1016/S0304-3894\(98\)00246-5](https://doi.org/10.1016/S0304-3894(98)00246-5)
- De Boom, A., Degrez, M., Hubaux, P., & Lucion, C. (2011). MSWI boiler fly ashes: Magnetic separation for material recovery. *Waste Management*, 31(7), 1505–1513. <https://doi.org/10.1016/j.wasman.2011.01.002>
- del Valle-Zermeño, R., Gómez-Manrique, J., Giro-Paloma, J., Formosa, J., & Chimenos, J. M. (2017). Material characterization of the MSWI bottom ash as a function of particle size. Effects of glass recycling over time. *Science of the Total Environment*, 581-582, 897–905. <https://doi.org/10.1016/j.scitotenv.2017.01.047>
- Department of Interior. (2022, February 22). *U.S. Geological Survey Releases 2022 List of Critical Minerals* / U.S. Geological Survey. [www.usgs.gov. https://www.usgs.gov/news/national-news-release/us-geological-survey-releases-2022-list-critical-minerals](https://www.usgs.gov/news/national-news-release/us-geological-survey-releases-2022-list-critical-minerals)
- Dou, X., Ren, F., Nguyen, M. Q., Ahamed, A., Yin, K., Chan, W. P., & Chang, V. W.-C. (2017). Review of MSWI bottom ash utilization from perspectives of collective characterization, treatment and existing application. *Renewable and Sustainable Energy Reviews*, 79, 24–38. <https://doi.org/10.1016/j.rser.2017.05.044>
- Elliott, J. E., Kamilli, R. J., Miller, W. R., & K Eric Livo. (1997). *VEIN AND GREISEN SN AND W DEPOSITS (MODELS 15a-c; Cox and Bagby, 1986; Reed, 1986a, b)*. <https://pubs.usgs.gov/of/1995/ofr-95-0831/CHAP9.pdf>
- Emsley, John (2001). "Manganese." *Nature's Building Blocks: An A-Z Guide to the Elements*. Oxford, UK: Oxford University Press. pp. 249–253. ISBN 978-0-19-850340-8.
- Environmental Protection Agency. (2019, February 15). *Energy Recovery from the Combustion of Municipal Solid Waste (MSW)* / US EPA. US EPA. <https://www.epa.gov/smm/energy-recovery-combustion-municipal-solid-waste-msw>

- Environmental Protection Agency. (2020a). *Advancing Sustainable Materials Management: 2018 Fact Sheet Assessing Trends in Materials Generation and Management in the United States*. https://www.epa.gov/sites/default/files/2020-11/documents/2018_ff_fact_sheet.pdf
- Environmental Protection Agency. (2020b). *Best Practices for Solid Waste Management: A Guide for Decision-Makers in Developing Countries*. https://www.epa.gov/sites/default/files/2020-10/documents/master_swmg_10-20-20_0.pdf
- European Commission. (2020, September). *Critical raw materials*. Single-Market-Economy.ec.europa.eu. https://single-market-economy.ec.europa.eu/sectors/raw-materials/areas-specific-interest/critical-raw-materials_en
- Force, E. R., Morgan, B. A., & Herz, N. (1977). GEOLOGY AND RESOURCES OF TITANIUM. In M. C. Blake Jr. (Ed.), *Geological Survey Professional*. United States Government Printing Office. <https://pubs.usgs.gov/pp/0959a-f/report.pdf>
- Fu, S., Lu, J. M., & Yuan, F. Q. (2018). Multivariate analysis of Co, Fe and Ni leaching from tailings following simulated temperature change. *IOP Conference Series: Earth and Environmental Science*, 191, 012125. <https://doi.org/10.1088/1755-1315/191/1/012125>
- Funari, V., Braga, R., Bokhari, S. N. H., Dinelli, E., & Meisel, T. (2015). Solid residues from Italian municipal solid waste incinerators: A source for “critical” raw materials. *Waste Management*, 45, 206–216. <https://doi.org/10.1016/j.wasman.2014.11.005>
- Gao, X., Yuan, B., Yu, Q. L., & Brouwers, H. J. H. (2017). Characterization and application of municipal solid waste incineration (MSWI) bottom ash and waste granite powder in alkali activated slag. *Journal of Cleaner Production*, 164, 410–419. <https://doi.org/10.1016/j.jclepro.2017.06.218>
- Glossary: *Municipal waste - Statistics Explained*. (n.d.). Ec.europa.eu. https://ec.europa.eu/eurostat/statistics-explained/index.php?title=Glossary:Municipal_waste
- Goldschmidt, V. M. (1937). The principles of distribution of chemical elements in minerals and rocks. The seventh Hugo Müller Lecture, delivered before the Chemical Society on March 17th, 1937. *J. Chem. Soc.*, 0(0), 655–673. <https://doi.org/10.1039/jr9370000655>

- Guerrero, A., Fernández, E., Macías, A., & Goñi, S. (2000). Hydrothermal treatment of fly ash from municipal solid waste incineration. *Waste Materials in Construction Wascon 2000 - Proceedings of the International Conference on the Science and Engineering of Recycling for Environmental Protection, Harrogate, England 31 May, 1–2 June 2000*, 178–185. [https://doi.org/10.1016/s0713-2743\(00\)80030-6](https://doi.org/10.1016/s0713-2743(00)80030-6)
- Gupta, S. K., & Chen, K. Y. (1975). Partitioning of Trace Metals in Selective Chemical Fractions of Nearshore Sediments. *Environmental Letters*, 10(2), 129–158. <https://doi.org/10.1080/00139307509435816>
- Han, G.-C., Um, N.-I., You, K.-S., Cho, H.-C., & Ahn, J.-W. (2009). Recovery of Ferromagnetic Material by Wet Magnetic Separation in Coal Bottom Ash. *Geosystem Engineering*, 12(1), 9–12. <https://doi.org/10.1080/12269328.2009.10541292>
- Havlík, T. (2008). Phase Equilibrium of Copper Iron Sulphides. *Hydrometallurgy*, 29–59. <https://doi.org/10.1533/9781845694616.29>
- Holm, O., Wollik, E., & Johanna Bley, T. (2017). Recovery of copper from small grain size fractions of municipal solid waste incineration bottom ash by means of density separation. *International Journal of Sustainable Engineering*, 1–11. <https://doi.org/10.1080/19397038.2017.1355415>
- Hoornweg, D., & Bhada-Tata, P. (2012). What a Waste: A Global Review of Solid Waste Management. *What a Waste: A Global Review of Solid Waste Management*. <https://openknowledge.worldbank.org/handle/10986/17388>
- Hu, H.-Y., Liu, H., Zhang, Q., Zhang, P.-A., Li, A.-J., Yao, H., & Naruse, I. (2014). Sintering characteristics of CaO-rich municipal solid waste incineration fly ash through the addition of Si/Al-rich ash residues. *Journal of Material Cycles and Waste Management*, 18(2), 340–347. <https://doi.org/10.1007/s10163-014-0341-z>
- Hu, Y., Zhang, P., Chen, D., Zhou, B., Li, J., & Li, X. (2012). Hydrothermal treatment of municipal solid waste incineration fly ash for dioxin decomposition. *Journal of Hazardous Materials*, 207–208, 79–85. <https://doi.org/10.1016/j.jhazmat.2011.05.068>
- Hwang, I. H., Nakajima, D., Matsuto, T., & Sugimoto, T. (2008). Improving the quality of waste-derived char by removing ash. *Waste Management*, 28(2), 424–434. <https://doi.org/10.1016/j.wasman.2006.11.015>

- Ilyushechkin, A., He, C., & Hla, S. S. (2020). Characteristics of inorganic matter from Australian municipal solid waste processed under combustion and gasification conditions. *Waste Management & Research: The Journal for a Sustainable Circular Economy*, 39(7), 928–936. <https://doi.org/10.1177/0734242x20966655>
- Jankowski, J., Ward, C., French, D., & Groves, S. (2006). Mobility Of Trace Elements From Selected Australian Fly Ashes And Its Potential Impact On Aquatic Ecosystems. *Fuel*, 85(2), 243–256. <https://doi.org/10.1016/j.fuel.2005.05.028>
- Jiao, F., Zhang, L., Dong, Z., Namioka, T., Yamada, N., & Ninomiya, Y. (2016). Study on the species of heavy metals in MSW incineration fly ash and their leaching behavior. *Fuel Processing Technology*, 152, 108–115. <https://doi.org/10.1016/j.fuproc.2016.06.013>
- Jung, C. H., Matsuto, T., Tanaka, N., & Okada, T. (2004). Metal distribution in incineration residues of municipal solid waste (MSW) in Japan. *Waste Management*, 24(4), 381–391. [https://doi.org/10.1016/s0956-053x\(03\)00137-5](https://doi.org/10.1016/s0956-053x(03)00137-5)
- Jung, C.-H., & Osako, M. (2009). Leaching characteristics of rare metal elements and chlorine in fly ash from ash melting plants for metal recovery. *Waste Management*, 29(5), 1532–1540. <https://doi.org/10.1016/j.wasman.2008.08.014>
- Kaza, S., & Bhada-Tata, P. (2018). Decision Maker's Guides for Solid Waste Management Technologies. *Worldbank.org*. <https://doi.org/http://documents.worldbank.org/curated/en/125061538762440170/Decision-maker-s-guides-for-solid-waste-management-technologies>
- Kaza, Silpa, Lisa Yao, Perinaz Bhada-Tata, and Frank Van Woerden. 2018. What a Waste 2.0: A Global Snapshot of Solid Waste Management to 2050. Urban Development Series. Washington, DC: World Bank. DOI: 10.1596/978-1-4648-1329-0. License: Creative Commons Attribution CC BY 3.0 IGO
- Kemal, D. (2007). *The Effect of Ionic Electrolytes and pH on the Zeta Potential of Fine Coal Particles*. Turkish Journal of Chemistry: Vol. 31: No. 6, Article 3. <https://journals.tubitak.gov.tr/cgi/viewcontent.cgi?article=2431&context=chem>
- Kinnunen, M. K. (2006). A Study on Physical Separation Techniques for Recovery of Metals from Municipal Solid Waste Incineration (MSWI) Bottom Ash. *Aaltodoc.aalto.fi*. <https://aaltodoc.aalto.fi/handle/123456789/19817>

- Kirby, C. S., & Rimstidt, J. D. (1993). Mineralogy and surface properties of municipal solid waste ash. *Environmental Science & Technology*, 27(4), 652–660. <https://doi.org/10.1021/es00041a008>
- Kukier, U., Ishak, C. F., Sumner, M. E., & Miller, W. P. (2003). Composition and element solubility of magnetic and non-magnetic fly ash fractions. *Environmental Pollution*, 123(2), 255–266. [https://doi.org/10.1016/S0269-7491\(02\)00376-7](https://doi.org/10.1016/S0269-7491(02)00376-7)
- Kuo, N.-W., Ma, H.-W., Yang, Y.-M., Hsiao, T.-Y., & Huang, C.-M. (2007). An investigation on the potential of metal recovery from the municipal waste incinerator in Taiwan. *Waste Management (New York, N.Y.)*, 27(11), 1673–1679. <https://doi.org/10.1016/j.wasman.2006.11.009>
- Lassesson, H., & Steenari, B.-M. (2013). Speciation of Copper in Ash from a Fluidized-Bed Boiler Fired with Municipal Solid Waste. *Energy & Fuels*, 27(7), 3891–3897. <https://doi.org/10.1021/ef400386j>
- Liao, Y. (2006). *Correct and incorrect peak Identification in EDX Measurements*. [Www.globalsino.com](http://www.globalsino.com). <https://www.globalsino.com/EM/page1747.html>
- Liu, Y., Li, Y., Li, X., & Jiang, Y. (2008). Leaching behavior of heavy metals and PAHs from MSWI bottom ash in a long-term static immersing experiment. *Waste Management*, 28(7), 1126–1136. <https://doi.org/10.1016/j.wasman.2007.05.014>
- Loginova, E., Volkov, D. S., van de Wouw, P. M. F., Florea, M. V. A., & Brouwers, H. J. H. (2019). Detailed characterization of particle size fractions of municipal solid waste incineration bottom ash. *Journal of Cleaner Production*, 207, 866–874. <https://doi.org/10.1016/j.jclepro.2018.10.022>
- Lu, S. G., Chen, Y. Y., Shan, H. D., & Bai, S. Q. (2009). Mineralogy and heavy metal leachability of magnetic fractions separated from some Chinese coal fly ashes. *Journal of Hazardous Materials*, 169(1-3), 246–255. <https://doi.org/10.1016/j.jhazmat.2009.03.078>
- Mann, S., & Ritchie, G. (1993). The influence of pH on the forms of cadmium in four West Australian soils. *Soil Research*, 31(3), 255. <https://doi.org/10.1071/sr9930255>
- Mantovani, L., Tribaudino, M., Matteis, C. D., & Funari, V. (2021). Particle Size and Potential Toxic Element Speciation in Municipal Solid Waste Incineration (MSWI) Bottom Ash. *Sustainability*, 13(4), 1911. <https://doi.org/10.3390/su13041911>

- Menad, N., Kanari, N., & Save, M. (2014). Recovery of high-grade iron compounds from LD slag by enhanced magnetic separation techniques. *International Journal of Mineral Processing*, 126, 1–9. <https://doi.org/10.1016/j.minpro.2013.11.001>
- Morf, L. S., Gloor, R., Haag, O., Haupt, M., Skutan, S., Lorenzo, F. D., & Böni, D. (2013). Precious metals and rare earth elements in municipal solid waste – Sources and fate in a Swiss incineration plant. *Waste Management*, 33(3), 634–644. <https://doi.org/10.1016/j.wasman.2012.09.010>
- Muchova, L. (2010). *Wet physical separation of MSWI bottom ash* [PhD Thesis Dissertation].
- Muchova, L., Bakker, E., & Rem, P. (2008). Precious Metals in Municipal Solid Waste Incineration Bottom Ash. *Water, Air, & Soil Pollution: Focus*, 9(1-2), 107–116. <https://doi.org/10.1007/s11267-008-9191-9>
- Mulleneers, H. (2001). *Selective Separation of very small Particles by Flotation in Relation to Soil and Sediment Remediation* [PhD Thesis].
- Mutz, D., Gross, T., Hengevoss, D., & Hugi, C. (n.d.). *Waste-to-Energy Options in Municipal Solid Waste Management A Guide for Decision Makers in Developing and Emerging Countries*. Published by: Deutsche Gesellschaft für Internationale Zusammenarbeit (GIZ) GmbH. Retrieved July 23, 2022, from https://www.giz.de/en/downloads/GIZ_WasteToEnergy_Guidelines_2017.pdf
- Nithiya, A., Saffarzadeh, A., & Shimaoka, T. (2018). Hydrogen gas generation from metal aluminum-water interaction in municipal solid waste incineration (MSWI) bottom ash. *Waste Management*, 73, 342–350. <https://doi.org/10.1016/j.wasman.2017.06.030>
- Norori-McCormac, A., Brito-Parada, P. R., Hadler, K., Cole, K., & Cilliers, J. J. (2017). The effect of particle size distribution on froth stability in flotation. *Separation and Purification Technology*, 184, 240–247. <https://doi.org/10.1016/j.seppur.2017.04.022>
- Okamoto, H. (1990). The Fe-P (iron-phosphorus) system. *Bulletin of Alloy Phase Diagrams*, 11(4), 404–412. <https://doi.org/10.1007/bf02843320>
- Olsen, K. (2006). *Bulk Solid Waste Incineration as a Source of Energy: Environmental Success Story, Expensive Diversion, or a Little of Both?* Montclair.edu; Montclair State University. <https://msuweb.montclair.edu/~olsenk/burn.htm>
- Pan, Y., Wu, Z., Zhou, J., Zhao, J., Ruan, X., Liu, J., & Qian, G. (2013). Chemical characteristics and risk assessment of typical municipal solid waste incineration (MSWI) fly ash in China.

- Journal of Hazardous Materials*, 261, 269–276.
<https://doi.org/10.1016/j.jhazmat.2013.07.038>
- Park, S., Kim, M., Lim, Y., Yu, J., Chen, S., Woo, S. W., Yoon, S., Bae, S., & Kim, H. S. (2021). Characterization of rare earth elements present in coal ash by sequential extraction. *Journal of Hazardous Materials*, 402, 123760. <https://doi.org/10.1016/j.jhazmat.2020.123760>
- Peiravi, M., Ackah, L., Guru, R., Mohanty, M., Liu, J., Xu, B., Zhu, X., & Chen, L. (2017). Chemical extraction of rare earth elements from coal ash. *Minerals & Metallurgical Processing*, 34(4), 170–177. <https://doi.org/10.19150/mmp.7856>
- Piantone, P., Bodéan, F., & Chatelet-Snidaro, L. (2004). Mineralogical study of secondary mineral phases from weathered MSWI bottom ash: implications for the modelling and trapping of heavy metals. *Applied Geochemistry*, 19(12), 1891–1904. <https://doi.org/10.1016/j.apgeochem.2004.05.006>
- Piantone, P., Bodéan, F., Derie, R., & Depelsenaire, G. (2003). Monitoring the stabilization of municipal solid waste incineration fly ash by phosphation: mineralogical and balance approach. *Waste Management*, 23(3), 225–243. [https://doi.org/10.1016/s0956-053x\(01\)00058-7](https://doi.org/10.1016/s0956-053x(01)00058-7)
- Pienkoß, F., Abis, M., Bruno, M., Grönholm, R., Hoppe, M., Kuchta, K., Fiore, S., & Simon, F.-G. (2021). Heavy metal recovery from the fine fraction of solid waste incineration bottom ash by wet density separation. *Journal of Material Cycles and Waste Management*, 24(1), 364–377. <https://doi.org/10.1007/s10163-021-01325-1>
- Pradhan, S., & Mohanta, S. (2020). A method to perform float-and-sink test for separation of coal samples of various densities and determination of “Probable Error” and “Imperfection.” *IOP SciNotes*, 1(2), 024403. <https://doi.org/10.1088/2633-1357/abaf36>
- Prameswara, G., Prista Tyassena, F. Y., Pasaribu, M., & Novitha Febryanza, I. (2022). Kinetika Leaching Ni dan Fe dari Bijih Laterit Tipe Limonite Morowali. *Journal of Research on Chemistry and Engineering*, 3(2746-0401), 57–62. <http://dx.doi.org/10.52759/reactor.v3i2.57>
- PubChem. (2021). *The PubChem Project*. NIH National Library of Medicine; National Library of Medicine. <https://pubchem.ncbi.nlm.nih.gov/>

- Ramachandra Rao, S. (2006). Physical and Physico-Chemical Processes. *Resource Recovery and Recycling from Metallurgical Wastes*, 35–69. [https://doi.org/10.1016/s0713-2743\(06\)80088-7](https://doi.org/10.1016/s0713-2743(06)80088-7)
- Reimann, D. O. (1989). Heavy Metals in Domestic Refuse and Their Distribution in Incinerator Residues. *Waste Management & Research: The Journal for a Sustainable Circular Economy*, 7(1), 57–62. <https://doi.org/10.1177/0734242x8900700107>
- Rissler, J., Klementiev, K., Dahl, J., Steenari, B.-M., & Edo, M. (2020). Identification and Quantification of Chemical Forms of Cu and Zn in MSWI Ashes Using XANES. *Energy & Fuels*, 34(11), 14505–14514. <https://doi.org/10.1021/acs.energyfuels.0c02226>
- Rusian Anatolievich Kiper. (n.d.). *zinc hydroxide*. Chemister.ru. Retrieved March 7, 2023, from <http://chemister.ru/Database/properties-en.php?dbid=1&id=4200>
- Saffarzadeh, A., & Takayuki, S. (2014). Occurrence and Significance of Secondary Iron-rich Products in Landfilled MSWI Bottom Ash. *International Journal of Waste Resources*, 04(03). <https://doi.org/10.4172/2252-5211.1000150>
- Saqib, N., & Bäckström, M. (2015). Distribution and leaching characteristics of trace elements in ashes as a function of different waste fuels and incineration technologies. *Journal of Environmental Sciences*, 36, 9–21. <https://doi.org/10.1016/j.jes.2015.03.006>
- Settimo, F., Bevilacqua, P., & Rem, P. (2004). Eddy Current Separation of Fine Non-Ferrous Particles from Bulk Streams. *Physical Separation in Science and Engineering*, 13(1), 15–23. <https://doi.org/10.1080/00207390410001710726>
- Shim, Y.-S., Kim, Y.-K., Kong, S.-H., Rhee, S.-W., & Lee, W.-K. (2003). The adsorption characteristics of heavy metals by various particle sizes of MSWI bottom ash. *Waste Management*, 23(9), 851–857. [https://doi.org/10.1016/S0956-053X\(02\)00163-0](https://doi.org/10.1016/S0956-053X(02)00163-0)
- Shim, Y.-S., Rhee, S.-W., & Lee, W.-K. (2005). Comparison of leaching characteristics of heavy metals from bottom and fly ashes in Korea and Japan. *Waste Management*, 25(5), 473–480. <https://doi.org/10.1016/j.wasman.2005.03.002>
- Smith, Y. R., Nagel, J. R., & Rajamani, R. K. (2019). Eddy current separation for recovery of non-ferrous metallic particles: A comprehensive review. *Minerals Engineering*, 133, 149–159. <https://doi.org/10.1016/j.mineng.2018.12.025>
- Somasundaran, P. (1986). An Overview of the Ultrafine Problem. *Mineral Processing at a Crossroads*, 1–36. https://doi.org/10.1007/978-94-009-4476-3_1

- Speiser, C., Baumann, T., & Niessner, R. (2000). Morphological and Chemical Characterization of Calcium-Hydrate Phases Formed in Alteration Processes of Deposited Municipal Solid Waste Incinerator Bottom Ash. *Environmental Science & Technology*, 34(23), 5030–5037. <https://doi.org/10.1021/es990739c>
- Sposito, G., Lund, L. J., & Chang, A. C. (1982). Trace Metal Chemistry in Arid-zone Field Soils Amended with Sewage Sludge: I. Fractionation of Ni, Cu, Zn, Cd, and Pb in Solid Phases. *Soil Science Society of America Journal*, 46(2), 260–264. <https://doi.org/10.2136/sssaj1982.03615995004600020009x>
- Stegemann, J. A., & Schneider, J. (1991, January 1). *Leaching Potential of Municipal Waste Incinerator Bottom ASH as a Function of Particle Size Distribution* (J. J. J. M. Goumans, H. A. van der Sloot, & Th. G. Aalbers, Eds.). ScienceDirect; Elsevier. <https://www.sciencedirect.com/science/article/abs/pii/S0166111608703972>
- Struis, R. P. W. J., Ludwig, C., Lutz, H., & Scheidegger, A. M. (2004). Speciation of Zinc in Municipal Solid Waste Incineration Fly Ash after Heat Treatment: An X-ray Absorption Spectroscopy Study. *Environmental Science & Technology*, 38(13), 3760–3767. <https://doi.org/10.1021/es0346126>
- Šyc, M., Krausová, A., Kameníková, P., Šomplák, R., Pavlas, M., Zach, B., Pohořelý, M., Svoboda, K., & Punčochář, M. (2018). Material analysis of Bottom ash from waste-to-energy plants. *Waste Management*, 73, 360–366. <https://doi.org/10.1016/j.wasman.2017.10.045>
- Šyc, M., Simon, F. G., Hykš, J., Braga, R., Biganzoli, L., Costa, G., Funari, V., & Grosso, M. (2020). Metal recovery from incineration bottom ash: State-of-the-art and recent developments. *Journal of Hazardous Materials*, 393, 122433. <https://doi.org/10.1016/j.jhazmat.2020.122433>
- Takayuki Shimaoka, S. A. (2014). Occurrence and Significance of Secondary Iron-rich Products in Landfilled MSWI Bottom Ash. *International Journal of Waste Resources*, 04(03). <https://doi.org/10.4172/2252-5211.1000150>
- Tang, P., Florea, M. V. A., Spiesz, P., & Brouwers, H. J. H. (2015). Characteristics and application potential of municipal solid waste incineration (MSWI) bottom ashes from two waste-to-energy plants. *Construction and Building Materials*, 83, 77–94. <https://doi.org/10.1016/j.conbuildmat.2015.02.033>

- Tessier, A., Campbell, P. G. C., & Bisson, M. (1979). Sequential extraction procedure for the speciation of particulate trace metals. *Analytical Chemistry*, 51(7), 844–851. <https://doi.org/10.1021/ac50043a017>
- Tian, S., Yu, M., Wang, W., Wang, Q., & Wu, Z. (2009). Investigating the Speciation of Copper in Secondary Fly Ash by X-ray Absorption Spectroscopy. *Environmental Science & Technology*, 43(24), 9084–9088. <https://doi.org/10.1021/es902039x>
- Tiseo, I. (2020, November 25). *Global municipal solid waste generation by region*. Statista. <https://www.statista.com/statistics/916592/global-generation-of-municipal-solid-waste-by-region/>
- Tiseo, I. (2022, June 22). *U.S. municipal solid waste generation*. Statista. <https://www.statista.com/statistics/186256/us-municipal-solid-waste-generation-since-1960/>
- Tuan, Y.-J., Paul Wang, H., Chang, J.-E. ., Chao, C.-C. ., & Tsai, C.-K. . (2010). Speciation of copper in the thermally stabilized slag. *Nuclear Instruments and Methods in Physics Research Section A: Accelerators, Spectrometers, Detectors and Associated Equipment*, 619(1-3), 316–318. <https://doi.org/10.1016/j.nima.2010.01.023>
- UNEP, & ISWA. (2015). *Global Waste Management Outlook*. United Nations Environment Programme and International Solid Waste Association. https://wedocs.unep.org/bitstream/handle/20.500.11822/9672/-Global_Waste_Management_Outlook-2015Global_Waste_Management_Outlook.pdf.pdf?sequence=3&isAllowed=
- Vateva, I., & Laner, D. (2020). Grain-Size Specific Characterisation and Resource Potentials of Municipal Solid Waste Incineration (MSWI) Bottom Ash: A German Case Study. *Resources*, 9(6), 66. <https://doi.org/10.3390/resources9060066>
- Veasey, T. J., & Wills, B. A. (1991). Review of methods of improving mineral liberation. *Minerals Engineering*, 4(7-11), 747–752. [https://doi.org/10.1016/0892-6875\(91\)90062-z](https://doi.org/10.1016/0892-6875(91)90062-z)
- Verbinnen, B., Billen, P., Van Caneghem, J., & Vandecasteele, C. (2016). Recycling of MSWI Bottom Ash: A Review of Chemical Barriers, Engineering Applications and Treatment Technologies. *Waste and Biomass Valorization*, 8(5), 1453–1466. <https://doi.org/10.1007/s12649-016-9704-0>

- Vilar, S., Gutierrez, A., Antezana, J., Carral, P., & Alvarez, A. (2005). A comparative study of three different methods for the sequential extraction of heavy metals in soil. *Toxicological & Environmental Chemistry*, 87(1), 1–10. <https://doi.org/10.1080/02772240410001665553>
- Wan, X., Wang, W., Ye, T., Guo, Y., & Gao, X. (2006). A study on the chemical and mineralogical characterization of MSWI fly ash using a sequential extraction procedure. *Journal of Hazardous Materials*, 134(1-3), 197–201. <https://doi.org/10.1016/j.jhazmat.2005.10.048>
- Wang, G. C. (2016). Nonferrous metal extraction and nonferrous slags. *The Utilization of Slag in Civil Infrastructure Construction*, 35–61. <https://doi.org/10.1016/b978-0-08-100381-7.00003-3>
- Wang, Q., Ko, J. H., Liu, F., & Xu, Q. (2021). Leaching characteristics of heavy metals in MSW and bottom ash co-disposal landfills. *Journal of Hazardous Materials*, 416, 126042. <https://doi.org/10.1016/j.jhazmat.2021.126042>
- Wei, Y., Shimaoka, T., Saffarzadeh, A., & Takahashi, F. (2011). Alteration of municipal solid waste incineration bottom ash focusing on the evolution of iron-rich constituents. *Waste Management*, 31(9-10), 1992–2000. <https://doi.org/10.1016/j.wasman.2011.04.021>
- Wei, Y., Mei, X., Shi, D., Liu, G., Li, L., & Shimaoka, T. (2017). Separation and characterization of magnetic fractions from waste-to-energy bottom ash with an emphasis on the leachability of heavy metals. *Environmental Science and Pollution Research*, 24(17), 14970–14979. <https://doi.org/10.1007/s11356-017-9145-8>
- Wiles, C. C. (1996). Municipal solid waste combustion ash: State-of-the-knowledge. *Journal of Hazardous Materials*, 47(1-3), 325–344. [https://doi.org/10.1016/0304-3894\(95\)00120-4](https://doi.org/10.1016/0304-3894(95)00120-4)
- Wills, B. A., & Finch, J. A. (2016a). Comminution. In *Wills' Mineral Processing Technology* (pp. 109–122). Elsevier Ltd. <https://doi.org/10.1016/b978-0-08-097053-0.00005-4>
- Wills, B. A., & Finch, J. A. (2016b). Crushers. In *Wills' Mineral Processing Technology* (pp. 123–146). Elsevier Ltd. <https://doi.org/10.1016/b978-0-08-097053-0.00006-6>
- Wills, B. A., & Finch, J. A. (2016c). Grinding Mills. In *Wills' Mineral Processing Technology* (pp. 147–179). Elsevier Ltd. <https://doi.org/10.1016/b978-0-08-097053-0.00007-8>
- Wills, B. A., & Finch, J. A. (2016d). Industrial Screening. *Wills' Mineral Processing Technology*, 181–197. <https://doi.org/10.1016/b978-0-08-097053-0.00008-x>

- Xia, Y., He, P., Shao, L., & Zhang, H. (2017). Metal distribution characteristic of MSWI bottom ash in view of metal recovery. *Journal of Environmental Sciences*, 52, 178–189. <https://doi.org/10.1016/j.jes.2016.04.016>
- Yang, Y., Balentina, CF., Brouwer, D., Xiao, Y., Voncken, JHL., & Boom, R. (2008). Metal recovery and refining from MSW incineration bottom ash. In B. Mishra, C. Ludwig, & S. Das (Eds.), *Proceedings of the Global Symposium on Recycling, Waste Treatment and Clean Technology, REWAS 2008* (pp. 1285-1294). TMS.
- Yao, J., Li, W.-B., Kong, Q.-N., Wu, Y.-Y., He, R., & Shen, D.-S. (2010). Content, mobility and transfer behavior of heavy metals in MSWI bottom ash in Zhejiang province, China. *Fuel*, 89(3), 616–622. <https://doi.org/10.1016/j.fuel.2009.06.016>
- Yao, Q., Samad, N. B., Keller, B., Seah, X. S., Huang, L., & Lau, R. (2014). Mobility of heavy metals and rare earth elements in incineration bottom ash through particle size reduction. *Chemical Engineering Science*, 118, 214–220. <https://doi.org/10.1016/j.ces.2014.07.013>
- Yin, K., Chan, W. P., S/O Tamilselvam, K., Chen, W. Q., Mohamad Latiff, N. B., Heberlein, S., & Lisak, G. (2021). Redistribution of mineral phases of incineration bottom ash by size and magnetic separation and its effects on the leaching behaviors. *Environmental Pollution*, 290, 118015. <https://doi.org/10.1016/j.envpol.2021.118015>
- Youcai, Z. (2017). Heavy Metals and Recycling of Bottom Ash. *Pollution Control and Resource Recovery: Municipal Solid Wastes Incineration*, 83–117. <https://doi.org/10.1016/b978-0-12-812165-8.00003-2>
- Yu, Y., Ma, L., Cao, M., & Liu, Q. (2017). Slime coatings in froth flotation: A review. *Minerals Engineering*, 114, 26–36. <https://doi.org/10.1016/j.mineng.2017.09.002>
- Zhang, H. Speciation of zinc in the weathered MSWI bottom ash by XAFS. Abstracts of Papers, 255th ACS National Meeting & Exposition, New Orleans, LA, United States, March 18–22, 2018, INOR-407, 2018.
- Zhang, H., He, P.-J., & Shao, L.-M. (2008). Fate of heavy metals during municipal solid waste incineration in Shanghai. *Journal of Hazardous Materials*, 156(1-3), 365–373. <https://doi.org/10.1016/j.jhazmat.2007.12.025>
- Zhang, W., & Honaker, R. (2020). Characterization and recovery of rare earth elements and other critical metals (Co, Cr, Li, Mn, Sr, and V) from the calcination products of a coal refuse sample. *Fuel*, 267. <https://doi.org/10.1016/j.fuel.2020.117236>

Zhang, W., Xue, Y., & Cui, Z. (2017). Effect of Size on the Structural Transition and Magnetic Properties of Nano-CuFe₂O₄. *Industrial & Engineering Chemistry Research*, 56(46), 13760–13765. <https://doi.org/10.1021/acs.iecr.7b03468>

Appendix A: Particle Size Distribution

Fit the data set entered to the equation:

$$Y = n * X - n * \ln(DN)$$

where: $Y = \ln(-\ln(R))$

$$X = \ln(D)$$

Raw BA sample

D	R	X	Y		
Sieve, μm	Cumulative %Retained			Fitted Y	Fitted % retained
420	-				0.0%
236	0.5%	5.47	1.67	1.61	0.7%
167	5.5%	5.12	1.06	0.92	8.2%
121	40.5%	4.79	-0.10	0.26	27.3%
85	53.2%	4.44	-0.46	-0.44	52.6%
57	68.8%	4.04	-0.98	-1.25	75.0%
40	87.8%	3.70	-2.04	-1.94	86.6%
26	100.0%	3.26		-2.81	94.2%
			$R^2 =$	0.9743	
n=	2.009534		(Note: R^2 is relative to the derived X and Y, and not D and R.)		
$n * \ln(D_N)$	-9.37263				
D_N	106.068				

UB-1: BA sample subjected to 10 min of grinding

D	R	X	Y		
Sieve, μm	Cumulative %Retained			Fitted Y	Fitted % retained
420	-				0.0%
236	3.4%	5.47	1.22	1.18	3.8%
167	7.4%	5.12	0.96	0.96	7.4%
121	12.4%	4.79	0.74	0.74	12.2%
85	20.9%	4.44	0.45	0.51	18.8%
57	28.9%	4.04	0.22	0.25	27.7%
40	33.5%	3.70	0.09	0.02	35.9%
26	100.0%	3.26		-2.81	94.2%
			$R^2 =$	0.9883	
n=	0.656073		(Note: R^2 is relative to the derived X and Y, and not D and R.)		
$n * \ln(D_N)$	-2.40231				
D_N	38.92543				

UB-2: BA sample subjected to 30 min grinding

D	R	X	Y		
Sieve, μm	Cumulative %Retained			Fitted Y	Fitted % retained
420	-				0.0%
236	1.2%	5.47	1.49	1.40	1.7%
167	4.2%	5.12	1.16	1.14	4.4%
121	11.7%	4.79	0.77	0.89	8.7%
85	17.1%	4.44	0.57	0.63	15.2%
57	25.5%	4.04	0.31	0.33	24.8%
40	30.6%	3.70	0.17	0.07	34.1%
26	100.0%	3.26		-2.81	94.2%
			$R^2 =$	0.9688	
n=	0.750198		(Note: R^2 is relative to the derived X and Y, and not D and R.)		
n * ln (D _N)	-2.70185				
D _N	36.65387				

UB-3: BA sample subjected to 60 min of grinding

D	R	X	Y		
Sieve, μm	Cumulative %Retained			Fitted Y	Fitted % retained
420	-				0.0%
236	0.5%	5.47	1.66	1.68	0.5%
167	0.9%	5.12	1.56	1.58	0.8%
121	1.1%	4.79	1.50	1.48	1.2%
85	1.4%	4.44	1.45	1.37	1.9%
57	3.5%	4.04	1.21	1.26	3.0%
40	4.4%	3.70	1.14	1.15	4.2%
26	100.0%	3.26		-2.81	94.2%
			$R^2 =$	0.9603	
n=	0.299239		(Note: R^2 is relative to the derived X and Y, and not D and R.)		
n * ln (D _N)	0.044995				
D _N	0.860394				

UB-3: BA sample subjected to 90 min of grinding

D	R	X	Y		
Sieve, μm	Cumulative % Retained			Fitted Y	Fitted % retained
420	-				0.0%
236	0.2%	5.47	1.83	1.85	0.2%
167	0.2%	5.12	1.80	1.78	0.3%
121	0.4%	4.79	1.72	1.71	0.4%
85	0.6%	4.44	1.64	1.63	0.6%
57	1.0%	4.04	1.54	1.55	0.9%
40	1.3%	3.70	1.47	1.48	1.3%
26	100.0%	3.26		-2.81	94.2%
			R² =	0.9876	
n=	0.211949		(Note: R ² is relative to the derived X and Y, and not D and R.)		
n * ln (D_N)	0.692005				
D_N	0.038199				

Appendix B: Permission for Release

Bunge, 2019



Sharon Escalante Pedraza <sepedraza@vt.edu>

Permission to use figures and information

3 messages

Sharon Escalante Pedraza <sepedraza@vt.edu>
To: "umtec@ost.ch" <umtec@ost.ch>

Tue, Apr 4, 2023 at 3:33 PM

Hello,

My name is Sharon Escalante Pedraza, a second-year master's student in the Mining and Minerals Engineering program at Virginia Tech.

For the last 2 years, I have been working on a project called "Municipal Solid Waste Incineration Ash Characterization and Physical Characterization". The results from this study will be included in my thesis. However, as part of the first chapter, related to the Literature Review, I would like to include information and Figures from the report called "Recovery of Metals from Waste Incineration Bottom Ash by Rainer Bunge and published in 2019. More specifically, information related to the BA composition and the description of the different physical concentration processes. This book has been properly cited in the thesis, but it is a requirement from Virginia Tech to have the proper author/publisher authorization.


I am attaching the document, which has free access online so that you can identify the information I am requiring.

Thank you, I hope to hear back from you soon.

Do not hesitate to ask more information or question, I will be happy to answer them

--

Sharon E. Pedraza
Graduate Student
Mining and Minerals Engineering
Virginia Tech
P: (540) 998 1558

 Metals_from_MWIBA_6_2019.pdf
3037K

UMTEC Institut für Umwelt- und Verfahrenstechnik | OST - Ostschweizer Fachhochschule
<umtec@ost.ch>

Sun, Apr 9, 2023 at 3:02 AM

To: Sharon Escalante Pedraza <sepedraza@vt.edu>

Dear Ms. Pedraza,

Thank you for your e-mail. I have forwarded your message to Dr. Prof. Rainer Bunge. I think, you will hear from him soon.

Yours sincerely,

Fabienne Früh

Assistentin Institutsleitung UMTEC

fabienne.frueh@ost.ch

OST – Ostschweizer Fachhochschule

Institut für Umwelt- und Verfahrenstechnik | [Oberseestrasse 10](#) | 8640 Rapperswil | Switzerland | <https://www.ost.ch> | <http://www.umtec.ch> |

OST – Ostschweizer Fachhochschule ist der Zusammenschluss aus FHS St.Gallen, HSR Rapperswil und NTB Buchs.

[Quoted text hidden]

Rainer Bunge <rainer.bunge@ost.ch>
To: "sepedraza@vt.edu" <sepedraza@vt.edu>

Sun, Apr 9, 2023 at 3:31 AM

Dear Sharon

I consent with your request and herewith authorize you to use the contents of my publication "Recovery of Metals from Waste Incineration Bottom Ash" in whichever way you consider suitable. Also, I would be grateful if you sent me a copy of your theses as PDF. By the way – if Tom Meloy is still around (which I doubt...), extend my very best regards to him. I did my PhD with Doug Fuerstenau at Berkeley and met Tom on a number of occasions. He is/was a brilliant scientist and also quite a character who has impressed me very considerably 😊

Whishing you good success with your theses and all the best,

Rainer

Prof. Dr. Rainer Bunge

Ostschweizer Fachhochschule OST

Institut für Umwelt- und Verfahrenstechnik UMTEC

[Oberseestrasse 10](#) , CH 8640 Rapperswil

+41 (0)58 257 4862, www.umtec.ch , rainer.bunge@ost.ch

UMTEC: "Wir erforschen technische Probleme nicht. Wir lösen sie!"

World Bank Group

© 2018 International Bank for Reconstruction and Development / The World Bank
1818 H Street NW, Washington, DC 20433
Telephone: 202-473-1000; Internet: www.worldbank.org

Some rights reserved.

1 2 3 4 21 20 19 18

This work is a product of the staff of The World Bank with external contributions. The findings, interpretations, and conclusions expressed in this work do not necessarily reflect the views of The World Bank, its Board of Executive Directors, or the governments they represent. The World Bank does not guarantee the accuracy of the data included in this work. The boundaries, colors, denominations, and other information shown on any map in this work do not imply any judgment on the part of The World Bank concerning the legal status of any territory or the endorsement or acceptance of such boundaries.

Nothing herein shall constitute or be considered to be a limitation upon or waiver of the privileges and immunities of The World Bank, all of which are specifically reserved.

Rights and Permissions



This work is available under the Creative Commons Attribution 3.0 IGO license (CC BY 3.0 IGO) <http://creativecommons.org/licenses/by/3.0/igo>. Under the Creative Commons Attribution license, you are free to copy, distribute, transmit, and adapt this work, including for commercial purposes, under the following conditions:

Attribution—Please cite the work as follows: Kaza, Silpa, Lisa Yao, Perinaz Bhada-Tata, and Frank Van Woerden. 2018. *What a Waste 2.0: A Global Snapshot of Solid Waste Management to 2050*. Urban Development Series. Washington, DC: World Bank. doi:10.1596/978-1-4648-1329-0. License: Creative Commons Attribution CC BY 3.0 IGO

Translations—If you create a translation of this work, please add the following disclaimer along with the attribution: *This translation was not created by The World Bank and should not be considered an official World Bank translation. The World Bank shall not be liable for any content or error in this translation.*

Adaptations—If you create an adaptation of this work, please add the following disclaimer along with the attribution: *This is an adaptation of an original work by The World Bank. Views and opinions expressed in the adaptation are the sole responsibility of the author or authors of the adaptation and are not endorsed by The World Bank.*